OPTIMIZATION OF USING POLYMERIC AND MIXED MATRIX PVA AMINE-BASED MEMBRANES FOR CO_2/N_2 AND CO_2/CH_4 SEPARATION

IRIS SAMPUTU

Thesis submitted to the University of Ottawa
in partial Fulfillment of the requirements for the
degree of
Master of Applied Science in Chemical Engineering

Department of Chemical and Biological Engineering
Faculty of Engineering
University of Ottawa

ABSTRACT

Separation of CO_2, the main global warming causing greenhouse gas, from other flue gases and from biogas has become of great interest due to the predicted effects of global warming that the world is already starting to experience. This research focuses on the separation of CO_2 from CH_4 and N_2 gases using polymeric and mixed matrix membranes. Amine-based poly vinyl alcohol (PVA) polymeric membranes that had previously shown good gas separation results were adapted for use in this research. The physical aging of the adapted membrane was initially analyzed for 37 days and it was observed that the membrane stabilized after 21 days. The adapted membrane was then optimized using a 2^6 factorial design to improve the membranes' performance with respect to CO_2/N_2 and CO_2/CH_4 selectivity when tested using single gas permeation experiments at near atmospheric conditions. This was done with the membrane components: PVA, formaldehyde, poly (allylamine hydroxide), potassium hydroxide, water and 2-aminoisobutyric acid. Zeolite 13X and ZIF-8 powdered adsorbents were incorporated in the optimized membranes to prepare mixed-matrix membranes with the goal of bettering the separation performance of the membranes. Membrane characterization was done on the best performing membranes through spectroscopy, microscopy, and contact angle measurements. This study concluded with feed pressure tests on the overall best performing membranes. The performance of the fabricated membranes was compared to other polymeric and mixed-matrix membranes and Robeson's upper bound line. Overall, the polymeric optimized membranes seemed to perform better than the filled mixed matrix membranes due to the introduction of agglomerations and cracks with both the filler materials. Also, the separation performance of the membrane improved with a decrease in pressure. At 1.5 absolute pressure, the optimized membrane was able to achieve a CO_2/N_2 and CO_2/CH_4 selectivity of 5.94 and 2.13 respectively with a CO_2 permeability of 15,813 Barrer.

ACKNOWLEDGEMENTS

Firstly, I would like to express my extreme gratitude to my supervisor Dr. F. Handan Tezel for supporting and guiding me throughout my graduate degree. I would like to thank her for helping me become a better researcher, her advice throughout the years and for helping me improve my communication skills both orally and in writing. I would also like to thank Franco Ziroldo and Gerard Nina for all the technical support they have provided me as well as for answering all my questions. I would like to thank Lara Tansug for helping to edit this thesis. Also, I would like to thank my other colleagues in the Tezel e-SMART group and in the Chemical and Biological Engineering department; Dana Li, Amirhosein Jahanshahi, Suboohi Shervani and Fatemeh Abedi for answering all my questions and for all the suggestions and training that they have provided me throughout my project. I would also like to thank Temilade Openinyi, Adoyeji Balogun, Gabriel Akinyemi and Onika Maraj for all their encouragement during my graduate studies.

Finally, I would like to thank my parents, sisters, family and friends for all the encouragement and support they have continually provided during the last two years of my graduate studies. I would like to thank NSERC (Natural Sciences and Engineering Council of Canada) and ECO-Canada for providing funding.

STATEMENT OF CONTRIBUTION AND COLLABORATORS

I hereby declare that solely I have written the work presented in this thesis under the direct supervision of Dr. F. Handan Tezel. I performed the entirety of the experiments discussed in this work. The design of the gas permeation set-up was done by Lauren Rose with feedback from Dr. F. Handan Tezel, Louis Tremblay, Franco Ziroldo and Gerard Nina. The membrane synthesis procedure was adapted by myself with feedback from Dr. Tezel using the reference procedure from the paper written by Jian Zou and Winston Ho. The factorial design optimization was suggested by Dr Tezel with implementation and design and synthesis of the membranes done by myself. Bhavya Bhatt tested the membranes made in the factorial design study. The aging test membranes was suggested by me. I made the aging test membranes with testing by Bhavya Bhatt. The incorporation of adsorbents was suggested by Dr. Tezel, the choice of adsorbents, membrane synthesis and testing were done by me. The feed pressure tests were also suggested by Dr. Tezel with membrane synthesis and testing done by me.

TABLE OF CONTENTS

ABSTRACT ii
ACKNOWLEDGEMENTS iii
STATEMENT OF CONTRIBUTION AND COLLABORATORS iv
LIST OF FIGURES viii
LIST OF TABLES ix
CHAPTER 1: INTRODUCTION 1
1.1 THESIS OBJECTIVES 3
1.2 THESIS OUTLINE 3
1.3 REFERENCES 5
CHAPTER 2: LITERATURE REVIEW OF POLYMERIC AND MIXED-MATRIX MEMBRANES USED FOR THE SEPARATION OF CARBON DIOXIDE AND NITROGEN AND CARBON DIOXIDE AND METHANE 7
2.1 ABSTRACT 7
2.2 INTRODUCTION 8
2.2.1 World energy demand 8
2.2.2 Greenhouse gas emissions and climate change 8
2.2.3 Carbon capture and storage 10
2.2.4 Separation technologies 11
2.2.5 CO_2, CH_4 and N_2 properties 12
2.2.6 CO_2 separation through membranes 13
2.2.7 CO_2/N_2 and CO_2/CH_4 separation conditions 21
2.2.8 Membrane defects 22
2.3 ORGANIC (POLYMERIC) MEMBRANES FOR CO_2/N_2 AND CO_2/CH_4 SEPARATION 23
2.3.1 PVA based membranes 25
2.3.2 PDMS 27
2.3.3 2-PD/2-ME 28
2.3.4 PEBAX based membranes 28
2.3.5 PTMSP 32
2.3.6 PIM 32
2.3.7 Bio-PITB 33
2.3.8 XL-PEGDA 34
2.3.9 PNB-Si(OEt)-Si(OEtOMe) 35
2.3.10 Overview of polymeric membrane materials for CO_2/N_2 and CO_2/CH_4 separation 35
2.4 MIXED-MATRIX MEMBRANES FOR CO_2/N_2 SEPARATION 37
2.4.1 Zeolite filled membranes for CO_2/N_2 separation 40
2.4.2 Metal organic framework filled membranes for CO_2/N_2 separation 43

2.4.3 Summary of mixed-matrix membranes for CO_2/N_2 separation..... 51
2.5.1 Zeolite filled membranes for CO_2/CH_4 separation..... 53
2.5.2 Metal organic framework filled membranes for CO_2/CH_4 separation..... 57
2.5.3 Summary of mixed-matrix membranes for CO_2/CH_4 separation..... 61
2.6 NOMENCLATURE..... 62
2.7 GREEK SYMBOLS..... 62
2.8 ABBREVIATIONS..... 63
2.9 REFERENCES..... 65
CHAPTER 3: APPLICATION OF A 2^6-FACTORIAL DESIGN OPTIMIZATION FOR POLY (VINYL ALCOHOL) BASED MEMBRANE SYNTHESIS FOR CO_2 /N_2 AND CO_2/CH_4 SEPARATION..... 79
3.1 ABSTRACT..... 79
3.2 INTRODUCTION..... 80
3.3 EXPERIMENTAL..... 84
3.3.1 Factorial design..... 84
3.3.2 Membrane development procedure..... 86
3.3.3 Aging test procedure..... 89
3.3.4 Single gas permeation experiment procedure..... 90
3.3.5 Characterization of synthesized membranes..... 92
3.4 RESULTS AND DISCUSSION..... 94
3.4.1 Physical aging study..... 94
3.4.2 Membrane characterization..... 95
3.4.3 Factorial design study for CO_2/N_2 and CO_2/CH_4 selectivity..... 100
3.4.4 Literature Comparison..... 107
3.5 CONCLUSIONS..... 109
3.6 APPENDIX..... 111
3.7 NOMENCLATURE..... 114
3.8 GREEK SYMBOLS..... 114
3.9 ABBREVIATIONS..... 115
3.10 REFERENCES..... 116
CHAPTER 4: ZEOLITE-13X- AND ZIF-8 FILLED PVA MIXED MATRIX MEMBRANES FOR USE IN CO_2/N_2 AND CO2/CH4 SEPARATION..... 124
4.1 ABSTRACT..... 124
4.2 INTRODUCTION..... 125
4.3 EXPERIMENTAL..... 129

4.3.1 Membrane development procedure 129
4.3.2 Feed pressure test procedure 132
4.3.3 Single gas permeation experiment procedure 133
4.3.4 Characterization of synthesized membranes 136
4.4 RESULTS AND DISCUSSION 137
4.4.1 Membrane characterization 137
4.4.2 Zeolite 13X filler tests 142
4.4.3 ZIF-8 filler tests 144
4.4.4 Feed pressure tests 146
4.4.5 Comparison with membranes from literature 149
4.5 CONCLUSIONS 154
4.6 NOMENCLATURE 155
4.7 GREEK SYMBOLS 155
4.8 ABBREVIATIONS 156
4.9 REFERENCES 157
CHAPTER 5: CONCLUSIONS AND RECOMMENDATIONS 163

LIST OF FIGURES

Figure 2.1: Schematic of a membrane separation process 14
Figure 2.2: SEM images of the parent and the impregnated nanoparticles, (top left: ZSM-5, top right: Fe-ZSM-5, bottom left: P-ZSM-5, and bottom right: Mn-ZSM [74]. 56
Figure 2.3: SEM images of Zn/Co-ZIF carbonized at 600 °C for different durations: (a) Zn/Co-ZIF, (b) C-ZIF-2H, (c) C-ZIF-4H, (d) C-ZIF-8H, (e) C-ZIF-12H, and (f) C-ZIF-24H [98]. ……...58
Figure 3.1: Schematic diagram of single gas permeation setup used in this study 91
Figure 3.2: CO_2, N_2 and CH_4 permeabilities as a function of day tested from day 1 to day 37. 95
Figure 3.3: Top membrane surface area SEM images of membrane 13 (left) and 61 (right) at X5000 magnification 97
Figure 3.4: Cross- sectional images of base membrane at X100 magnification (left) and X800 magnification (right) 97
Figure 3.5: FTIR spectroscopy image of the base membrane, membrane 13 and membrane 61 99
Figure 3.6: Contact angle measurements of the base membrane, membrane 13 and membrane 61. 100
Figure 3.7: Weight factors of individual and combined component factors for CH_4/N_2 selectivity. 104
Figure 3.8: Weight factors of individual and combined component factors for CO_2/CH_4 selectivity. 105
Figure 3.9: Weight factors of individual and combined component factors for CO_2/N_2 selectivity 106
Figure 3.10: Comparison with membranes from literature and Robeson plot. 108
Figure 4.1: Schematic of single gas permeation setup used in this study. 135
Figure 4.2: Zeolite 13X filled membranes at ×1,000 magnification (left) and at ×3,000 magnification (right). 137
Figure 4.3: ZIF-8 filled membranes at ×1,000 magnification (left) and at ×3,000 magnification (right). 138
Figure 4.4: FTIR spectroscopy image of membrane 13 with and without zeolite 13X filler and ZIF-8 filler 139
Figure 4.5: FTIR spectroscopy image of membrane 61 with and without zeolite 13X filler and ZIF-8 filler. 139
Figure 4.6: Contact angle measurements of the base membrane and membrane 13 with and zeolite 13X filler and ZIF-8 filler 141
Figure 4.7: Contact angle measurements of the base membrane and membrane 61 with and without zeolite 13X filler and ZIF-8 filler 141
Figure 4.8: Permeation test results for different zeolite 13X weight % filled membrane 13. 143
Figure 4.9: Permeation test results for different zeolite 13X weight % filled membrane 61. 143
Figure 4.10: Permeation test results for different ZIF-8 weight % filled membrane 13. 145
Figure 4.11: Permeation test results for different ZIF-8 weight % filled membrane 61. 145
Figure 4.12: N_2, CH_4 and CO_2 permeability for membrane 13 at different feed pressures 147
Figure 4.13: CO_2/N_2 and CO_2/CH_4 selectivity values at different feed pressures for membrane 13. 147
Figure 4.14: N_2, CH_4 and CO_2 permeability for membrane 61 at different feed pressures 149
Figure 4.15: CO_2/N_2 and CO_2/CH_4 selectivity values at different feed pressures for membrane 61. 149
Figure 4.16: CO_2/N_2 Robeson plot of polymeric membranes 153
Figure 4.17: CO_2/CH_4 Robeson plot of polymeric membranes 153

LIST OF TABLES

Table 2.1: Summary of important CO_2, CH_4 and N_2 gas properties. 13
Table 2.2: Common polymeric membranes used for CO_2 separation. These membranes are listed in decreasing order of CO_2/N_2 selectivity. 23
Table 2.3: Permeabilities of common polymeric membranes used for CO_2 separation. These membranes are listed in decreasing order of CO_2/N_2 selectivity. 24
Table 2.4: Common mixed-matrix membranes for CO_2/N_2 separation and their acronyms used. 37
Table 2.5: Mixed Matrix membranes studied in the literature for CO_2/N_2 separation and their permeabilities and selectivities at specified conditions. 39
Table 2.6: CO_2 permeability and selectivity values for pure PEBA, Uio-66-PEBA and UiO-66-PEBA-NH_2 membranes tested in both dry and humid states [82]. 47
Table 2.7: Common mixed-matrix membranes for CO_2/CH_4 separation and their acronyms 52
Table 2.8: Mixed Matrix membranes studied in the literature for CO_2/N_2 separation and their permeabilities and selectivities at specified conditions 53
Table 3.1: Summary of important CO_2, CH_4 and N_2 properties[11]. 83
Table 3.2: Upper and lower limits for components used in the optimization study. Each of these components were taken as different factors in preparing the membranes. These factors were labelled from A to F, as shown in this table. 86
Table 3.3: Gases used for the experiments in this study and their grades and purities. 89
Table 3.4: Material development concentrations, CO_2 permeability, CO_2/N_2 and CO_2/CH_4 selectivity values for the base membrane, membrane 13 and membrane 61 96
Table 3.5: Maximum and minimum permeability and selectivity data observed in this study. 100
Table 3.6: Comparison with membranes from literature 107
Table 3.7: Summary of results from factorial design 111
Table 4.1: Summary of results from 2^6 factorial design study on PVA amine-based membranes. 129
Table 4.2: Gases used for the research experiment and their grades and purities 133
Table 4.3: Summary of zeolite 13X and ZIF-8 filled mixed matrix membranes 150
Table 4.4: Performance of common polymeric membranes for CO_2/N_2 and CO_2/CH_4 separation 152

CHAPTER 1: INTRODUCTION

Continual global warming has become a global concern with policy makers, and particularly the Intergovernmental Panel on Climate Change (IPCC) warning that the earth should not warm more than 2°C higher than pre-industrial revolution temperatures. The average global temperatures have already increased by a little over 1°C since 1880[1]. In order for this to happen, the cumulative carbon emissions released between 2011 and 2050 need to be limited to around 1,100 gigatonnes of Carbon dioxide[2]. Consequently, Various international multilateral environment agreements have been organized to sync the reduction of greenhouse gas emissions between international countries such as the Montreal Protocol in 1999 and more recently the Paris agreement of 2015[3,4]. This is because as detailed by IPCC after analyzing the effects of climate change over the past two decades, climate change so far has caused shrinkage of glaciers, thawing of permafrost, later freezing and earlier breakup of ice on rivers and lakes. This is all in addition to the lengthening of mid to high latitude growing seasons, declines in plant and animal populations and earlier emergence of insects, flowering of trees and egg-laying in birds[5]. Other predicted effects of global warming as the earth continues to warm include floods, insect infestations, spread of disease, wildfire and drought which is predicted to affect a lot of the biodiversity on the earth from plants to all animals alike[6]. For these reasons, there has been a real effort to decrease the amount of greenhouse gas emissions emitted from fossil fuels, the major contributor to global warming.

The main greenhouse gases in the earth's atmosphere are water vapor (H_2O), carbon dioxide (CO_2), methane (CH_4), nitrous oxide (N_20) and ozone (O_3). Most of the greenhouse gas emissions leading to the climate change experienced in the earth are from CO_2. In fact, the atmospheric CO_2 concentration has increased by 35% since preindustrial times. This has been especially brought

about by the emission from fossil fuel combustion and to a lesser extent by land conversion and cement production[7,8]. Although fossil fuels are being phased out in an attempt to use more environmentally friendly energy sources, the International Energy Agency World Energy Outlook predicts that fossil fuels will remain significant for many decades[9]. It is, therefore, necessary to find a way to reduce the net CO_2 emitted into the atmosphere. Carbon Capture and Storage (CCS) is a growing method of doing this where it involves the removal of CO_2 from streams where it is produced such as at a power plant. This is followed by the transport of CO_2 to a safe location for long-time storage[10]. This paper focuses on post-combustion CO2 capture, that is separation of CO_2 from nitrogen (N_2).

Separation of CO_2 from CH_4 was also explored for application in natural gas sweetening. Natural gas sweetening is necessary as CO_2 lowers the Btu content of natural gas and it makes the natural gas corrosive which prevents the transportation of natural gas[11]. Other methods currently used for natural gas sweetening that is absorption and adsorption have fouling and corrosion issues; this has prompted the exploration of the use of membranes for CO_2 /CH_4 separation. CO_2 separation from CH_4 was also studied as a method of lowering the environmental footprint in the process of harnessing energy from the power generating sector[11]. Other applications for the separation of CO_2 from CH_4 are in the enhancement of the oil recovery process and in the upgrading of biogas[12].

1.1 THESIS OBJECTIVES

The main objectives of this research project were:

1. To perform an extensive literature search on polymeric and mixed matrix membranes used for CO_2/ N_2 separation and CO_2/ CH_4 separation.
2. To develop and optimize a Polyvinyl alcohol (PVA) and amine-based membrane for CO_2/ N_2 and CO_2/ CH_4 separations at near atmospheric conditions. This was done by adapting a workable procedure from literature. Test the stability of the developed membrane over time and study the effect of aging. Implement a factorial design to optimize the fabricated membrane for CO_2/N_2 and CO_2/CH_4 separation. The fabricated membranes were tested through single gas permeation tests.
3. Fabrication of mixed-matrix membranes by incorporating the use of ZIF-8 and zeolite 13 X particles within the previously optimized membranes with the same goal of bettering the performance of the membrane with respect to CO_2/N_2 and CO_2 /CH_4 separation. The effect of increasing the feed pressure and consequently the pressure difference was then observed with the 2 best optimized membranes.

1.2 THESIS OUTLINE

This thesis consists of a total of five chapters. Chapter 1 introduces the motivation behind the thesis project, namely why CO_2/ N_2 and CO_2/ CH_4 separations are important. It talks about the increasing world energy demand and the resulting global warming coming from green house gas emissions released from burning fossil fuels. This chapter also gives a brief outline of methods of carbon capture and storage and other gas separation technologies currently being used. The chapter then briefly describes membrane technology for gas separations and the operation of these membranes. Finally, the chapter is concluded with the thesis objectives and outlines.

Chapter 2 involves an extensive literature review of polymeric and mixed-matrix membranes currently being used for CO_2/N_2 separation as well as for CO_2/CH_4 separation. This chapter contains excerpts from 2 literature review papers to be submitted to the Journal of Membrane Science. Moreover, this chapter specifically looks at zeolites and metal organic frameworks as fillers. Herein, this chapter looks at the best performing membranes in terms of their selectivity for CO_2 over N_2 and over CH_4.

Chapter 3 describes the results obtained in adapting a PVA and amine-based membrane for CO_2/N_2 and CO_2/ CH_4 separation. It describes the results of the stability and aging of the membrane obtained by testing the membrane over a period of 35 days. Thereafter, this chapter describes results obtained by employing a 2^6 factorial design to optimize the adapted PVA- amine base membrane in terms of its selectivity for CO_2 over N_2 and over CH_4. Results of the membrane characterization done using FTIR, SEM and a goniometer were also presented. The performance of the best membrane is also compared to the base membrane and other membranes from literature.

Chapter 4 describes results obtained from incorporating ZIF-8 and zeolite 13X fillers at different weight percentages to the previously optimized membranes from chapter 3. Thereafter, the results from feed pressure tests on the 2 best performing membranes of the last 2 chapters are presented. Results of the membrane characterization done using FTIR, SEM and a goniometer are also presented. Finally, a comparison with the base membrane as well as other membranes from literature is done.

Chapter 5 summarizes the results obtained from chapters 3 and 4 and gives recommendations based on the results obtained.

1.3 REFERENCES

[1] IPCC News from Policy and Legislation News from Policy and Legislation Intergovernmental Panel on Climate Change IPCC Second Assessment Synthesis of Scientific-Technical Information Relevant to Interpreting Article 2 of the UN Framework Convention on Climate Change 1995', n.d.

[2] C. McGlade, P. Ekins, The geographical distribution of fossil fuels unused when limiting global warming to 2°C, Nature. 517 (2015) 187–190. https://doi.org/10.1038/nature14016.

[3] UNEP, Handbook on data reporting under the Montreal Protocol, 1999.

[4] V. Popovski, The Implementation of the Paris Agreement on Climate Change, First edit, Routledge, London, 2018.

[5] Intergovernmental Panel on Climate Change (IPCC) third assessment report : hearing before the Committee on Commerce, Science, and Transportation, United States Senate, One Hundred Seventh Congress, first session, May 1, 2001., Intergov. Panel Clim. Chang. Third Assess. Rep. Hear. before Comm. Commer. Sci. Transp. United States Senat. One Hundred Seventh Congr. First Sess. May 1, 2001. . (2004). https://heinonline.org/HOL/Page?handle=hein.cbhear/cbhearings71893&id=1&div=&collection=congrec (accessed June 16, 2021).

[6] J. Kerr, Changing Ecosystems: Effects of global warming, Facts on File, Inc., New York, 2010.

[7] N.R. Table, N.R. Table, I. Isbn, P. Downloaded, S.P. Books, S.P. Books, Canada ' s options for a domestic greenhouse gas emissions trading program, 2020.

[8] J.A. Dunne, S.C. Jackson, J. Harte, Greenhouse Effect, Encycl. Biodivers. Second Ed. 4

(2013) 18–32. https://doi.org/10.1016/B978-0-12-384719-5.00068-X.

[9] International Energy Agency (IEA), World Energy Outlook 2019, OECD, 2019. https://doi.org/10.1787/caf32f3b-en.

[10] J. Gibbins, H. Chalmers, Chapter 2. Fossil Power Generation with Carbon Capture and Storage (CCS): Policy Development for Technology Deployment, Carbon Capture. (2010) 41–64. https://doi.org/10.1039/9781847559715-00041.

[11] M. Stewart, K. Arnold, Gas Sweetening and Processing Field Manual, Gas Sweeten. Process. F. Man. (2011).

[12] N. Norahim, P. Yaisanga, K. Faungnawakij, T. Charinpanitkul, C. Klaysom, Recent Membrane Developments for CO2 Separation and Capture, Chem. Eng. Technol. 41 (2018) 211–223. https://doi.org/10.1002/CEAT.201700406.

CHAPTER 2: LITERATURE REVIEW OF POLYMERIC AND MIXED-MATRIX MEMBRANES USED FOR THE SEPARATION OF CARBON DIOXIDE AND NITROGEN AND CARBON DIOXIDE AND METHANE

2.1 ABSTRACT

There has been an increase in the world energy demand over the years and in turn an increase in the demand for fossil fuels. The increased use of fossil fuels over the years has caused an increase in the carbon dioxide (CO_2) being emitted which has, in turn, caused an increase in the greenhouse gases emitted to the atmosphere over the years. In the interest of reducing CO_2 emissions, membranes have been studied for CO_2 capture in post-combustion capture, pre-combustion capture, and oxyfuel combustion. CO_2 separation from methane (CH_4) has also been studied in an attempt to make biogas a viable renewable fuel source. This literature search was done for the separation of CO_2 from flue gases and in particular from N_2 for application in post-combustion CO_2 capture as well as CO_2 separation from CH_4 in natural gas processing plants. The different types of membranes studied were polymeric and mixed-matrix membranes.

With polymeric membranes, the best performing membrane from the literature search presented was the 2-PD/2-ME membrane for CO_2/N_2 separation with a CO_2/N_2 selectivity of 162 and PVA-PAAm with a CO_2/CH_4 selectivity of 58. With the mixed-matrix membranes reviewed, the best performing membrane for CO_2/N_2 and CO_2/CH_4 separation respectively were the 1657/CuZnIF membrane with a CO_2/N_2 selectivity of 200.2 and MOF-76(Y)-30 with a CO_2/CH_4 selectivity of 60.5. Metal Organic Framework containing mixed-matrix membranes were the better performing mixed-matrix membrane type.

Key words: Post-combustion CO_2 capture, CO_2/N_2 separation, CO_2/CH_4 separation, polymeric membranes, mixed-matrix membranes.

2.2 INTRODUCTION

2.2.1 World energy demand

With an increasing world population, the world energy consumption is increasing as well. This consumption is primarily fossil fuel-based. The world population has increased by 77% from 1978 to 2018 and with this, the energy consumption has almost doubled (from 270.5 EJ to 580 EJ) [1]. Most of this energy consumption stems from iron and steel, chemical and petrochemical, non-metallic mineral, non-ferrous metals, transport equipment, machinery, mining and quarrying, food and tobacco, paper, pulp and printing, textile and leather, wood and wood products, and the construction industries. Currently, the main fossil fuel sources used are coal, coal products, natural gas, and oil. The iron and steel industry is the main industrial consumer of these fossil fuels [2].

This upsurge in the energy demand is due to the increase in the world population, since population increase results in production increase within the above-listed industries. Moreover, the continuing economic and industrial growth of developing countries has led to a further increase in energy demands. Therefore, because both the world population and the industrialization of developing countries are projected to increase in the coming years, an increase in the world energy demand is to be expected as well. One way to mitigate the issue is by encouraging or expanding the use of renewable energy sources like wind, solar and nuclear power [3,4].

2.2.2 Greenhouse gas emissions and climate change

Fossil fuels provide more than 80% of the energy consumed in today's world. The production of fossil fuels however leads to the emission of greenhouse gases [4]. Therefore, an increase in the world energy demand will in turn lead to an increase in fossil fuels being burned for energy and consequently to an increase in the greenhouse gases being emitted into the atmosphere. This in turn is leading to the climate change effects being felt in today's world.

One of the major causes of climate change as mentioned above is greenhouse gas emissions. Greenhouse gases receive and distribute earth's radiation. These gases absorb the heat in gas molecules and then re-radiate it back to the earth. This increases earth's surface temperature. Since the gases stay in the atmosphere long after their release, their prolonged re-radiative activity increases the earth's surface temperature for longer than required [5]. The main greenhouse gases in the earth's atmosphere are water vapor (H_2O), carbon dioxide (CO_2), methane (CH_4), nitrous oxide (N_2O), and ozone (O_3). Most of the greenhouse gas emissions leading to the climate change experienced on earth are from CO_2. In fact, the atmospheric CO_2 concentration has increased by 35% since preindustrial times. This has been especially brought about by the emissions from fossil fuel combustion and to a lesser extent by land conversion and cement production [5,6]. This increased global warming poses a huge threat to the agricultural industry but also to most of the other industries from the mining industry to the insurance industry [7–9]. Various international multilateral environmental agreements have been organized to synchronize the reduction of greenhouse gas emissions between international countries such as the Montreal Protocol in 1999 and more recently the Paris agreement of 2015 [10,11].

Although fossil fuels are being phased out in an attempt to use more environmentally friendly energy sources, the International Energy Agency World Energy Outlook predicts that fossil fuels will remain significant for many decades [12]. It is, therefore, necessary to find a way to reduce the net CO_2 emitted into the atmosphere. Carbon Capture and Storage (CCS) is a growing method of doing this where it involves the removal of CO_2 from areas of mass production, such as at a power plant. This is followed by the transport of CO_2 to a safe location for long-term storage [13], which in some case is followed by the Reverse Water Gas Shift (RWGS) reaction and then by the Fischer-Tropsch reaction where the previously stored CO_2 is used to produce a hydrocarbon. This

CO_2 can also be used as a raw material to produce other valuable chemicals and/or permanently stored underground. CO_2 separation from CH_4 has also been studied as a method of lowering the environmental footprint in the process of harnessing energy from the biogas power generating sector [14].

2.2.3 Carbon capture and storage

Carbon capture and storage as discussed above is one of the methods of reducing CO_2 emissions being released into the atmosphere. It is a more effective and cheaper method when implemented on large stationary CO_2 sources. The Intergovernmental Panel on Climate Change (IPCC) assessed the most appropriate targets for CCS as power plants and in particular fossil fuel power plants [15]. There are three main methods of carbon capture currently under investigation: pre-combustion capture, post-combustion capture, and the oxyfuel system. Pre-combustion capture involves partially oxidizing the fuel and then reacting it with steam to form a CO_2 and H_2 mixture which can thereafter be separated. Post-combustion capture involves the separation of CO_2 from flue gases after fuel combustion, where the main component of flue gases is N_2 gas [16]. Oxyfuel combustion involves fuel combustion in an oxygen-rich gas mixture that lacks nitrogen. The flue gases consequently produced from this combustion contain primarily CO_2 as well as easily separated water and other impurities.

Pre-combustion capture has been applied and proven to work at the megatonne-per-year scale but has not been fitted to an operational power plant due to the inability of total continuous operation. Pre-combustion capture is advantageous in that it can be applied to multiple fuels and it prevents CO_2 emissions from ever entering the atmosphere. Conversely, in post-combustion CO_2 gas is separated from flue gases that have already been produced from burning fossil fuels. It is disadvantageous in that the equipment is very large and a lot of utilities are necessary for this

process, however, once installed and running it is easy to upgrade without a fundamental impact on the plant. Oxyfuel combustion on the other hand is disadvantageous in that it requires relatively high operating temperatures as well as the more expensive oxygen-rich combustion gas[17,18]. Both post-combustion and oxyfuel combustions require a unit operation for the separation of CO_2 from syngas. Post-combustion capture technologies however have the highest potential to be retrofitted to traditional pulverized coal power plants compared to the pre-combustion and oxyfuel technologies [19].

Another solution to the increasing energy demand and the need for alternative forms of renewable energy is natural gas, mainly composed of methane. However, natural gas has a high concentration of carbon dioxide among other impurities which need to be removed before natural gas can be used as a viable renewable energy source, through natural gas sweetening. There are also several reasons beyond the direct environmental implications for why these impurities should be removed from the gas as early as possible in the process. Natural gas sweetening and particularly CO_2 removal from CH_4 is necessary as CO_2 lowers the Btu content of natural gas and it makes the natural gas corrosive which prevents the transportation of natural gas [14]. Needless to say, the removal of CO_2 from natural gas also directly reduces the carbon footprint of its combustion. For all of these reasons, a large array of technologies has emerged in the hopes of removing this impurity efficiently. This work, therefore, focuses on CO_2/ CH_4 separation as well as CO_2/ N_2 separation.

2.2.4 Separation technologies

The technologies currently employed in the post-combustion separation of CO_2 from N_2 include absorption, adsorption, and membrane capture methods. Absorption can be both through physical and chemical absorption. The leading technology of industrial gaseous CO_2 capture is by using

liquid amine absorption. However, both solid adsorption and the use of membranes have been explored as valid options. The amine absorption method though popular is disadvantageous because it requires higher energy consumption, more careful operator attention, and solvent regeneration. The use of membranes on the other hand is advantageous in that they are more environmentally friendly and they form a low-energy separation method that requires less space. The most valuable property of these membranes however is their ability to control the rate of permeation of different gases in a mixture [20]. The use of membranes is also more preferred as they are also more easily installed and operated [21].

Some of the technologies currently available for the removal of CO_2 from natural gas include cryogenic distillation, absorption/adsorption, and membrane separation. The latter two options are the most commonly used alternatives [22,23]. Membrane separation has been of great interest in recent years for a number of reasons. When compared to methods such as cryogenic distillation, the energy requirements for membrane separation are significantly lower, and the required equipment is much simpler and more easily maintained. Because this method is capable of running continuously, and maintenance may be as simple as replacing the membranes, it is also less costly in terms of operational downtime. Additionally, the fabrication of membranes can be achieved with materials that are environmentally friendly [22,24,25]. Between the ecological fabrication and lower energy requirements, this method can have a lower carbon footprint overall when compared to other CO_2 separation technologies, while still performing with high efficiency.

2.2.5 CO_2, CH_4 and N_2 properties

The CO_2, CH_4 and N_2 properties that allow for their separation include the kinetic diameter, polarizability and quadrupole moments as shown in Table 2.1. The quadrupole moment of carbon

dioxide is much higher than that of nitrogen and methane and so the polarizability of carbon dioxide is much larger than that of nitrogen and methane [26].

Table 2.1: Summary of important CO_2, CH_4 and N_2 gas properties.

	Property		
Molecule	**Kinetic diameter (Å)**	**Polarizability (Å^3)**	**Quadrupole moment (DÅ)**
CO_2	3.30	2.507	4.30
CH_4	3.80	2.448	0.02
N_2	3.64	1.710	1.54

2.2.6 CO_2 separation through membranes

Membrane separation is a unit operation that uses a semi-permeable material to selectively allow components of a gas or liquid to be separated from other gaseous or liquid constituents. The driving force is pressure as well as the presence of a concentration gradient. Here gaseous or liquid components move from regions of high concentration to those of low concentration. In membrane separations the two products are usually miscible, the separating agent is a semi-permeable barrier, and a sharp separation is often difficult to achieve. Factors considered when working in a gas permeation experiment are: the category of membranes, pore size, and properties of gases used during the experiments. As previously mentioned, there are three major targets for membrane separation for CO_2 capture: the post-combustion separation of CO_2 from the flue gases, CO_2 separation from natural gas, and pre-combustion separation of CO_2 from H_2 [27]. As previously mentioned, this paper will be focusing on the post-combustion separation of CO_2 from flue gases and in particular from nitrogen gas as well as its separation from CH_4 using polymeric and mixed matrix membranes for biogas and natural applications.

2.2.6.1 Membrane performance

The performance of a membrane in the separation of two gases is described by the permeability and selectivity of the membrane in gas separation. Membrane permeability is the ease with which a gaseous or liquid particle is able to pass through a film/membrane. A membrane permeation setup is illustrated as shown in Figure 2.1:

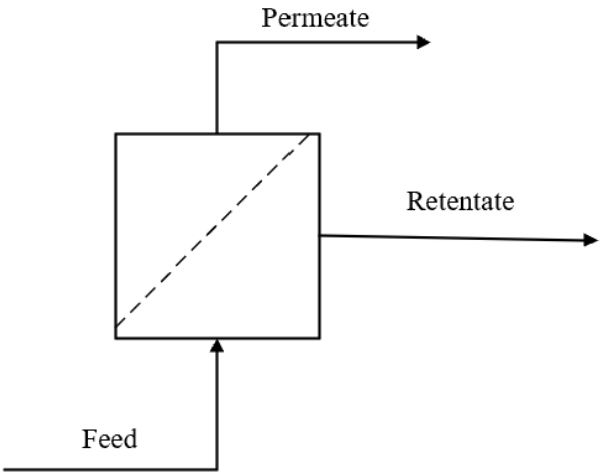

Figure 2.1: Schematic of a membrane separation process

Here a gas feed mixture is fed into the membrane. Some of the gaseous components interact favourably and reversibly with the membrane or are small enough to pass through the membrane's pores; these are termed as permeable and are allowed to permeate through the membrane, exiting as the permeate, whereas the components that do not favourably interact with the membrane exit from the retentate side.

Permeability of a gas in membrane is defined as the sum of the fluxes flowing through the membrane. This flux is presented by Equation (1).

$$N_A = -D_{AB}\frac{\partial c_A}{\partial z} + x_A^*(N_A + N_B) \quad (1)$$

where N_A (mol/cm^2·s) is the molar flux of component A through an area of the membrane, N_B [mol/cm^2·s] is the molar flux of component B, D_{AB} [cm^2/s] is the diffusivity of gas A within the membrane, c_A [mol/cm^3] is the concentration of component A, x_A^* is the mole fraction of A in membrane and z [cm] represents distance in the membrane. Since the mole fraction of A in the membrane is usually very small, this makes the second term in the right hand side of (1), which represents the bulk flow in the membrane, negligible in comparison to the first term in the right hand side of (1), which represents the diffusion term in the membrane. This assumption simplifies Equation (1) into Fick's first law of diffusion shown in Equation (2).

$$J_A = -D_{AB}\frac{\partial c_A}{\partial z} \tag{2}$$

Where J_A (mol/cm^2·s) represents the diffusive flux of component A through the membrane.

The concentration of A, c_A, shown in Equation (3) is expressed as follows:

$$c_A = Sp_A \tag{3}$$

This is substituted into Equation (2) as shown in Equation (4) below:

$$J_A = -D_{AB}S\frac{\partial p_A}{\partial z} \tag{4}$$

Where D_{AB} (mol/cm^3·cmHg) represents the diffusivity of component A in B, p_A (cmHg) is the partial pressure of A and S is the solubility of gas A in the membrane.

The solution-diffusion theory model can also be utilized to characterize membrane permeability. In this model, it is assumed that the gas will dissolve and move through the membrane through

molecular diffusion. The mass transfer of this model can be expressed in terms of permeability P_A of gas A [mol/s·cm·cmHg] as illustrated in Equation (5).

$$P_A = D_{AB}S \tag{5}$$

When this expression of permeability is substituted into Equation (4) and rearranged, Equation (6) can be used to express the permeability of A in terms of the diffusive flux, J_A, the membrane thickness, δ, and the change in partial pressure of gas A, Δp_A.

$$P_A = \frac{J_A \delta}{\Delta p_A} \tag{6}$$

Since the diffusive flux is the volumetric flow rate per area, the substitution shown in Equation (7) can be made for J_A,

$$P_A = \frac{F_A \delta}{\Delta p_A A} \tag{7}$$

where F_A is the volumetric flow rate [cm^3/s] taken at STP conditions and A is the surface area of the membrane[cm^2]. A system not operating at STP conditions must use a modified version of Equation 7 as shown in Equation (8).

$$P_A = F_A \frac{T_{STP}}{T_{feed}} \frac{p_{feed}}{p_{STP}} \frac{\delta}{\Delta p_A A} \tag{8}$$

Where T_{STP} is the temperature of gas at STP conditions [K] and p_{STP} is the pressure of 1 mol of gas at STP conditions [cmHg]. The permeability in the membrane, P_A, is expressed in units of [cm^3(STP)·cm/(s·cm^2·cmHg], whereas they are typically expressed in units of Barrer. The conversion between the 2 units is displayed in Equation (9) [28].

$$1\ Barrer = 10^{-10}\frac{cm^3(STP)\ cm}{cm^2\ s\ cmHg} \quad (9)$$

The permeability of gases is dependent on the solubility, size and diffusivity of the gases.

The membrane selectivity is defined as the preferred permeability of the membrane towards one component over other the other component, calculated from the pure component permeability values. This is calculated using Equation (10) for selectivity of gas A over gas B.

$$\alpha^*_{A/B} = \frac{P_A}{P_B} \quad (10)$$

where $\alpha^*_{A/B}$, is the ideal selectivity of gas A relative to gas B and P_i is the pure component permeability of gas i where i is either A or B [28].

The separation factor for the mixtures can be defined for a 2 component feed system as shown in Equation (11)

$$\alpha_{A/B} = \frac{y_A/y_B}{x_A/x_B} \quad (11)$$

where x_A and x_B are the mole fractions of component A and B in the feed and y_A and y_A are the mole fractions of component A and B in the permeate. $\alpha_{A/B}$ is the separation factor.

Assuming zero stage cut conditions where the stage cut is the permeate's molar flow rate over the feed's molar flow rate, the separation factor can be calculated from the ideal selectivity. This is calculated using Equation (12) [27] below when the permeate and feed pressures are known.

$$\alpha_{A/B} = \alpha^{*}_{A/B}\left(\frac{x_A(\alpha_{A/B} - 1) + 1 - (\frac{p_l}{p_h})\alpha_{A/B}}{x_A(\alpha_{A/B} - 1) + 1 - (\frac{p_l}{p_h})}\right) \quad (12)$$

where x_A is the mole fraction of component A in the feed, $\alpha_{A/B}$ is the separation factor, $\alpha^{*}_{A/B}$ is the ideal selectivity, $p_h$and p_l are the feed and permeate pressures, respectively.

2.2.6.2 Types of membranes used for separation

Membranes used for gaseous separations are categorized based on two properties: the material of construction and the membrane pore sizes. Using the pore size property, membranes can fall into either the mesoporous, microporous, or dense (non-porous) categories. Mesoporous membranes have pore sizes greater than 50 nm and are usually used to separate larger molecules from a solution. Mesoporous membrane pore sizes range from 2 to 50 nm and are mostly used for ultrafiltration processes. Dense (non-porous) membranes have pore sizes of less than 0.3 nm and are commonly used for gaseous separations, nanofiltration and reverse osmosis. Using the material of construction property, membranes can be categorized into organic, inorganic and mixed-matrix membranes. Organic membranes are usually polymeric in nature, made from either natural or synthetic polymers. Natural polymers include wool, rubber and cellulose whereas synthetic polymers are produced by polymerization of a monomer by condensation or addition reactions. On the other hand, inorganic membranes are usually either zeolite type materials or carbon-based and act as molecular sieves. Contrarily, mixed-matrix membranes are hybrid polymeric membranes containing nanomaterials in their polymer matrices [29,30].

The main driving force of the mass transfer through most membranes is the pressure gradient across the membrane. Depending on the properties of the membrane the permeability of the membrane for a particular gas is also determined by the physio-chemical interactions between the diffusing species and the membrane constituents.

2.2.6.3 Organic (polymeric) membranes

Polymeric membranes are polymer-based membranes. The most widely used polymers used to make membranes include polysulfone (PSF), cellulose acetates, (poly(2,6-dimethyl-1,4-phylene oxide)) (PPO), aramids (aromatic polyamides), poly (dimethylsiloxane) (PDMS), polycarbonates, polymers of intrinsic microporosity (PIMs) and polyimide (PI)[31]. These polymeric membranes are further categorized based on their glass transition and melting temperature as either glassy or rubbery. Glassy polymeric membranes are those made from polymers after heating them below their glass transition temperatures, while rubbery membranes are made after heating the membrane-making solution above the glass transition temperature [32]. Rubbery membranes have more flexible polymeric chains compared to glassy polymeric membranes as they have more movement in the composing monomer chains. This higher chain mobility allows the rubbery polymers to form denser layers and therefore smaller pores whereas glassy polymers are better suited to form microporous membranes [33,34]. Rubbery polymers are often characterized by high permeabilities and low selectivities with examples including PDMS, Polyether block amide (PEBAX) and Polyvinyl Alcohol (PVA). Glassy polymers on the other hand have high selectivities and low permeabilities. The most common of these glassy polymers include PSF, Polyethersulfone (PES), Polyethylenimine (PEI), PI and 2,2′-bis(3,4′dicarboxyphenyl) hexafluoropropane dianhydride(6FDA)-2,4,6-trimethyl-1,3-phenylenediamine (TMPDA) 6FDA-TMPDA[31].

The separation performance of polymeric membranes is restricted by the trade-off between selectivity and permeability as illustrated by empirical Robeson's curve defining the upper limit in polymeric membranes [33]. This curve illustrates that with increasing permeability of a membrane comes decreasing separation factor, decreasing selectivity.

Supported liquid membranes (SLM) form a smaller category of polymeric membranes used for separation. They consist of a microporous membrane with an embedded solvent, which does the separation of two or more components. SLM have shown to be the most useful as they combine extraction, diffusion, stripping, and regeneration into one step [35]. They have been researched as a growing alternative to polymeric membranes as they show enhanced gas separation and mechanical stability compared to polymeric membranes [36].

2.2.6.4 Inorganic membranes

Inorganic membranes are usually composed of either zeolites or carbon materials. They have appropriately sized pores for CO_2 separation and capture: in the separation from flue gases, inorganic membranes usually show strong affinities for CO_2 and show selectivity for CO_2 over CH_4 and flue gases like N_2. This is because inorganic membranes are usually amine based and able to interact with the polar CO_2, allowing its separation from non polar gases[30]. Inorganic membranes used for CO_2 capture are categorized based on their pore sizes. Here, there are two main categories: mesoporous membranes with pore sizes between 2-50 nm, and microporous membranes with pore sizes of less than 2 nm. Mesoporous membranes are prepared using amine grafted silicas. Inorganic microporous membranes used for CO_2 capture on the other hand are made up of either amine-functionalized silicas, stabilized silicas, zeolites and metal-organic frameworks (MOFs) or Zeolitic imidazolate framework (ZIFs) membranes [37].

2.2.6.5 Mixed-matrix membranes

Mixed-matrix membranes are defined as a family of hybrid membranes containing nanomaterials in their polymer matrices [38]. These nanomaterials are added to polymeric membranes since although membranes made solely of inorganic nanomaterials exhibit excellent gas transport performances, their scale-up is usually expensive – 150 times higher than polymeric membranes [39]. This is why the inorganic nanomaterials are incorporated into polymeric membranes. Mixed-matrix membranes are considered a viable membrane option over pure polymeric membranes because they preserve the processability of the membrane. Also, when nanomaterials with specific pore sizes are used with high permeability membranes, they can improve the selectivity of these membranes. Moreover, nanomaterials allow for modification of membrane surfaces due to the surface chemistry of nanomaterials. Therefore, by adding nanomaterials to polymeric membranes to make mixed-matrix membranes, their permeabilities and/or selectivities can be improved. The main challenge with mixed-matrix membranes is the non-uniformity in the dispersion of these inorganic nanomaterials which consequently affects the performance of these membranes in the separation of gases. This distribution is affected by the preparation procedure as well as the nanomaterial's surface chemistry, size and the polymer's chemistry and properties including its ability to dissolve the nanomaterial [29].

2.2.7 CO_2/N_2 and CO_2/CH_4 separation conditions

The conditions for post combustion CO_2 capture from N_2 are flue gas exhaust conditions which is feed at 150°C and atmospheric pressure that has about 15% of CO_2 and about 80% of N_2 composition with oxygen. Therefore, membranes that can operate at these conditions would be preferrable for CO_2 capture from N_2 This is because this would ensure the least amount of additional processing of the feed stream before separation [26-28].

About 50% of known natural gas reserves contain more than 2% of CO_2. In the liquid natural gas, the CO_2 concentration should be less than 0.005% per volume [27]. Therefore, membranes that are stable at cryogenic temperatures would be preferred for this CO_2/CH_4 separation.

2.2.8 Membrane defects

It is usually very difficult to develop defect-free membranes and as such it is important to characterize the transport through the defects. There are two methods of transportation through these pores namely: Knudsen flow and viscous flow. Here Knudsen flow describes flow through smaller pores whereas viscous flow describes flow through larger pores. In Knudsen flow the mean free path is grater than the pore diameter whereas for viscous flow, the mean free path is less than the pore diameter. In Knudsen flow there is collision between the permeant and the walls of the membrane and therefore there can be some selectivity with this kind of flow. With viscous flow the main interaction is between the permeating molecules [27].

2.3 ORGANIC (POLYMERIC) MEMBRANES FOR CO_2/N_2 AND CO_2/CH_4 SEPARATION

Commonly used polymeric membranes in CO_2/N_2 and CO_2/CH_4 separation are shown in Table 2.2 and Table 2.3. They have been listed in descending order of CO_2/N_2 selectivity.

Table 2.2: Common polymeric membranes used for CO_2 separation. These membranes are listed in decreasing order of CO_2/N_2 selectivity.

Membrane acronym	Membrane full name
PDMS	Poly(dimethylsiloxane)
PAAm-PVA	Polyallylamine-poly(vinyl alcohol)
PTMEG+PEBAX	Poly(tetramethylene ether) glycol + Polyether block amine
PTMSP	poly[1-(trimethylsilyl)-1-propyne]
PEBA/PSF	Polyether block amide/ polysulfone
PIM-1	Polymers of intrinsic microporosity-1
PIM-7	Polymers of intrinsic microporosity-2
PVA-PEG/PTFE	Poly(vinyl alcohol)- poly(ethylene glycol)/ Polytetrafluoroethylene
Bio-PITB-1	Polyimide incorporating Tröger's Base
Bio-PITB-2	Polyimide incorporating Tröger's Base
2-PD/2-ME	2-pyrrolidone/ 2-methoxyethanol
PEBAX	Polyether block amine
XL-PEGDA	Cross linked poly(ethylene glycil) diacrylate
PIM-CO-19	Polymers of intrinsic microporosity-CO-19
PIM-CO-15	Polymers of intrinsic microporosity-CO-15
TZPIM	Tetrazole-modified polymers of intrinsic microporosity
PEBAX/ PA-PPG	Polyether block amine / Poly(amide-c-poly(propylene glycol))
PVA+amines	Poly vinyl alcohol + formaldehyde + potassium hydroxide+ methanol+ poly (allylamine hydrochloride) + 2-aminoisobutyric acid
PNB-Si(DEt)-Si(OEtOMe)	Polynorborenes with alkoxy silyl pendant

Table 2.3: Permeabilities of common polymeric membranes used for CO_2 separation. These membranes are listed in decreasing order of CO_2/N_2 selectivity.

Membrane	CO_2 permeability (Barrers)	CO_2/CH_4	CO_2/N_2	Temperature (°C)	Feed Pressure absolute (atm)	Reference
PVA+ amines	1800	-	280	150	2	[40]
2-PD/2-ME	9.08×10^6	-	162	57	1.1	[41]
PAAm-PVA	2.4×10^5	58	80	25	1	[43]
$PTMEG_{0.8}$+PEBAX	325	22.5	70	25	15.8	[42]
XL-PEGDA	145	19.86	66	35	2.2	[44]
PVA-PEG/PTFE	1.85×10^7	-	56	30	2	[45]
$PEBAX_{1074}$	120	-	51	35	15	[46]
PEBAX/PA-PPG	79.7	14.0	34.7	25	1	[47]
PEBA/PSF	260	-	32	25	7.8	[48]
TZPIM	3076	24	31	25	-	[49]
PEBAX	150	7.5	29	55	15.8	[42]
PNB-Si(DEt)-Si(OEtOMe)	733.3	-	27.5	35	1	[50]
PIM-7	1100	17.74	26	30	1.3	[51]
PIM-1	2300	18.5	25	30	1.2	[51]
PIM-CO15	2000	15.38	24	30	1.5	[52]
Bio-PITB-2 (air-100)	1161	26	23	35	1	[53]
Bio-PITB-1 (vac)	1123	23	22	35	1	[53]
Bio-PITB-1(vac-100)	1008	25	22	35	1	[53]
Bio-PITB-1 (air-100)	1076	25	22	35	1	[53]
Bio-PITB-2 (vac)	1201	24	22	35	1	[53]
Bio-PITB-2 (vac-100)	1087	27	22	35	1	[53]
Bio-PITB-2 (air)	1384	23	22	35	1	[53]
Bio-PITB-1 (air)	1352	23	21	35	1	[53]
PIM-CO19	6100	10.52	19	30	1.5	[52]
PDMS	3800	28	9.5	35	1	[54]
PTMSP	28010	2.2	5.64	20-25	-	[55]

2.3.1 PVA based membranes

2.3.1.1 PVA + amines

Zou and Ho (2006) designed polymeric membranes made up of PVA but because of the weak mechanical properties of PVA, in order to improve the CO_2 permeability of the membrane as well as the CO_2/N_2 selectivity, formaldehyde was added as the main cross-linker along with potassium hydroxide, methanol, poly (allylamine hydrochloride) and 2-aminoisobutyric acid. Here the amino groups were added to increase the interaction of the membrane with the CO_2 penetrant, thereby allowing more CO_2 permeability through facilitated transport. To test the membrane performances, the gas permeation experiments were carried out between 1.5 atm and 3.0 atm pressure and at 110°C and 150°C. Mixed gas experiments were done with compositions of 17% CO_2, 1.0% CO, 37% N_2 and 45% H_2. Argon was used as a sweep gas with a flow rate of 30 cm^3/min and a specific volume of water was injected into both the sweep and feed gas. The CO_2 permeability was seen to decrease with an increase in feed pressure. The CO_2 permeability was also seen to increase with an increase in the moisture content on the sweep side. The CO_2 permeability and the CO_2/N_2 selectivity were also seen to decrease with an increase in temperature. At 150°C and 2 atm pressure, the maximum CO_2 permeability was obtained to be 1800 Barrer and the CO_2/N_2 selectivity was obtained as 280 [40].

2.3.1.2 PAAm-PVA

PVA membranes have been shown to have high gaseous permeabilities and be mechanically strong [43]. The PAAm portion of the PAAm-PVA membrane was selected because it is an amine-based carrier that has been shown to increase the CO_2 permeability by increasing facilitated transport of CO_2. This is through a reversible reaction of the amino group with CO_2, where PAAm seemed to have a high concentration of such interacting primary amine groups. The PAAm portion of the

membranes makes the membranes brittle when dry because of PAAm's precipitation and coagulation. This is why PVA is added to the PAAm to impart mechanical strength. Also, because both PVA and PAAm are hydrophilic, water is retained within the membrane and more water retention in the membrane has been linked to better permeability performance of hydrophilic based membranes. Mixed binary gas experiments were studied with this membrane with compositions of 20% CO_2 and 80% N_2 and with compositions of 10% CO_2 and 90% CH_4 [43]. With an increase of PAAm content, the gas permeance initially increases up to 10% PAAm composition point and then decreases gradually. 10% PAAm was the best performing membrane for CO_2/N_2 separation, achieving a CO_2 permeance of 2.4×10^5 Barrer with a CO_2/N_2 selectivity of 80 at 0.1MPa. 20% PAAm was the best performing membrane for CO_2/CH_4 separation achieving a CO_2 permeance of 2.6×10^5 Barrer with a CO_2/CH_4 selectivity of 58 at 0.1MPa. The feed gas pressure was also varied from 0.5 MPa to 1.5 MPa in this study and the CO_2/N_2 and CO_2/CH_4 selectivities were seen to decrease with an increase in feed gas pressure. This is because the CO_2 permeance increase was higher than that of CH_4 and N_2 with an increase in feed pressure. There was also an increase in CO_2 permeance with an increase in PAAm concentration up to the 20wt% loading weight where an increase in PAAm decreased the crystallinity of the membrane up to the 20wt%. This established the observed inverse relationship between membrane crystallinity and permeance [43].

2.3.1.3 PVA-PEG/PTFE

PVA membranes cross-linked with glutaraldehyde membranes and cross-linked further with amine rich (poly(ether imine)) dendrimer generations were studied by Kunalan et al (2021) [45]. Poly tetrafluoroethylene was used as the ultrafiltration membrane support. The amine functionalities were chosen to be incorporated in the polymer as they have been shown to result in higher permeabilities and higher selectivities because of their chelation abilities with the electro-deficient

CO_2. Mixed gas experiments were carried out with compositions of 15% CO_2 and 85% N_2. An optimal CO_2 permeability was determined to be 1.85×10^6 Barrer at a feed pressure of 2×10^5 Pa at 30°C. Here the CO_2/N_2 selectivity was determined to be 56. With an increase in feed pressure, the CO_2 permeability increased up to 2×10^5 Pa and above 2.2×10^5 Pa the CO_2 permeability started decreasing. However, the N_2 permeation remained constant. This meant that the optimal pressure for CO_2/N_2 separation was at 2.2×10^5 Pa. Lastly, with an increase in temperature both the CO_2 and the N_2 permeances increased [45].

2.3.2 PDMS

PDMS is a rubbery polymer that is liquid-like. It has been reported as the most permeable rubbery polymer and has been used commercially in many gaseous separation applications. PDMS has also been reported to be more permeable to organic vapors than to supercritical gases. Permeability of gases in the PDMS membranes is defined by the solution-diffusion mechanism. The permeability and selectivity properties of the gases to be separated are trade-off properties described by Robeson's upper limit. The selectivity of PDMS membranes is reported to be mostly governed by a difference in solubility, whilst being a weak function of the size of the penetrating gas. When tested with single gas experiments at 35℃ with a feed pressure of 1 atm, a CO_2 permeability of 3800 Barrer and a CO_2/ N_2 and CO_2/ CH_4 selectivity of 9.5 and 3.2 were obtained respectively[46,56]. Senthilkumar et al (2007) also reported PDMS membranes with a CO_2 permeability of 200 Barrer and CO_2/N_2 selectivity of 34.2 when single gas experiments were carried out [31,57].

The permeability of both the gases was directly proportional to the pressure difference Δp, (the difference between the feed and the permeate pressure) and with an increase in this pressure difference, there was an increase in permeability of the penetrant. The addition of a PDMS-PEG

50% quantity to PEBAX 1657 block copolymer has been shown to increase the CO_2 permeability by a factor of 5 [58].

2.3.3 2-PD/2-ME

Thin-film composite (TFC) membranes with added amines were studied by Pang et al. (2020) [41] and in particular, a mixed solvent comprising 2-PD and 2-ME was used to prepare polyethersulfone (PES) substrate membranes which were thereafter used for gas separations. TFC membranes usually comprise of a dense top layer that is mainly responsible for the separation and a porous substrate layer that provides major mechanical support. PES was the substrate layer with 2-PD/ 2-ME as the dense top layer. TFC membranes were chosen due to the low CO_2 concentration and the limited transmembrane driving force associated with flue gases. There was an increase in CO_2 permeance with the addition of 2-ME due to the increased pore size and therefore porosity. There was also an increase in CO_2 permeance with the increase in the 2-PD/2-ME weight ratio to the PES substrate. Mixed gas experiments were used to test the permeability with a gas mixture containing 20% CO_2 and 80% N_2 with Argon as the sweep gas. With a 2-ME/2-PD ratio of 1.5, the optimized membrane was able to show the highest CO_2 permeance of 9.08×10^6 Barrer with a CO_2/N_2 selectivity of 162 [41].

2.3.4 PEBAX based membranes

Pebax is a block copolymer (thermoplastic elastomer) that consists of two segments: a polyamide hard segment and a polyether soft segment. The polyamide hard segment imparts high mechanical strength for the membrane for stability purposes whereas the softer polyether allows high permeation through its flexible chains. Pebax has been modified with a variety of other polymers to be better suited for the separation of gases[42].

2.3.4.1 PTMEG+PEBAX

In the study done by Rabiee et al. (2015) [42], PTMEG was added to $Pebax_{1657}$ because of the higher diffusion, solubility and permeability imparted by the less rigid structure of the PTMEG. This is because PTMEG is of low molecular weight and with low molecular weight comes more free fractional volume and reduction in membrane crystallinity. With an increase in PTMEG concentration, there was an increase in CO_2 permeability and a decrease in CO_2/N_2 and CO_2/CH_4 selectivity was observed. 20%, 40%, 60% and 80% PTMEG were tested. Single pure gas permeation tests were performed. The pure $Pebax_{1657}$ membrane had a permeability of 100 Barrer with a CO_2/N_2 selectivity of 80 and CO_2/CH_4 selectivity of 15 at 4 bar at room temperature. With an increase in PTMEG percentage to the highest tested value of 80%, the $Pebax_{1657}$ +$PTMEG_{0.8}$ had an increased CO_2 permeability of 225 with a decreased CO_2/N_2 selectivity of 65 and a CO_2/CH_4 selectivity of 15. For a higher pressure of 16 bar the pure $Pebax_{1657}$ membrane had a higher CO_2 permeability of 150 Barrer with a higher CO_2/N_2 and CO_2/CH_4 selectivity of 85 and 17.5, respectively. With an increase in PTMEG to 80% at the same 16 bar pressure, the $Pebax_{1657}$ +$PTMEG_{0.8}$ had a further increased CO_2 permeability of 325 with a slightly decreased CO_2/N_2 selectivity of 70 and an increased CO_2/CH_4 selectivity of 22.5.

A temperature study was also carried out. With an increase in temperature, the CO_2 permeability was increased and the CO_2/N_2 selectivity was decreased for both the pure $Pebax_{1657}$ membrane and the $Pebax_{1657}$ +$PTMEG_{0.8}$ membrane. As previously mentioned, the pure $Pebax_{1657}$ membrane had a permeability of 100 Barrer with a CO_2/N_2 selectivity of 80 and CO_2/CH_4 selectivity of 15 at 4 bar and at room temperature (25°C). With an increase in PTMEG to the highest tested 80%, the $Pebax_{1657}$ +$PTMEG_{0.8}$ had an increased CO_2 permeability of 225 with a decreased CO_2/N_2 selectivity of 65 and CO_2/CH_4 selectivity of 14. When a higher temperature of 55°C was tested,

the pure $Pebax_{1657}$ membrane had a lower CO_2 permeability of 175 Barrer with a lower CO_2/N_2 and CO_2/CH_4 selectivity of 28 and 7.5 respectively. With an increase in PTMEG percentage to 80% at the same temperature (55°C), the $Pebax_{1657}$ +$PTMEG_{0.8}$ had an increased CO_2 permeability of 325 with a slightly increased CO_2/N_2 and CO_2/CH_4 selectivity of 35 and 12 respectively. Therefore, with an increase in temperature and pressure, the CO_2/N_2 and CO_2/CH_4 selectivities were decreased and increased, respectively. A decrease in CO_2/N_2 and CO_2/CH_4 selectivity was also observed with an increase in PTMEG concentration from 0% to 80% [42].

2.3.4.2 PEBAX+PEG-DME

In this case, oligomers of poly (ethylene) glycol dimethyl ether (PEG-DME) are added to Pebax to increase CO_2, N_2 permeability while maintaining CO_2/N_2 selectivity. This was done because although Pebax is very permeable, the CO_2 permeability increases with higher Pebax content. When the Pebax content is increased, however, it increases the chances of crystallization due to the longer Pebax chains that are able to be formed. This is why PEG-DME is considered as an option to increase CO_2, N_2 permeability while maintaining CO_2/N_2 selectivity since it acts as a plasticizer. Five different loading weights: 10%, 20% 30%, 40% and 50% PEG-DME were studied by Huang et al and Yave et al using single pure gas permeability tests [61,62]. The CO_2/N_2 selectivity is generally constant and then decreases after 30wt% loading when tested at 303K. The glass transition temperature of the membrane initially increases then decreases with loading weight. With 50% weight percent of PEG-DME to Pebax, a CO_2 permeability of 606 Barrer was identified with a CO_2/N_2 selectivity of 44. With 30% weight percent of PEG-DME to Pebax, a CO_2 permeability of 300 Barrer was identified with a CO_2/N_2 selectivity of 46 [61,62].

2.3.4.3 PEBA/PSF

PEBA is a copolymer consisting of a hard polyamide segment and a soft polyether segment. PEBA was chosen as a potential membrane for gaseous separations due to the high permeability it showed for polar gases. This is because of the strong affinity of the polar gases to the polyether block. For the separation of CO_2 from N_2, the fact that CO_2 is polar whereas N_2 is not means that CO_2 will be more selectively permeable than N_2. This PEBA/PSF membrane was tested by Liu et al. (2014) [48] at different temperatures and pressures using single gas permeability tests. There was an increase in both CO_2 and N_2 permeability with an increase in temperature where the three temperatures tested were 25°C, 40°C, and 60°C. There was also an increase in just the permeability of CO_2 with an increase in pressure where the pressure range tested was from 25 psig to 200 psig. This is because of the plasticization of the membrane by CO_2 with an increase in pressure. A CO_2 permeability of 260 Barrer was obtained and a CO_2/N_2 selectivity of 32 was obtained at 25°C and 100 psig [48].

2.3.4.4 PEBAX/PA-PPG

Zhu et al. (2019) [47] designed PEBAX/PA-PPG through a polycondensation reaction where these copolymers were blended to up to 60% with commercially available $Pebax_{2533}$ and the blended membranes were then tested with CO_2 and N_2 within a 25°C-55°C temperature range at an atmospheric feed pressure. The best results were obtained with a 50%-60% $Pebax_{2533}$/PA-PPG blend at 25°C. The CO_2 permeability under these conditions was 79.7 Barrer with a CO_2/N_2 selectivity of 34.7 and a CO_2/CH_4 selectivity of 14.0. The pure $Pebax_{2533}$ membrane without any PA-PPG had a CO_2 permeability of 226 Barrer with a CO_2/N_2 selectivity of 25.1 and a CO_2/CH_4 selectivity of 6.7. The PA-PPG blend was shown to increase the CO_2/N_2 and CO_2/CH_4 selectivity because of the bulky fluorine group in the blend as well as the CO_2-philic ether group. There was

a decrease in both CO_2 and N_2 permeabilities with an increase in $Pebax_{2533}$/PA-PPG concentration, also an increase in CO_2/N_2 selectivity. An optimally functioning membrane was obtained at 50%-60% $Pebax_{2533}$/PA-PPG blend. Overall, however, there was a decrease in CO_2/N_2 and CO_2/CH_4 selectivities with an increase in temperature [47].

2.3.5 PTMSP

PTMSP is known as one of the most permeable glassy polymeric membranes and has been tested for different gas separation applications. This membrane has been shown to have high gas permeabilities with lower selectivities. The higher gas permeabilities are reported to be due to the high excess free volume in the PTMSP polymer. For the particular study done by Nakagawa et al (1987) [55], pure single gas experiments were done. These experiments were done with pure PTMSP and PTMSP with a dioctyl phthalate (DOP) additive. It was found that there was a direct relationship between the DOP additive and CO_2/N_2 selectivity and an inverse relationship with the CO_2/CH_4 selectivity. The addition of DOP greatly reduced the permeability of all gases. The CO_2 permeability for pure PTMSP was identified as 28010 Barrer and the CO_2/N_2 and CO_2/CH_4 selectivities were identified to be 5.64 and 2.2, respectively at room temperature. With the addition of 3.4% of DOP, the CO_2 permeability was identified as 1336 Barrer and the CO_2/N_2 and CO_2/CH_4 selectivities were identified as 12.59 and 7.2, respectively at room temperature [55].

2.3.6 PIM

Polymers of intrinsic microporosity are often formed through polycondensation of aromatic tetrahydroxy and tetrahalogented monomers. Consequently, they have a rigid backbone structure containing spirocenters, which disrupts the efficient chain-packing and leads to higher polymer-free fractional volume and therefore higher gas permeabilities. PIMs are also soluble in organic solvents enabling their good processability for membrane fabrication. Because of these properties,

they have improved solubility which reduces the trade-off effect between permeability and selectivity seen in membranes [59].

PIM-1 and PIM-7 combined the high permeability and selectivity properties through the increased stiffness of the polymers from the increased interchain spacing. PIM-1, therefore, showed a high CO_2 permeability of 2300 Barrer with CO_2/N_2 and CO_2/CH_4 selectivities of 25 and 18 respectively, at 30°C and approximately atmospheric feed pressure. PIM-7 on the other hand showed a CO_2 permeability of 1100 Barrer with CO_2/N_2 and CO_2/CH_4 selectivities of 26 and 17, respectively under the same conditions [51]. Another version of this PIM-1 membrane has been shown to have a CO_2 permeability of 3464 Barrer with a CO_2/N_2 selectivity of 23[63]. PIM-1 is, therefore, better for the CO_2/N_2 separation and PIM-7 is better for the CO_2/CH_4 separation,

PIMs have been functionalized with polar groups to further improve the CO_2 permeability and the CO_2/N_2 selectivity. PIM-CO15 when compared to PIM-1 has additional oxygen atoms in the spirobischromane moiety resulting in higher CO_2 solubility and higher CO_2 permeability. CO_2-philic pendant tetrazole groups have also been added to PIMs to increase CO_2 selectivity over N_2 because N-containing tetrazole groups have an affinity towards CO_2 through Lewis acid-base interactions but not N_2. Among the modified PIMs, the one with the highest CO_2 permeability is PIM-EA-TB with a permeability of 7140 Barrer and the one with the highest CO_2/N_2 selectivity is TZPIM-2 with a CO_2/N_2 selectivity of 31 [49,52,59].

2.3.7 Bio-PITB

Thermally rearranged polymers have shown outstanding gas transport behavior resulting in improved permeabilities [53]. Tröger's base (TB) polymers are made by incorporating highly stiff moieties into polymers to improve membrane rigidity. TB polymerization is easily realized

through polymerization using functionalized diamines or by polyimidization using ready-made TB containing monomers. Additionally, Bio PITBs showed diffusion selectivity as the permeabilities followed the order of kinetic diameters for all gases except for CO_2. Bio PITB-1 and Bio PITB-2 are synthesized from a lignin by-product. These synthesized membranes were dried in either vacuum conditions, at 120°C for 24 hours or under atmospheric conditions. Some of the synthesized membranes were tested right after their synthesis while others were tested 100 days after synthesis. Single pure gas permeation tests were carried out. A summary of the results obtained was shown in Table 2.3. The membrane with the highest permeability for CO_2 was Bio PITB-2 membrane dried in room temperature conditions and tested right after synthesis. The membrane with the highest CO_2/N_2 selectivity was the Bio PITB-2 membrane dried in room temperature conditions and tested 100 days after synthesis. The membrane with the highest CO_2/CH_4 selectivity was the Bio PITB-2 membrane dried in a vacuum and tested 100 days after synthesis. The membranes dried in room temperature conditions had higher CO_2 permeabilities compared to those dried in vacuum. Bio PITB-2 membranes had slightly higher CO_2 permeabilities compared to Bio PITB-1 membranes. The 100-day waiting time between synthesis and testing for the membranes resulted in lower permeabilities for CO_2 [53].

2.3.8 XL-PEGDA

Increasing the ether oxygen in polymers has been shown to increase the CO_2/N_2 selectivity[44,59]. To prevent PEO from crystallizing when long PEO chains are used in the making of polymeric membranes, cross-linked Poly (ethylene glycol) diacrylate (PEGDA) is used. Single pure gas permeation tests were done: using these membranes, a CO_2 permeability of 110 Barrer with a CO_2/N_2 selectivity of 50 was achieved. The membranes showed an increase in gas permeabilities with an increase in feed pressure. The N_2 permeability decreased with a decrease in XL-PEGDA

concentration while the CO_2 concentration increased. The CO_2/N_2 selectivity was optimized at 20% XL-PEGDA concentration. At 35°C and 2.2 atm, a CO_2 permeability of 145 Barrer with a CO_2/N_2 selectivity of 66 was observed [44,59].

2.3.9 PNB-Si(OEt)-Si(OEtOMe)

Polynorbornene membranes constitute polymerized norbornenes, which are bridged cyclic hydrocarbons. These membranes are glassy polymeric membranes with alkoxy silyl groups added to increase the gas permeabilities of the membranes due to the low gas permeabilities of polynorbornenes. With an increase in the concentration of the alkoxy silyl component, the CO_2 permeability is seen to decrease for PNB-Si(OEt)-Si(OEtOMe) with the CO_2/N_2 selectivity first increasing then decreasing. An optimum CO_2/N_2 selectivity of 27.5 was obtained at an equal concentration of PNB-Si(OEt) and the Si(OEtOMe) components. The CO_2 permeability at this equal PNB-Si(OEt)-Si(OEtOMe) ratio was obtained to be 733.3 Barrer [50].

2.3.10 Overview of polymeric membrane materials for CO_2/N_2 and CO_2/CH_4 separation

Different polymeric membranes have been used in the literature for the separation of CO_2 from N_2 and CH_4. The membrane that had the highest CO_2 permeability is the PVA-PEG/PTFE membrane with a permeability of 1.85×10^7 Barrer. Alternatively, the membrane that had the highest CO_2/N_2 selectivity was the PVA+ amines membrane where a selectivity of 280 was obtained. The membrane that had the highest CO_2/CH_4 selectivity was the PAAm-PVA membrane where a selectivity of 58 was obtained.

When the separation factors of the best performing membranes were analyzed assuming zero-stage cut condition, the performance of the membranes decreased dramatically with the PVA+amines membrane CO_2/N_2 having a separation factor of 2.5 at 150°C and 2 atmosphere. The

same occurred for the PVA-PEG/PTFE membrane whose CO_2/N_2 separation factor was equal to about 2.3 at 30°C and 2 atmospheres. It is also important to note that although these membranes did perform well they had an active layer thickness above 1µm, the cut off for the industrially used thin film membranes and when making thinner membranes there is usually introduction of defects [26]. Here, the thicknesses of the PVA+ amines membrane were between 20µm- 80µm, the thickness of the PVA-PEG/PTFE membrane was about 10µm. and the thickness of the PAAm-PVA membrane was about 3µm. Taking all this into consideration and based on the ideal selectivity and permeabilities reported, the best performing membrane from the literature search presented is the PAAm-PVA membrane with a CO_2 permeability of 2.4×10^5 Barrer and a CO_2/N_2 and CO_2/CH_4 selectivity of 80 and 58, respectively. PVA membranes also generally showed good performance with high permeabilities and high selectivities.

2.4 MIXED-MATRIX MEMBRANES FOR CO_2/N_2 SEPARATION

Mixed-matrix membranes can be subdivided into different categories depending on the membrane filler material. Namely, these are: zeolite filler membranes, metallic organic frameworks, carbon-based fillers, silica-based and other fillers. Table 2.4 outlines zeolite-filled membranes and metal organic framework filled membranes that are used for CO_2/N_2 separation.

Table 2.4: Common mixed-matrix membranes for CO_2/N_2 separation and their acronyms used

Type of mixed-matrix membranes	Membrane acronym	Membrane full name
Zeolite filled membranes	$[Cu(6L)]^{2+}$@13X(15wt%)	Schiff base macrocyclic copper complex in the FAU super-cages of zeolite 13X.
	PES/PDMS/SAPO-34	30 wt% Small pore size zeolite (SAPO-34) in PES matrix with PDMS coating
	PEBA-zeolite 13X	1 wt% zeolite 13X in PEBA matrix
	Mn-ZSM-5	Manganese impregnated Zeolite Socony Mobil–5
	PDMS/zeolite 4A/ PAN 15A%	15 wt% zeolite 4A in Polydimethylsiloxane matrix on Polyacrylonitrile support
	P8FAU-NH_2	1 wt% NH_2-functionalized faujasite in poly (ether block amide) matrix
	PU-Z12	12 wt% zeolite 4A in polyurethane matrix
	PES +SAPO-34	% Small pore size zeolite (SAPO-34) in Polyethersulfone matrix
Metal Organic Framework filled membranes	PG-PN40	40 wt% NOTT-300 (metal-hydroxyl-functionalized porous solid) in poly (ether block amide) matrix under pure gas conditions
	MG-PN40	40 wt% NOTT-300 (metal-hydroxyl-functionalized porous solid) in poly (ether block amide) matrix under mixed gas conditions
	MOF-76(Y)-30	Metal Organic Framework of Yttrium and 1,3,4-benzene-tricarboxylate
	1657/CuZnIF	Copper zinc bimetallic imidazolate framework in poly (ether block amide) matrix
	ZIF0302/d-PI	Zeolitic imidazolate framework-302 in a dense PI matrix

(Table 2.4 continuation)		
Type of mixed-matrix membranes	**Membrane acronym**	**Membrane full name**
Metal Organic Framework filled membranes	UiO-66-PEBA	Zirconium-based Metal Organic Framework (Uio-66) poly (ether block amide)
	UiO-66-PEBA-NH_2	Zirconium-based Metal Organic Framework (Uio-66) poly (ether block amide)-NH_2
	PIMs with P-NPs	Polymer of Intrinsic Microporosity with pearl necklace nanoparticles
	PVAm+ PANI@CNTs GO	Polyvinylamine + Polyaniline-coated carbon nanotubes in graphene oxide
	Polyetheramine M2070 + Pebax 1657	polyetheramine (M2070)-carbon nanotubes + Pebax1657
	UiO-66 + Al_2O_3	Zirconium-based Metal Organic Framework (Uio-66) + Al_2O_3
	Pebax + ZIF-8	Pebax+ ZIF-8 (Basolite® Z1200)
	Pebax + ZIF-67	Pebax+ ZIF- 67 (Basolite® Z1200)
	PIM-1+ MUF-15	Polymer of Intrinsic Microporosity-1 + (Massey University Framework-15)
	PDXLA +MOP-3	poly(1,3 dioxolane) acrylate + metal-organic polyhedron-3
	Ppy nanospheres with mesoporous shells + Pebax1657	Polypyrrole nanospheres with mesoporous shells + Pebax1657
	PIM-Py-X	Anion filled Pyridine-based Polymers of Intrinsic Microporosity

The permeabilities of the listed membranes in Table 2.4 at specific temperatures and pressures are shown in Table 2.5.

Table 2.5: Mixed Matrix membranes studied in the literature for CO_2/N_2 separation and their permeabilities and selectivities at specified conditions.

Membrane	CO_2 permeability (Barrer)	N_2 permeability (Barrer)	CO_2/N_2	Temperature (°C)	Pressure (atm)	Reference
$[Cu(6L)]^{2+}$@13X(15wt%)	1034.1	8.8	117	25	2	[64]
1657/CuZnIF	190.52	1.0	200.2	30	13.8	[65]
PVAm+ PANI@CNTs GO	2.6×10^{6}	1.7×10^{4}	149.8	25	1	[66]
P8FAU-NH_2	122	1.0	117	25	11.8	[67]
Pebax + ZIF-67	162.0	2.0	81.0	35	10.9	[68]
Polyetheramine M2070 + Pebax 1657	332	4.611	72	25	1	[69]
PIM-Py-X	6205	99.3	62.5	-	-	[70]
PDXLA +MOP-3	580	9.4	62	35	-	[71]
PG-PN40	395	6.5	61.2	25	9.9	[24]
Pebax + ZIF-8	117.9	2.0	59.0	35	10.9	[68]
MG-PN40	356	6.1	58.4	25	9.9	[24]
MOF-76(Y)-30	27.3	0.5	58	25	-	[72]
PEBA-zeolite 13X	194.1	3.4	56.5	25	13.8	[73]
Mn-ZSM-5	134.3	2.6	51.7	25	-	[74]
Ppy nanospheres with mesoporous shells + Pebax1657	274	6.8	40.1	35	2	[75]
Uio-66 + Al_2O_3	1.1×10^{8}	3.6×10^{6}	31.3	-	-	[76]
PIM-1+ MUF-15	3.7×10^{4}	1451.4	25.5	20	1	[77]
PDMS/zeolite 4A/ PAN 15A%	1.2×10^{4}	508.4	23.8	25	3.0	[78]
PU-Z12	81.6	3.5	23.6	25	10	[79]
ZIF0302/d-PI	0.1	6.2×10^{-3}	16.1	35	4.0	[80]
PIMs with P-NPs	1.5×10^{4}	1013.3	15	35	1	[22]
PES/PDMS/SAPO-34	2.9×10^{4}	2.3×10^{3}	12.5	25	19.7	[81]
PES +SAPO-34	6.4×10^{6}	5.2×10^{5}	12.5	25	19.7	[81]
UiO-66-PEBA	139.7	60.7	2.3	25	3.0	[82]
Uio-66-PEBA-NH_2	130.2	72.2	1.8	25	3.0	[82]

2.4.1 Zeolite filled membranes for CO_2/N_2 separation

2.4.1.1 $[Cu(6L)]^{2+}$@13X(15wt%)

$[Cu(6L)]^{2+}$@13X membranes were prepared by encapsulating Schiff base macrocyclic copper complexes in the FAU super-cages of zeolite 13X [64]. Metal ion complexes that have macrocyclic ligands are promising membrane components due to their tunable properties attributed to the substituents design. Their properties are influenced by both the type of coordinated ligands in their complexes and the metal ions. Zeolite 13X was chosen as the filler due to its high promise for CO_2/N_2 seperation. With an increase in the zeolite loading from 5% to 20%, there was an increase in the CO_2 permeability and the CO_2/N_2 selectivity with an optimal performing membrane at a 15% zeolite 13X loading. At 15wt% loading of zeolite 13X, the CO_2 permeability was 1034.1 Barrer with a CO_2/N_2 selectivity of 38.3 at 25°C at 2 atm – which was a 96% increase from the pure 6FDA-duferne membrane with a CO_2 permeability and a CO_2/N_2 selectivity of 455.2 Barrer and 15.4, respectively. Higher amounts of filler loading, above 15wt%, led to undesirable molecular transport through the membrane which further led to the decreased CO_2/N_2 selectivity [64].

2.4.1.2 PES/PDMS/SAPO-34

PES/ PDMS/ SAPO-34 membranes consist of a PES component, PDMS and SAPO-34 component. The PES glassy polymer component was chosen due to its high glass transition temperature and good mechanical stability. PDMS is a rubbery polymer component that was selected due to its high gas permeability and its good adhesion with fillers; it however has a low selectivity for CO_2. SAPO-34 was therefore added to the PES/ PDMS blend to improve the CO_2 gas permeation [81]. SAPO-34-filled membranes possess high selectivity for CO_2 because of their pore size of 3.8 nm. An increase in SAPO-34 loading caused an increase in permeability for all gases without a

significant difference in the mixed matrix membrane's CO_2 selectivity. The mixed matrix membrane blend PES/PDMS/SAPO-34 displayed an optimum CO_2 permeability of 2.89×10^4 Barrer and a CO_2/N_2 selectivity of 12.45 at 25℃ and 19.7 atm [81].

2.4.1.3 PEBA-zeolite 13X

Asghari et al. (2018) [73] have designed polyether block amide (PEBA) membranes incorporated with zeolite 13X deposited onto a Polysulfone/ Polyester (PSf/ PE) layer. Zeolite 13X was selected as the filler due to its preferential selectivity for CO_2 when used as an adsorbent for CO_2 in flue gas separation [83]. PE was used as one of the layers for its mechanical advantage as a support layer. PSf was the hydrophobic second layer chosen to increase the permeability of the gases due to its hydrophobicity. PEBA was used due to its superior gas separation properties, particularly those favoring CO_2 separation. The mixed matrix membrane blend PEBA-zeolite 13X displayed an optimum CO_2 permeability of 194.12 Barrer and a CO_2/N_2 selectivity of 56.5 at 25℃ and 13.8 atm [73].

2.4.1.4 Mn-ZSM-5

Rostamizadeh et al. (2020) [74] designed mixed matrix membranes using fillers made of transition metal oxides based on manganese (Mn) modifier agents in ZSM-5 nanoparticles. PEBA was impregnated with these ZSM-5 loaded with manganese at various loading weight percentages. PEBA + Mn-ZSM-5 mixed matrix membrane with a Mn-ZSM-5 loading of 9wt% was able to increase the permeability of the membrane for CO_2 by 44%. The mixed matrix membrane blend PEBA with a 59wt% loading of Mn-ZSM-5 displayed an optimum CO_2 permeability of 134.3 Barrer and a CO_2/N_2 selectivity of 51.7 [74].

2.4.1.5 PDMS/zeolite 4A/ PAN 15A%

PDMS/ zeolite 4A/ PAN 15% was a mixed matrix thin film composite membrane (MMTFCM) [78]. The membrane was made from a mixed matrix membrane PDMS/ zeolite 4A mix coated on a polyacrylonitrile ultrafiltration membrane. The performance of MMTFCM is dependent on the thickness of the membranes where thinner membranes have higher gas permeances and are therefore more commercially advantageous. Zeolite 4A was chosen as a filler in the MMTFCM because they have a unique cage-like structure with an average diameter of 11.2 Angstroms and an effective pore diameter of 3.8 Angstroms allowing separation of CO_2 from N_2. A 15wt% loading of the PDMS/ zeolite 4A had an optimal performance for the separation of CO_2 from N_2. The mixed matrix membrane blend PAN with a 15wt% loading of PDMS/zeolite 4A displayed an optimum CO_2 permeability of 12099.5 Barrer and a CO_2/N_2 selectivity of 23.8 at 25°C and 3 atm [78].

2.4.1.6 P8FAU-NH_2

These mixed matrix membranes were prepared through zeolite faujasite (FAU) embedded with NH_2 (amine) which was chosen due to the selectivity it has shown for CO_2. The filler FAU-NH_2 was embedded on the PEBA chain. While it was observed that increasing the particle loading of FAU, increased CO_2 permeability; an optimum performance was observed with a 1 wt% amine loading. The mixed matrix membrane blend PEBA with a 1wt% loading of P8FAU-NH_2 displayed an optimum CO_2 permeability of 122 Barrer and a CO_2/N_2 selectivity of 117 at 25°C and 12 atm [67].

2.4.1.7 PU-Z12

PU-Z12 mixed matrix membranes were made from polyurethane (PU) embedded with zeolite 4A at different zeolite contents of 6wt%, 12 wt%, 18wt% and 24wt%. PU-Z12 with a 12 wt% zeolite

4A weight content was the best performing membrane of the different percentages tested in terms of CO_2 permeability and selectivity. The mixed matrix membrane blend PU with a 12wt% loading of zeolite 4A displayed an optimum CO_2 permeability of 81.63 Barrer and a CO_2/N_2 selectivity of 23.6 at 25°C and 10 atm [79].

2.4.1.8 PES +SAPO-34

The PES +SAPO-34 membrane was prepared through the phase-inversion method (Haider et al., 2020) [81]. This membrane was prepared using different SAPO-34 concentrations. At 20 bar and 25°C and with a SAPO-34 concentration of 30%, this membrane was seen to have a CO_2 permeability of 6.4×10^6 Barrer and a CO_2/N_2 selectivity of 12.45. An increase in the permeability of CO_2 was observed up to 30 % SAPO-34. The CO_2/N_2 selectivity was seen to increase up to 20% SAPO-34 and decrease thereafter [81].

2.4.2 Metal organic framework filled membranes for CO_2/N_2 separation

2.4.2.1 MOF-81/PIM-1

Chen et al. (2020) [84] studied Metal Organic Framework (MOF-81) microporous filler in PIM-1 microporous polymer matrix. MOF-81 was selected due to its microporous structure which provided fast channel for gas transportation through the increased free fractional volume. MOF-81 is also CO_2-philic and has a strong adsorption capacity for CO_2 because of the interaction between the hydroxyl group in the MOF-81/PIM-1 and its Zr clusters. After 90 days of aging, the CO_2 permeability of this mixed matrix membrane remained above 70% showing its good anti-aging performance. MOF-81/PIM-1 displayed a CO_2 permeability of 9686 Barrer and a CO_2/N_2 selectivity of 27 at 35°C and 4 atm [84].

2.4.2.2 PEBA-8h

This mixed matrix membrane PEBA-8h was prepared by Cheng et al. (2020) [85] through zeolitic imidazolate framework (Zn/Co-ZIF) nanoparticles which were carbonized and then loaded into Pebax 1657 copolymer. Zn/Co-ZIF had a large BET surface area and good porosity which reduced its gas transfer resistance, and therefore increased gas permeability. PEBA-8h displayed a CO_2 permeability of 102.5 Barrer and a CO_2/N_2 selectivity of 52.1 at 35°C and 4 atm [85].

2.4.2.3 PEBA-2533/ZIF-8 (35%)

Zeolitic imidazolate framework-8 (ZIF-8) is an inorganic filler used with PEBAX-2533 polymer matrix. ZIF-8 was chosen because of its high thermal and chemical stability and its selectivity for CO_2. The membrane was tested for gas permeability in both dry and humid conditions. The permeability of the membrane for CO_2 increased with an increase in ZIF-8 loading in both dry and humid conditions. There was an increase in gas permeability of all the gases with an increase in pressure as well from 2 bar to 6 bar. The mixed matrix membrane blend PEBA-2533/ZIF-8 with a 35wt% loading of ZIF-8 displayed an optimum CO_2 permeability of 1287 Barrer and a CO_2/N_2 selectivity of 32.3 at room temperature at 2 atm [86].

2.4.2.4 10% Zn $(pyrz)_2(SIF_6)$

This mixed matrix membrane was made by Gong et al. (2015) [87] using Zn $(pyrz)_2(SIF_6)$ metal-organic framework filler embedded in cross-linked polyetehene oxide (XLPEO). Zn $(pyrz)_2(SIF_6)$ is a MOF with square grids of zinc and pyrazine pillared by hexafluorosillicate (SIF_6^{2-}) anions. Together they formed one-dimensional channels with a 3.8 Angstrom diagonal diameter which allows them to be good candidates for fillers used in membranes used for the separation of CO_2 from flue gas. The mixed matrix membrane blend XLPEO + Zn $(pyrz)_2(SIF_6)$ with a 10wt%

loading of Zn (pyrz)$_2$(SIF_6) displayed an optimum CO_2 permeability of 670 Barrer and a CO_2/N_2 selectivity of 29 at 25°C at 1 atm [87].

2.4.2.5 PG-PN40 and MG-PN40

Mixed matrix membranes in this paper (Habib et al., 2020) [24] were prepared by combining MOF NOTT-300 filler and Pebax 1657. They were then tested in pure gas conditions (PG-PN40) and mixed gas conditions in exposure to methane, carbon dioxide and nitrogen (MG-PN40). NOTT-300 is an inexpensive and energy-efficient MOF reported from The University of Nottingham which was chosen because of its selectivity for CO_2 as shown by researchers from this university. An increase in filler loading of the NOTT-300 increased the free fractional volume of the membrane and decreased its glass transition temperature. Higher permeabilities were noted when tested in pure gas conditions compared to mixed gas conditions. PG-PN40 displayed a CO_2 permeability of 395 Barrer and a CO_2/N_2 selectivity of 61.2 at 25°C and 10 atm whereas MG-PN40 displayed a CO_2 permeability of 356 Barrer and a CO_2/N_2 selectivity of 58.36 under the same conditions [24].

2.4.2.6 MOF-76(Y)-30

Bano et al. (2020) [72] prepared a mixed matrix membrane by incorporating MOF-76 yttrium nanocrystals into Matrimind 5218. MOF-76 has a metal center of Yttrium (Y^{+3}) which is a group 3 member with a large ionic radius facilitating the formation of stable 3D networks. Increasing MOF-76(Y) in the Matrimind polymer matrix increases the performance of the matrix by decreasing the activation energies of the membranes. This increase in the MOF-76(Y) in the membrane matrix increases the permeability of the membrane for CO_2 and the CO_2/N_2 selectivity. MOF-76(Y)-30 with a 30wt% loading of MOF-76(Y) displayed an optimum CO_2 permeability of 27.29 Barrer and a CO_2/N_2 selectivity of 58 at 25°C and 10 bar operating pressure [72].

2.4.2.7 1657/CuZnIF

This study prepared mixed matrix membranes by embedding copper-zinc imidazolate framework particles (CuZnIF) in Pebax 1657 matrix [65]. Different weight percentages of the CuZnIF were added to this Pebax 1657 matrix in the range of 0.1wt% to 10wt%. There was increased CO_2 permeability with the increased concentration of the CuZnIF in the membrane matrix up to a loading of 1 wt% of CuZnIF. This showed the existence of interaction between CuZnIF and CO_2 molecules. Kardani et al. (2020) [65] also noted an increase in the CO_2 permeability of these membranes with an increase in the feed pressure. 1657/CuZnIF with a 1wt% loading of CuZnIF displayed an optimum CO_2 permeability of 190.52 Barrer and a CO_2/N_2 selectivity of 200.18 at 30°C and 13.8 atm [65].

2.4.2.8 ZIF0302/d-PI

Ghanem et al. (2020) [80] reported mixed matrix membranes made by incorporating Zeolitic Imidazolate Framework (ZIF-302) in a polyimide matrix (PI). ZIFs have been researched as potential fillers in the preparation of membranes used for the post-combustion separation of CO_2 as they reduce the overall density of the membrane, making the membranes more permeable while increasing the membrane selectivity for CO_2. The selectivity is increased by modifying the active dipole site with a nitrogen atom in the membranes that use ZIF-302 as fillers. The additional nitrogen enhances the thermodynamic affinity of CO_2 to the membrane thus increasing its selectivity for CO_2. ZIF-302 increased the CO_2/N_2 selectivity of the membrane 19 times compared to that of pure PI [80].

2.4.2.9 UiO-66-PEBA, UiO-66-PEBA-NH_2

UiO-66 is a new class of Zirconium-based porous Metal Organic Frameworks. Two versions of this membrane were made: Uio-66-PEBA and UiO-66-PEBA-NH_2. The membrane was tested in

both dry and humid conditions where the humid condition's relative humidity was 85%. The results obtained for the CO_2 permeability and the CO_2/N_2 selectivity by Shen et al. (2016) at 3 atm feed pressure and 25°C are summarized in Table 2.6 [82].

Table 2.6: CO_2 permeability and selectivity values for pure PEBA, Uio-66-PEBA and UiO-66-PEBA-NH_2 membranes tested in both dry and humid states [82].

Membrane Type	Dry State CO_2 permeability (Barrer)	CO_2/N_2 selectivity	Humid State CO_2 permeability (Barrer)	CO_2/N_2 selectivity
Pure PEBA	51.5	42.1	71.6	43.2
UiO-66-PEBA	96.3	56.6	139.7	61.1
UiO-66-PEBA-NH_2	87.0	66.1	130.2	72.2

There was increased CO_2 permeability and CO_2/N_2 selectivity for all the humid state membranes compared to the dry state membranes. This is because water vapour facilitated the transport of *CO_2*. Also, the incorporation of the MOF to the pure PEBA increased the CO_2 permeability and the CO_2/N_2 selectivity due to the enhanced polymer-MOF interaction. A further increase in CO_2 permeability and the CO_2/N_2 selectivity was seen with the UiO-66-PEBA-NH_2 membrane also because of the CO_2-philic effect of the amino-functionalized group [82].

2.4.2.10 PIMs with P-NPs

Pearl necklace nanoparticles were chosen as they are MOF membranes that are used for gas separations because of the gas permeance sizes of 0.3 nm to 0.5 nm, and the ease in incorporating MOFs into polymer matrices. The nanoparticles are pearl- necklace-shaped because particles with anisotropy tend to form a linked structure in a composite material. At 1 atm and 35°C and with a P-NP concentration of 50%, this membrane was seen to have an optimal CO_2 permeability of 1.52×10^4 Barrer and a CO_2/N_2 selectivity of 15. The formation of voids between polymer and

nanoparticles or within nanoparticles aggregates causes an increase in permeability with an increase in CO_2/N_2 selectivity through the formation of new gas permeable space [22].

2.4.2.11 PVAm + PANI@CNTs-GO

These membranes were prepared by coating a mixed dispersion of polyaniline-coated carbon nanotubes in graphene oxide layers on a polyvinylamine support. The graphene oxide layers are used to regulate interlayer spacing. 1wt% PANI@CNTs-GO showed the best carbon dioxide separation performance with a CO_2 permeance of 2.6×10^6 Barrer with a CO_2/N_2 selectivity of 122.4 at 1 atm and 25°C [66]. This was an increase in both the permeability and selectivity of pure PVAm. The improved transport of CO_2 was attributed to the amine groups, the facilitated transport carriers. CO_2 permeance was seen to decrease with an increase in feed pressure from 1 bar to 5 bar because of a decrease in the number of facilitated transport carriers. With an increase in temperature from 25°C to 80°C, both the CO_2 permeance and CO_2/N_2 selectivity decreased [66].

2.4.2.12 Polyetheramine M2070, Pebax 1657

Polyetheramine (M2070) – carbon nanotubes have been incorporated into the Pebax-1657 polymeric matrix. The functional NH groups of polyetheramine improved CO_2 permeability and CO_2/N_2 selectivity by 442% and 77% respectively. The CO_2 permeability and CO_2/N_2 selectivity at 25°C and 1 atm were determined to be 332 Barrer and 72, respectively [69].

2.4.2.13 UiO-66 + Al_2O_3

Zirconium-based membranes have attracted widespread attention due to their highly tailorable pore aperture and adsorption behaviour caused by functional group decoration. These functional groups are further attributed with good thermal and chemical stabilities under harsh conditions. The study prepared porous α-Al_2O_3 hollow polycrystalline UiO-66 through a solvothermal process

[76]. The high CO_2/N_2 selectivity was attributed to the high affinity between CO_2 and the hydroxylated Zr_6 cluster in UiO-66 framework. The CO_2/N_2 selectivity was higher with this membrane compared to other polycrystalline MOF membranes. The CO_2 permeability and CO_2/N_2 selectivity was determined to be 1.124×10^8 Barrer and 31.3 respectively [76].

2.4.2.14 Pebax + ZIF-8 and Pebax +ZIF-67

Zeolitic Imidazolate Frameworks (ZIFs) are a family of MOFs with a zeolite topology in which the metal clusters are reconnected by imidazole linkers. They have large diameter cages with narrow pores in the range of CO_2's kinetic diameter. ZIF-8 has a framework of a Zn(II) metal center bridged to N_2. For ZIF-67, the Zn metal center is replaced by Cobalt. When both of the membrane types were tested, with an increase in ZIF content there was an increase in the free fractional volume of the membrane and therefore an increase in the permeability of the membranes[68]. An increase in CO_2/N_2 selectivity was also noted with an increase in ZIF-67 content. The CO_2 permeability and CO_2/N_2 selectivity at 35°C and 10.86 atm for the Pebax+ZIF-8 was determined to be 117.9 Barrer and 1.998, respectively. Whereas the CO_2 permeability and CO_2/N_2 selectivity at 35°C and 10.86 atm for the Pebax+ZIF-67 was determined to be 162.0 Barrer and 2.0, respectively [68].

2.4.2.15 PIM-1+ MUF-15

MUF-15 was chosen as a filler in this membrane as it had shown promise with previous membranes even with low loadings of about 2%-5% by weight. MUF-15 enhances CO_2 separation because of the porosity enhancement in the PIM-1+MUF-15 membrane polymer matrix and the discriminating effect of the MUF-15 filler. A 2% loading of MUF-15 showed 155% higher CO_2 permeability with a CO_2/N_2 selectivity of 25.5 [77]. The incorporation of MUF-15 also prevented the aging-related performance degradation of PIM-1. The CO_2 permeability and CO_2/N_2 selectivity

at 20°C and 1 atm for the PIM-1 + MUF-15 were determined to be 3.701×10^4 Barrer and 25.5, respectively [77].

2.4.2.16 PDXLA +MOP-3

Metal-organic polyhedron (MOP-3) with a particle size of about 5 nm was dispersed in poly(1,3 dioxolane acrylate) (PDXLA). Liu et al. (2020) [71] chose MOP as a metal-organic framework type because of the variety of pore sizes and the structural diversity. As the weight percent of the incorporated MOP-3 increased from 0%-30%, the CO_2 permeability increased from 190 Barrer to 580 Barrer and CO_2/N_2 selectivity decreased from 70 to 62 at 35°C. The CO_2 permeability and CO_2/N_2 selectivity at 35°C for the PDXLA+ MOP-30% were determined to be 580 Barrer and 62, respectively [71].

2.4.2.17 PPy nanospheres with mesoporous shells + Pebax1657

Polypyrrole (PPy) nanospheres with mesoporous shells have been synthesized through chemical oxidation polymerization of pyrrole using silica mesosphere as templates[75]. These PPy nanospheres were incorporated into Pebax 1657 at 1% weight loading of the PPy. The mixed matrix membranes had a CO_2 permeability of 274 Barrer – more than double the permeability of a pure Pebax 1657 membrane. The CO_2 permeability and CO_2/N_2 selectivity at 35°C and 2 atm for the PPy nanospheres with mesoporous shells + Pebax1657 were determined to be 274 Barrer and 40.1, respectively. 1% was the optimum amount of loading for a high CO_2 permeability [75].

2.4.2.18 PIM-Py-X

Porous Ionic Polymers (PIPs) have shown highly selective CO_2 adsorption and compatibility with PIM-1 matrix. More significantly, the PIM-Py-X mixed matrix membranes efficiently facilitated transport, especially of CO_2 across the membrane. Different anion fillers were tested including

acetate anion (Ac^-), BF_4^- and Cl^-. Of these anions, PIM-Py-Ac is the most efficient at CO_2 separation. Among the anion fillers, the effectiveness in CO_2 separation in accordance of the most effective is: PIM-Py-Ac-15 followed by PIM-Py-BF_4-15 then PIM-Py-Cl-15 followed by just PIM-1. The CO_2 permeability and CO_2/N_2 selectivity for the PIM-Py-Ac-15 were determined to be 6205 Barrer and 62.5, respectively [70].

2.4.3 Summary of mixed-matrix membranes for CO_2/N_2 separation

After studying many different mixed-matrix membranes, the one that had the highest permeability for CO_2 was found to be the Uio-66 + Al_2O_3 with a permeability of 1.1×10^8 Barrer. The membrane with the highest CO_2/N_2 selectivity was the 1657/CuZnIF membrane with a selectivity of 200.2. Because pure gas permeation tests were done it was not possible to analyze the separation factor of the membrane. Considering only the ideal selectivities and permeabilities the best performing mixed-matrix membrane from this study was the PVAm+PANI@CNTsGO membrane with a permeability of 2.6×10^6 Barrer and a selectivity of 149.8. This membrane also had a thickness of 900 nm, characteristic of thin film membranes. This also means that the membrane would not need to be reconfigured in order for it to be used industrially. Metal Organic Framework filled membranes were also generally better performing with higher CO_2/N_2 selectivities than zeolite filled membranes.

2.5 MIXED-MATRIX MEMBRANES FOR CO_2/CH_4 SEPARATION

Mixed-matrix membranes can be subdivided into different categories depending on the membrane filler material. Namely, these are: zeolite filler membranes, metallic organic frameworks, carbon-based fillers, silica-based and other fillers. Table 2.7 and 2.8 outline the results obtained with zeolite-filled membranes and metal organic framework filled membranes that are used for CO_2/CH_4 separation.

Table 2.7: Common mixed-matrix membranes for CO_2/CH_4 separation and their acronyms

Types of mixed-matrix membranes	Membrane acronym	Membrane full name
Zeolite filled membranes	$[Cu(6L)]^{2+}$@13X(15wt%)	Schiff base macrocyclic copper complex in the FAU super-cages of zeolite 13X.
	PES/PDMS/SAPO-34	30 wt% Small pore size zeolite (SAPO-34) in PES matrix with PDMS coating
	PEBA-zeolite 13X	1 wt% zeolite 13X in PEBA matrix
	Mn-ZSM-5	Manganese impregnated Zeolite Socony Mobil–5
	PDMS/zeolite 4A/ PAN 15A%	15 wt% zeolite 4A in Polydimethylsiloxane matrix on Polyacrylonitrile support
	P8FAU-NH_2	1 wt% NH_2-functionalized faujasite in poly (ether block amide) matrix
	P8FAU-SO_3	1 wt% SO_3-functionalized faujasite in poly (ether block amide) matrix
	PU-Z12	12 wt% zeolite 4A in polyurethane matrix
	PSu-Clino-BHPA	BHPA-modified clinoptilolite-type natural zeolite in PSu matrix
Metal Organic Framework filled membranes	PEBA- 8h	Zn/Co-ZIF carbonized at 600 °C for 8 hours in PEBA matrix
	PEBA-2533/ZIF-8	35 wt% ZIF-8 in PEBA matrix
	Zn(pyrz)2(SiF6)	Square grids of Zn and pyrazine pillared by hexafluorosilicate (SiF_6^{2-}) anions which form one-dimensional channels having a 3.8 Å diagonal dimension
	MG-PN40	40 wt% NOTT-300 in PEBA matrix under mixed gas conditions
	MOF-76(Y)-30	30 WT% MOF composed of Yttrium and 1,3,4-benzene-tricarboxylate in Matrimid matrix
	1657/CuZnIF	copper zinc bimetallic imidazolate framework in PEBA matrix
	PG-PN40	40 wt% NOTT-300 (metal-hydroxyl-functionalized porous solid) in poly (ether block amide) matrix under pure gas conditions
	ZIF0302/d-PI	Zeolitic imidazolate framework-302 in a dense PI matrix

Table 2.8: Mixed Matrix membranes studied in the literature for CO_2/N_2 separation and their permeabilities and selectivities at specified conditions

Membrane	CO_2 permeability (Barrer)	CO_2 /CH_4	Temperature (°C)	Pressure (atm)	Reference
$[Cu(6L)]^{2+}$@13X(15wt%)	1034.1	42.2	-	2	[64]
PES/PDMS/SAPO-34	2.9×10^4	4.5	25	20	[88]
PEBA-zeolite 13X	194.1	56	25	14	[73]
Mn-ZSM-5	134.3	33.6	-	-	[74]
PDMS/zeolite 4A/ PAN 15A%	1.2×10^4	8.2	25	3	[89]
P8FAU-SO_3	110	31	35	12	[67]
PU-Z12	81.6	7.4	25	10	[79]
PSu-Clino-BHPA	22.8	22.8	35	3.5	[90]
PEBA- 8h	102.5	16.4	25	9.9	[91]
PEBA-2533/ZIF-8	1287	9	ambient	2	[86]
Zn(pyrz)2(SiF6)	620	27	25	1	[87]
MG-PN40	340	33.24	25	10	[92]
MOF-76(Y)-30	27.3	60.5	25	-	[72]
1657/CuZnIF	190.5	56.9	30	14	[93]
PG-PN40	395	36.3	25	10	[92]
ZIF0302/d-PI	0.1	31.2	35	4.1	[80]

2.5.1 Zeolite filled membranes for CO_2/CH_4 separation.

Zeolites are among the most commonly used materials for fillers in MMMs. This is due to their combination of high performance and low cost, as well as their sub-nanometer pores, resistance to CO_2-induced plasticization, and superior selectivity for CO_2 over CH_4 compared to many polymeric membranes [94]. The term "zeolite" encompasses a wide range of different materials, having been derived from the Greek words for "boiling stone". These materials are generally aluminosilicates with distinctive rigid structures that feature many channels and cavities [95]. This cage-like structure contributes to the ability of most zeolites to provide a molecular sieving effect, which often results in increased selectivity for MMMs. In addition to this, many zeolites interact favourably with CO_2, increasing its overall solubility in the membrane. The latter effect was observed in the study by Alavi et al. (2017) [89] which examined the incorporation of zeolite 4A

into a PDMS matrix. The polar hydroxyl groups of the zeolite 4A interacted with the quadrupole moments of CO_2 to improve CO_2 adsorption in the membrane. Additionally, the zeolite particles acted to reinforce the structure of the membrane in order to reduce compaction at higher pressures, which allowed a higher permeability to be maintained at such conditions. The results of incorporating 15 wt.% zeolite 4A into the membrane at a pressure of 3 bar yield a CO_2 permeability of 12099.5 Barrer, and CO_2/CH_4 selectivity of 8.2 [89].

Alternatively, the incorporation of zeolite particles may be used to alter the structure of a membrane, as seen in the study completed by Asghari et al. (2018) [96], which employed zeolite 13X as a filler for PEBA-based membranes. The incorporation of the nano-zeolite particles into the membrane served to improve its sorption capacity by increasing the fractional free volume. Additional improvement was achieved through the use of a protective PDMS layer which plugged pinhole defects, thereby increasing the selectivity of the membrane. The results of this synthesis were a promising CO_2 permeability of 194.12 Barrer, as well as CO_2/CH_4 selectivity of 56 [96]. A similar structural modification was employed in the research conducted by Haider et al. (2020), which looked at the incorporation of SAPO-34 zeolite particles into a PES membrane with a PDMS coating [88]. While the selectivity of the membrane did not change significantly with the filler loading, the addition of SAPO-34 particles increased the fractional free volume of the MMM, resulting in higher permeabilities for both gases. The PDMS coating somewhat decreased these permeabilities but increased the selectivity due to its interactions with CO_2. The final product from this paper had a CO_2 permeability of 28879.65 Barrer (converted from a permeance of 641.77 GPU) and CO_2/CH_4 selectivity of 4.45.

If the zeolite particles do not have significant polar properties on their own, another solution lies in their functionalization or the incorporation of other molecules. Such an alteration was done by

Rostamizadeh et al. (2020) in their study of MMMs produced with ZSM-5 as a filler for a PEBA polymer matrix [74]. In addition to the pure ZSM-5, alternatives were also examined in the form of ZSM-5 that had been impregnated by manganese (Mn), iron (Fe), and phosphorus (P). The SEM images of the untreated and impregnated filler can be seen in Figure 2.2**.** The results from this research show that all of the modified membranes, except for those with phosphorus, exhibited better gas separation performance than the original PEBA membranes. The improved performance of the modified membranes was attributed to three major factors, the first of which being that the ZSM-5 mesopores were penetrated by the polymer chains, resulting in narrower pores. For the samples which included the Mn and Fe particles, improvements were due to the dealumination phenomenon caused by the impregnation in addition to the ability of CO_2 to interact with the polar surface of the ZSM-5 nanoparticles. The impregnation had certain drawbacks, however, and resulted in the negation of some of the effects from the ZSM-5. In the cases of Mn and Fe, the effects from the dealumination phenomenon were enough to counteract this, but the same was not the case for the phosphorus containing sample. The highest-performing MMM in their study was the 9% Mn-ZSM-5 membrane, which showed an increase in the permeability of CO_2 by 97% (to 134.3 Barrer) when compared to the plain PEBA. Additionally, the CO_2/CH_4 selectivity was increased from 20.7 to 33.6.

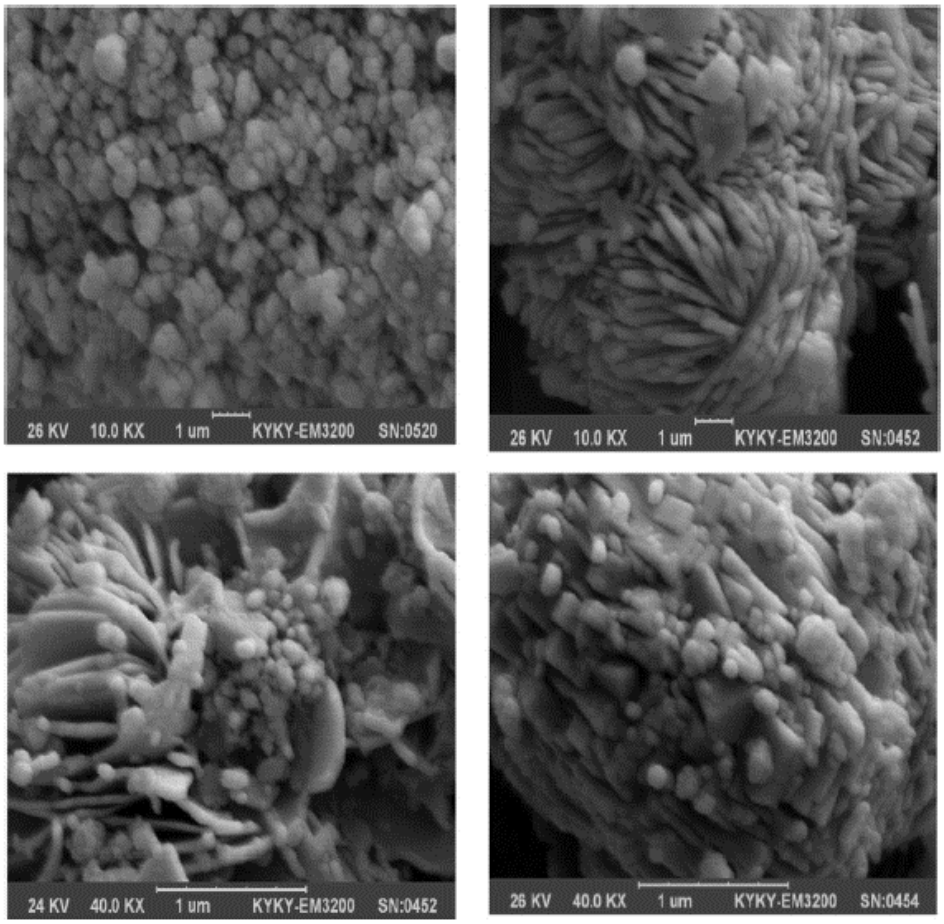

Figure 2.2: SEM images of the parent and the impregnated nanoparticles, (top left: ZSM-5, top right: Fe-ZSM-5, bottom left: P-ZSM-5, and bottom right: Mn-ZSM [74].

A summary of the performance of all zeolite-based MMMs examined in this review can be seen in Table 2.8. From this, it is evident that zeolites are promising materials for use as filler in MMMs. The mechanisms by which they are able to improve the gas separation performance of a membrane are diverse, which allows for the combination of various techniques in order to achieve an impressive final result. It should be noted that, while some of these MMMs succeeded in surpassing the Robeson's Upper Bound, their selectivities were still quite low (this was offset by extremely high permeabilities). When choosing a membrane for any given application, the specific requirements of that application should still be considered. In some cases, a membrane that fails

to surpass the upper bound by a small amount but has moderately high permeability and selectivity may be preferable to one which surpasses the bound with low selectivity.

2.5.2 Metal organic framework filled membranes for CO_2/CH_4 separation.

MOFs are rapidly becoming one of the most highly researched categories of filler for MMMs. These compounds are composed of metal ion centres that are linked by multidentate organic ligands [72,86]. The generally high performance of these materials as fillers in MMMs is attributed to their high surface area and adsorption capacity, excellent chemical and thermal properties, and the ability to tailor their pore size. Some MOFs may also increase the wetting between the filler and polymer matrix of a membrane, allowing for better interaction between these two phases [97]. Unfortunately, these materials also come at a higher cost than many of the other types of fillers, so their performance must be exceptional in order to justify their use on a large scale.

One category of MOFs, zeolitic imidazolate frameworks (ZIFs), is characterized by the structural similarity of its members to zeolites. The work of Cheng et al. (2020) [91].employs the use of Zn/Co-ZIF fillers in a PEBA matrix. The fillers were tested in their original state in addition to samples that had been carbonized at 600 °C for various lengths of time. SEM images of these particles after various carbonization times can be seen in Figure 2.3. The carbonization process altered the structure of the filler, reducing the particle size. The addition of the untreated filler drastically improved the permeability of the membrane by increasing the fractional free volume. This effect was reduced as the nanoparticles were broken down and became smaller with increasing carbonization time. Making up for this, however, is the improved CO_2 solubility that was achieved with increasing carbonization time, leading to higher selectivities for the MMM. The results of this study are that the MMM created with the untreated filler (PEBA-0H) had the highest CO_2 permeability (145.6 Barrer), while its selectivity remained very close to that of pure PEBA.

The best overall results were from the PEBA-8H sample (carbonization for 8 hours), which had a CO_2 permeability of 102.5 Barrer, and CO_2/CH_4 selectivity of 16.4 [91].

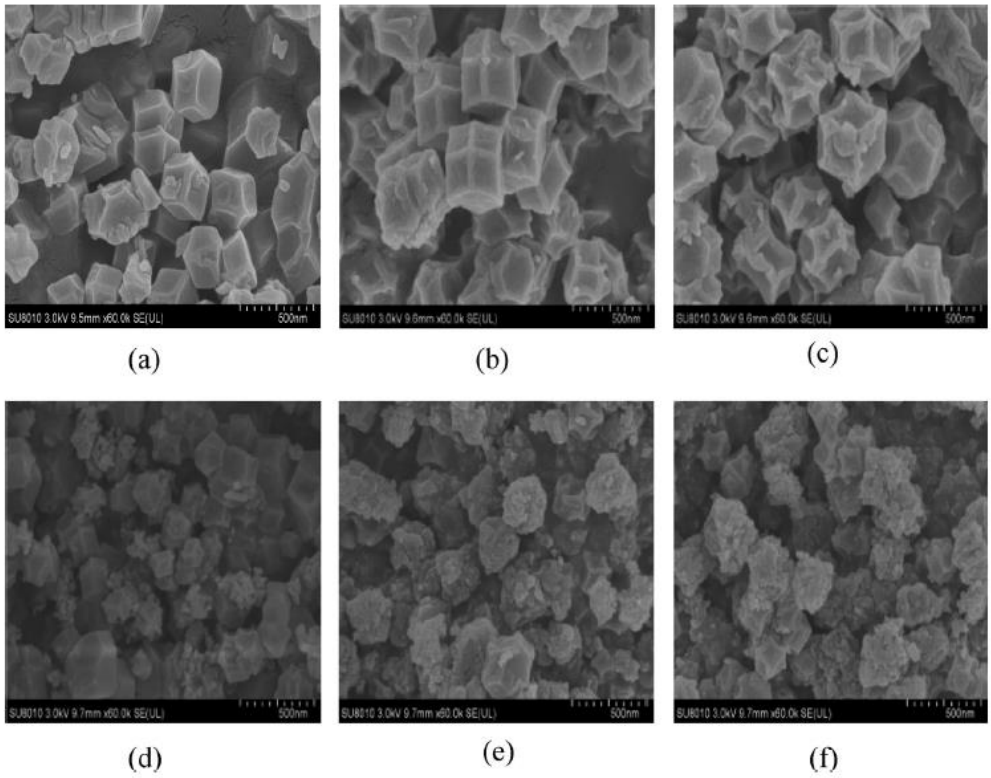

Figure 2.3: SEM images of Zn/Co-ZIF carbonized at 600 °C for different durations: (a) Zn/Co-ZIF, (b) C-ZIF-2H, (c) C-ZIF-4H, (d) C-ZIF-8H, (e) C-ZIF-12H, and (f) C-ZIF-24H [98].

The study by Nafisi and Hägg (2014) [86] also explored a PEBA-based membrane with a ZIF filler. In this case, ZIF-8 was used, and the MMMs that were produced were tested with both pure and mixed gases in dry and humidified conditions. While the permeability did increase with the introduction of the filler, possibly due to the disruption of chain packing which allowed for easier diffusion through the membrane, the selectivity did not increase as expected. The inorganic base layer was originally intended to increase selectivity based on its high CO_2 sorption capacity, but the opposite effect was observed to some degree, possibly owing to the porous structure of the filler or the relative thinning of the polymer-based layer as the filler loading was increased [86].

In their study, Gong et al. (2015) [87] explored the use of $Zn(pyrz)_2(SiF_6)$ crystals in an MMM with crosslinked PEO as the polymer matrix. The $Zn(pyrz)_2(SiF_6)$ filler consists of square grids of zinc and pyrazine that are pillared by hexafluorosilicate (SiF_6^{2-}) anions, creating one-dimensional channels that allowed for the mechanism of size exclusion to increase the selectivity of the membrane. The filler further improved selectivity due to its selective adsorption of CO_2. The crosslinked PEO maintained a high chain mobility which inhibited the formation of interfacial gaps between the polymer and filler. Both bulk and submicron crystals of $Zn(pyrz)_2(SiF_6)$ were tested in this study and while the submicron crystals demonstrated a somewhat lower CO_2 uptake when compared to the bulk crystals, their overall performance was higher than that of the MMMs containing bulk $Zn(pyrz)_2(SiF_6)$ crystals. The tests in this study were conducted with gas mixtures, with a measured CO_2 permeability of 620 Barrer in the CO_2/CH_4 mix. The CO_2/CH_4 selectivity for the membranes using a 10 wt% loading of the submicron particles was 27 [87].

Habib et al. (2020) [99] made use of a novel MOF that had been developed at Nottingham University, NOTT-300. NOTT-300 showed promise as a filler in MMMs due to its chemical stability, high uptake capacity, and exceptional abilities to capture harmful gases such as CO_2 and sulphur dioxide (SO_2). The MOF was incorporated into a polymeric matrix of PEBA and tested with both pure and mixed gases. The addition of the filler resulted in improved permeability by way of increased fractional free volume as well as a high affinity of NOTT-300 for CO_2. The latter also served to improve the selectivity of the MMM. While the overall measurements for permeability and selectivity were higher in the case of pure gases when compared to mixed gases, as expected, the relative increases in performance of the MMM compared to a pure PEBA membrane were almost identical, regardless of the gas composition. The permeability for the MMM showed a 354-380% increase, while the CO_2/CH_4 selectivity increased by around 70%

when compared to the value for the pure polymeric membrane. Under pure gas conditions, the CO_2 permeability was 395 Barrer, and the CO_2/CH_4 selectivity was 36.3 [24].

The work by Bano et al. (2020) [72] explores the use of a lanthanide-based MOF in the form of MOF-76(Y), which has yttrium (Y) acting as its metal centre. The large ionic radius of yttrium results in a high coordination demand, which in turn leads to a high coordination number and better connectivity so that stable 3D structures may be formed. The polymer matrix used in this case was Matrimid, which has polar sites that improved performance through their interactions with CO_2, leading to high CO_2 condensability. It was observed that increasing filler loading resulted in higher permeance and selectivity due to the transport pathways that are created by the MOF as well as its molecular sieving effects. The results of their experiments showed a CO_2 permeability of 27.29 Barrer and CO_2/CH_4 selectivity of 60.5 when converted from a relative performance increase of 67% from the pure polymeric membrane [72].

Overall, the use of MOFs as fillers in MMM has proven to be highly promising. The results for gas permeation tests from all of the MOF-related papers that were examined for this review can be seen in Table 2.8. While some compositions did not necessarily yield the expected results, it can be seen that further treatment of the filler particles, by way of heat treatment or functionalization, for example, can be employed to increase the performance of MMMs that would otherwise be subject to the permeability-selectivity trade-off or simply underwhelming results. Despite their relatively higher cost when compared to many other possible inorganic fillers, the continued improvement of MOF performance in MMMs lends credence to the idea that their performance improvements could offset the additional cost.

2.5.3 Summary of mixed-matrix membranes for CO_2/CH_4 separation

After studying the different types of zeolites based and metal organic framework based mixed matrix membranes used for CO_2/CH_4 separation zeolitic based membranes were seen to be slightly better performing than MOF- based membranes. Because pure gas permeation tests were done, it was not possible to analyze the separation factor of the membrane. Considering only the ideal selectivities and permeabilities the best performing zeolitic membrane studied was $[Cu(6L)]^{2+}$@13X(15wt%) which had a CO_2 permeability and CO_2/CH_4 selectivity of 1034.1 Barrer and 42.2, respectively[64]. This membrane was also constructed to have a thickness between 60 nm to 80 nm characteristic of thin film membranes. This also means that this membrane would not need to be reconfigured into a thinner membrane, leading to an increase in membrane defects. On the other hand, the best performing MOF-based membrane was 1657/CuZnIF which had a CO_2 permeability and CO_2/CH_4 selectivity of 190.5 Barrer and 56.9, respectively[93].

2.6 NOMENCLATURE

A	Area of membrane (cm^2)
Barrer	10^{-10} cm^3(STP)cm/scm^2cmHg
F_i	Volumetric flow rate of component i at STP conditions (cm^3/s)
P_i	Permeability of the membrane for component i where i can be either CO_2, CH_4 or N_2 (Barrer)
p_{STP}	Pressure of 1 mol of gas at STP, 760cmHg was used (cmHg)
p_{feed}	Pressure of feed gas (psi)
p_h	Pressure of feed (psi)
p_l	Pressure of permeate (psi)
T_{STP}	Temperature of 1 mol of gas at STP conditions, 273.15K was used (Kelvin)
T_{feed}	Temperature of feed gas (Kelvin)

2.7 GREEK SYMBOLS

$\alpha^*_{A/B}$	Ideal selectivity based on pure component data (dimensionless)
$\alpha_{A/B}$	Separation factor (dimensionless)
Δp	Pressure difference measured at feed and permeate side (psi)

2.8 ABBREVIATIONS

Abbreviation	Definition
$[Cu(6L)]^{2+}$@13X(15wt%)	Schiff base macrocyclic copper complex in the FAU super-cages of zeolite 13X.
1657/CuZnIF	Copper zinc bimetallic imidazolate framework in poly (ether block amide) matrix
2-PD/2-ME	2-pyrrolidone/ 2-methoxyethanol
AIBA	2-Aminoisobutyric acid, also referred to as F
Bio-PITB-1	Polyimide incorporating Tröger's Base
Bio-PITB-1	Polyimide incorporating Tröger's Base
Bio-PITB-2	Polyimide incorporating Tröger's Base
Btu	British Thermal Unit
CCS	Carbon Capture and Storage
FTIR	Fourier Transform Infrared
IPCC	Intergovernmental Panel on Climate Change
MG-PN40	40 wt% NOTT-300 (metal-hydroxyl-functionalized porous solid) in poly (ether block amide) matrix under mixed gas conditions
Mn-ZSM-5	Manganese impregnated Zeolite Socony Mobil–5
MOF	Metal Organic Framework
MOF-76(Y)-30	Metal Organic Framework of Yttrium and 1,3,4-benzene-tricarboxylate
P8FAU-NH_2	1 wt% NH_2-functionalized faujasite in poly (ether block amide) matrix
PAAm-PVA	Polyallylamine-poly(vinyl alcohol)
PDMS	Poly(dimethylsiloxane)
PDMS/zeolite 4A/ PAN 15A%	15 wt% zeolite 4A in Polydimethylsiloxane matrix on Polyacrylonitrile support
PDXLA +MOP-3	poly(1,3 dioxolane) acrylate + metal-organic polyhedron-3
PEBA- 8h	Zn/Co-ZIF carbonized at 600 °C for 8 hours in PEBA matrix
PEBA/PSF	Polyether block amide/ polysulfone
PEBA-2533/ZIF-8	35 wt% ZIF-8 in PEBA matrix
PEBAX	Polyether block amine
Pebax + ZIF-67	Pebax+ ZIF- 67 (Basolite® Z1200)
Pebax + ZIF-8	Pebax+ ZIF-8 (Basolite® Z1200)
PEBAX/ PA-PPG	Polyether block amine / Poly(amide-c-poly(propylene glycol))
PEBA-zeolite 13X	1 wt% zeolite 13X in PEBA matrix
PES +SAPO-34	% Small pore size zeolite (SAPO-34) in Polyethersulfone matrix
PES/PDMS/SAPO-34	30 wt% Small pore size zeolite (SAPO-34) in PES matrix with PDMS coating
PG-PN40	40 wt% NOTT-300 (metal-hydroxyl-functionalized porous solid) in poly (ether block amide) matrix under pure gas conditions
PIM-1	Polymers of intrinsic microporosity-1
PIM-1+ MUF-15	Polymer of Intrinsic Microporosity-1 + (Massey University Framework-15)
PIM-7	Polymers of intrinsic microporosity-2

Abbreviation	Definition
PIM-CO-15	Polymers of intrinsic microporosity-CO-15
PIM-CO-19	Polymers of intrinsic microporosity-CO-19
PIM-Py-X	Anion filled Pyridine-based Polymers of Intrinsic Microporosity
PIMs with P-NPs	Polymer of Intrinsic Microporosity with pearl necklace nanoparticles
PNB-Si(DEt)-Si(OEtOMe)	Polynorborenes with alkoxy silyl pendant
Polyetheramine M2070 + Pebax 1657	polyetheramine (M2070)-carbon nanotubes + Pebax1657
Ppy nanospheres with mesoporous shells + Pebax1657	Polypyrrole nanospheres with mesoporous shells + Pebax1657
PSu-Clino-BHPA	BHPA-modified clinoptilolite-type natural zeolite in PSu matrix
PTMEG+PEBAX	Poly(tetramethylene ether) glycol + Polyether block amine
PTMSP	poly[1-(trimethylsilyl)-1-propyne]
PU-Z12	12 wt% zeolite 4A in polyurethane matrix
PVA	Polyvinyl alcohol
PVA+amines	Poly vinyl alcohol + formaldehyde + potassium hydroxide+ methanol+ poly (allylamine hydrochloride) + 2-aminoisobutyric acid
PVAm+ PANI@CNTs GO	Polyvinylamine + Polyaniline-coated carbon nanotubes in graphene oxide
PVA-PEG/PTFE	Poly(vinyl alcohol)- poly(ethylene glycol)/ Polytetrafluoroethylene
PVDF	Polyvinylidene difluoride
SEM	Scanning Electron Microscope
SLM	Supported liquid membranes
STP	Standard Temperature Pressure conditions, 1 atmosphere, 76cmHg and 273.15K
TZPIM	Tetrazole-modified polymers of intrinsic microporosity
UiO-66 + Al_2O_3	Zirconium-based Metal Organic Framework (Uio-66) + Al_2O_3
UiO-66-PEBA	Zirconium-based Metal Organic Framework (Uio-66) poly (ether block amide)
UiO-66-PEBA-NH_2	Zirconium-based Metal Organic Framework (Uio-66) poly (ether block amide)-NH_2
XL-PEGDA	Cross linked poly(ethylene glycil) diacrylate
ZIF	Zeolitic Imidazolate Framework
ZIF0302/d-PI	Zeolitic imidazolate framework-302 in a dense PI matrix
ZIF0302/d-PI	Zeolitic imidazolate framework-302 in a dense PI matrix
Zn(pyrz)2(SiF6)	Square grids of Zn and pyrazine pillared by hexafluorosilicate (SiF_6^{2-}) anions which form one-dimensional channels having a 3.8 Å diagonal dimension

2.9 REFERENCES

[1] T. Kober, H.W. Schiffer, M. Densing, E. Panos, Global energy perspectives to 2060 – WEC's World Energy Scenarios 2019, Energy Strategy. Rev. 31 (2020) 100523. https://doi.org/10.1016/j.esr.2020.100523.

[2] S. Fujimori, Y. Matsuoka, Development of method for estimation of world industrial energy consumption and its application, Energy Econ. 33 (2011) 461–473. https://doi.org/10.1016/j.eneco.2011.01.010.

[3] M. Laraia, Introduction to nuclear decommissioning: definitions and history, in: Nucl. Decommissioning, Elsevier, 2012: pp. 1–10. https://doi.org/10.1533/9780857095336.1.

[4] J. Yoon, Y. Sun, J.A. Rogers, Flexible Solar Cells Made of Nanowires/Microwires, in: Semicond. Nanomater. Flex. Technol. From Photovoltaics Electron. to Sensors Energy Storage, Elsevier Ltd., 2010: pp. 159–196. https://doi.org/10.1016/B978-1-4377-7823-6.00006-4.

[5] J.A. Dunne, S.C. Jackson, J. Harte, Greenhouse Effect, Encycl. Biodivers. Second Ed. 4 (2013) 18–32. https://doi.org/10.1016/B978-0-12-384719-5.00068-X.

[6] N.R. Table, N.R. Table, I. Isbn, P. Downloaded, S.P. Books, S.P. Books, Canada's options for a domestic greenhouse gas emissions trading program, 2020.

[7] J.D. Ford, T. Pearce, J. Prno, F. Duerden, L.B. Ford, M. Beaumier, T. Smith, Perceptions of climate change risks in primary resource use industries: A survey of the Canadian mining sector, Reg. Environ. Chang. 10 (2010) 65–81. https://doi.org/10.1007/s10113-009-0094-8.

[8] R. Garnaut, Climate change and the Australian agricultural and resource industries, Aust. J. Agric. Resour. Econ. 54 (2010) 9–25. https://doi.org/10.1111/j.1467-

8489.2009.00481.x.

[9] G.A. Berz, Global warming and the insurance industry, Interdiscip. Sci. Rev. 18 (1993) 120–125. https://doi.org/10.1179/isr.1993.18.2.120.

[10] UNEP, Handbook on data reporting under the Montreal Protocol, 1999.

[11] V. Popovski, The Implementation of the Paris Agreement on Climate Change, First edit, Routledge, London, 2018.

[12] International Energy Agency (IEA), World Energy Outlook 2019, OECD, 2019. https://doi.org/10.1787/caf32f3b-en.

[13] J. Gibbins, H. Chalmers, Chapter 2. Fossil Power Generation with Carbon Capture and Storage (CCS): Policy Development for Technology Deployment, Carbon Capture. (2010) 41–64. https://doi.org/10.1039/9781847559715-00041.

[14] M. Stewart, K. Arnold, Gas Sweetening and Processing Field Manual, Gas Sweeten. Process. F. Man. (2011).

[15] H.J. Herzog, Carbon Capture, The MIT Press, 2018. https://doi.org/10.7551/mitpress/11423.001.0001.

[16] S.A. Rackley, Overview of carbon capture and storage, in: Carbon Capture and Storage, Elsevier, 2017: pp. 23–36. https://doi.org/10.1016/b978-0-12-812041-5.00002-7.

[17] C. Cremer, Carbon capture and storage, Hydrog. Econ. Oppor. Challenges. 9780521882 (2009) 168–198. https://doi.org/10.1017/CBO9780511635359.007.

[18] F. J.D., F. T., P. S., M. H., S. R.D., Int. J. Greenh. gas Control, 2 (2008).

[19] H. Liu, R. Idem, P. Tontiwachwuthikul, Post-combustion CO_2 Capture Technology, Springer International Publishing, Regina, 2019. https://doi.org/10.1007/978-3-030-00922-9.

[20] J. Torstensen, R.M.L. Helberg, L. Deng, Ø.W. Gregersen, K. Syverud, PVA/nanocellulose nanocomposite membranes for CO_2 separation from flue gas, Int. J. Greenh. Gas Control. 81 (2019) 93–102. https://doi.org/10.1016/j.ijggc.2018.10.007.

[21] R. Xing, W.S.W. Ho, Crosslinked polyvinylalcohol-polysiloxane/fumed silica mixed matrix membranes containing amines for CO_2/H_2 separation, J. Memb. Sci. 367 (2011) 91–102. https://doi.org/10.1016/j.memsci.2010.10.039.

[22] Y. Kudo, H. Mikami, M. Tanaka, T. Isaji, K. Odaka, M. Yamato, H. Kawakami, Mixed matrix membranes comprising a polymer of intrinsic microporosity loaded with surface-modified non-porous pearl-necklace nanoparticles, J. Memb. Sci. 597 (2020) 117627. https://doi.org/10.1016/j.memsci.2019.117627.

[23] R. Nasir, H. Mukhtar, Z. Man, B.K. Dutta, M.S. Shaharun, M.Z. Abu Bakar, Mixed matrix membrane performance enhancement using alkanolamine solution, J. Memb. Sci. 483 (2015) 84–93. https://doi.org/10.1016/J.MEMSCI.2015.02.041.

[24] N. Habib, Z. Shamair, N. Tara, A.S. Nizami, F.H. Akhtar, N.M. Ahmad, M.A. Gilani, M.R. Bilad, A.L. Khan, Development of highly permeable and selective mixed matrix membranes based on Pebax®1657 and NOTT-300 for CO_2 capture, Sep. Purif. Technol. 234 (2020). https://doi.org/10.1016/j.seppur.2019.116101.

[25] X.Y. Chen, N. Tien-Binh, A. Romero, A. Patón, L. Sanchez-Silva, J.L. Valverde, S. Kaliaguine, D. Rodrigue, Gas Separation Properties of Mixed Matrix Membranes based on Polyimide and Graphite Oxide, J. Membr. Sci. Res. 6 (2020) 58–69. https://doi.org/10.22079/JMSR.2019.100069.1244.

[26] T.E. Rufford, S. Smart, G.C.Y. Watson, B.F. Graham, J. Boxall, J.C. Diniz da Costa, E.F. May, The removal of CO_2 and N_2 from natural gas: A review of conventional and

emerging process technologies, J. Pet. Sci. Eng. 94–95 (2012) 123–154. https://doi.org/10.1016/j.petrol.2012.06.016.

[27] J.D. Seader, E.J. Henley, Separation process principles, Choice Rev. Online. 36 (1999) 36-5112-36–5112. https://doi.org/10.5860/choice.36-5112.

[28] R. Singh, Introduction to Membrane Technology, Elsevier Ltd., Colorado Springs, 2015.

[29] A.A. Shamsabadi, H. Riazi, M. Soroush, Mixed matrix membranes for CO_2 separations, Elsevier Inc., 2018. https://doi.org/10.1016/B978-0-12-813645-4.00004-0.

[30] S. Nakao, K. Yogo, K. Goto, T. Kai, H. Yamada, Advanced CO_2 Capture Technologies, Springer International Publishing, Kyoto, 2020.

[31] E.P. Favvas, A. Figoli, R. Castro-Muñoz, V. Fíla, X. He, Polymeric membrane materials for CO_2 separations, 2018. https://doi.org/10.1016/B978-0-12-813645-4.00001-5.

[32] M. Porter, C., Handbook of Industrial Membrane technology, New Jersey, 1990.

[33] L.M. Robeson, The upper bound revisited, J. Memb. Sci. 320 (2008) 390–400. https://doi.org/10.1016/j.memsci.2008.04.030.

[34] L.M. Robeson, Correlation of separation factor versus permeability for polymeric membranes, J. Memb. Sci. 62 (1991) 165–185. https://doi.org/10.1016/0376-7388(91)80060-J.

[35] C. Zidi, R. Tayeb, M.B.S. Ali, M. Dhahbi, Liquid-liquid extraction and transport across supported liquid membrane of phenol using tributyl phosphate, J. Memb. Sci. 360 (2010) 334–340. https://doi.org/10.1016/j.memsci.2010.05.027.

[36] L.-Y. Kong, W.-D. Shan, S.-L. Han, T. Zhang, L.-C. He, K. Huang, S. Dai, Interfacial Engineering of Supported Liquid Membranes by Vapor Cross-Linking for Enhanced Separation of Carbon Dioxide, ChemSusChem. 11 (2018) 185–192.

https://doi.org/10.1002/cssc.201701851.

[37] M. Pera-Titus, Porous inorganic membranes for CO_2 capture: Present and prospects, Chem. Rev. 114 (2014) 1413–1492. https://doi.org/10.1021/cr400237k.

[38] M. Dehghani, M. Asghari, A.H. Mohammadi, M. Mokhtari, Molecular simulation and Monte Carlo study of structural-transport-properties of PEBA-MFI zeolite mixed matrix membranes for CO_2, CH_4 and N_2 separation, Comput. Chem. Eng. 103 (2017) 12–22. https://doi.org/10.1016/j.compchemeng.2017.03.002.

[39] G.L. Han, Z. Chen, L.F. Cai, Y.H. Zhang, J.F. Tian, H.H. Ma, S.M. Fang, Poly(vinyl alcohol)/carboxyl graphene mixed matrix membranes: High-power ultrasonic treatment for enhanced pervaporation performance, J. Appl. Polym. Sci. 137 (2020) 48526. https://doi.org/10.1002/app.48526.

[40] J. Zou, W.S.W. Ho, CO_2-selective polymeric membranes containing amines in crosslinked poly(vinyl alcohol), J. Memb. Sci. 286 (2006) 310–321. https://doi.org/10.1016/j.memsci.2006.10.013.

[41] R. Pang, K.K. Chen, Y. Han, W.S.W. Ho, Highly permeable polyethersulfone substrates with bicontinuous structure for composite membranes in CO_2/N_2 separation, J. Memb. Sci. 612 (2020) 118443. https://doi.org/10.1016/j.memsci.2020.118443.

[42] H. Rabiee, A. Ghadimi, S. Abbasi, T. Mohammadi, CO_2 separation performance of poly(ether-b-amide6)/PTMEG blended membranes: Permeation and sorption properties, Chem. Eng. Res. Des. 98 (2015) 96–106. https://doi.org/10.1016/j.cherd.2015.03.026.

[43] Y. Cai, Z. Wang, C. Yi, Y. Bai, J. Wang, S. Wang, Gas transport property of polyallylamine-poly(vinyl alcohol)/polysulfone composite membranes, J. Memb. Sci. 310 (2008) 184–196. https://doi.org/10.1016/j.memsci.2007.10.052.

[44] H. Lin, T. Kai, B.D. Freeman, S. Kalakkunnath, D.S. Kalika, The effect of cross-linking on gas permeability in cross-linked poly(ethylene glycol diacrylate), Macromolecules. 38 (2005) 8381–8393. https://doi.org/10.1021/ma0510136.

[45] S. Kunalan, K. Dey, P.K. Roy, V. Velachi, P.K. Maiti, K. Palanivelu, N. Jayaraman, Efficient facilitated transport PETIM dendrimer-PVA-PEG/PTFE composite flat-bed membranes for selective removal of CO_2, J. Memb. Sci. 622 (2021) 119007. https://doi.org/10.1016/j.memsci.2020.119007.

[46] V.I. Bondar, B.D. Freeman, I. Pinnau, Gas Transport Properties of Poly (ether-b-amide) Segmented, J. Polym. Sci. Part B Polym. Physics,. 38 (2000) 2051–2062.

[47] T. Zhu, X. Yang, Y. Zheng, X. He, F. Chen, J. Luo, Preparation of poly(ether-block-amide)/poly(amide-co-poly(propylene glycol)) random copolymer blend membranes for CO2/N2 separation, Polym. Eng. Sci. 59 (2019) E14–E23. https://doi.org/10.1002/pen.24828.

[48] L. Liu, A. Chakma, X. Feng, Preparation of hollow fiber poly(ether block amide)/polysulfone composite membranes for separation of carbon dioxide from nitrogen, Chem. Eng. J. 105 (2004) 43–51. https://doi.org/10.1016/j.cej.2004.08.005.

[49] N. Du, H.B. Park, G.P. Robertson, M.M. Dal-Cin, T. Visser, L. Scoles, M.D. Guiver, Polymer nanosieve membranes for CO_2-capture applications, Nat. Mater. 10 (2011) 372–375. https://doi.org/10.1038/nmat2989.

[50] Y. Han, W.S.W. Ho, Recent developments on polymeric membranes for CO_2 capture from flue gas, J. Polym. Eng. 40 (2020) 529–542. https://doi.org/10.1515/polyeng-2019-0298.

[51] P.M. Budd, K.J. Msayib, C.E. Tattershall, B.S. Ghanem, K.J. Reynolds, N.B. McKeown, D. Fritsch, Gas separation membranes from polymers of intrinsic microporosity, J. Memb.

Sci. 251 (2005) 263–269. https://doi.org/10.1016/j.memsci.2005.01.009.

[52] D. Fritsch, G. Bengtson, M. Carta, N.B. McKeown, Synthesis and gas permeation properties of spirobischromane-based polymers of intrinsic microporosity, Macromol. Chem. Phys. 212 (2011) 1137–1146. https://doi.org/10.1002/macp.201100089.

[53] X. Hu, W.H. Lee, J.Y. Bae, J. Zhao, J.S. Kim, Z. Wang, J. Yan, Y.M. Lee, Highly permeable polyimides incorporating Tröger's base (TB) units for gas separation membranes, J. Memb. Sci. 615 (2020) 118533. https://doi.org/10.1016/j.memsci.2020.118533.

[54] M. Mukaddam, E. Litwiller, I. Pinnau, Gas Sorption, Diffusion, and Permeation in Nafion, Macromolecules. 49 (2016) 280–286. https://doi.org/10.1021/acs.macromol.5b02578.

[55] T. Nakagawa, T. Saito, S. Asakawa, Y. Saito, Polyacetylene derivatives as membranes for gas separation, Gas Sep. Purif. 2 (1988) 3–8. https://doi.org/10.1016/0950-4214(88)80035-5.

[56] T.C. Merkel, V.I. Bondar, K. Nagai, B.D. Freeman, I. Pinnau, Gas Sorption, Diffusion, and Permeation in Poly(dimethylsiloxane) The permeability of poly(dimethylsiloxane) [PDMS] to, J Polym Sci B Polym Phys. 38 (2000) 415–434. https://doi.org/10.1002/(SICI)1099-0488(20000201)38:3.

[57] U. Senthilkumar, B.S.R. Reddy, Polysiloxanes with pendent bulky groups having amino-hydroxy functionality: Structure-permeability correlation, J. Memb. Sci. 292 (2007) 72–79. https://doi.org/10.1016/j.memsci.2007.01.014.

[58] S.R. Reijerkerk, M.H. Knoef, K. Nijmeijer, M. Wessling, Poly(ethylene glycol) and poly(dimethyl siloxane): Combining their advantages into efficient CO_2 gas separation membranes, J. Memb. Sci. 352 (2010) 126–135.

https://doi.org/10.1016/j.memsci.2010.02.008.

[59] J. Liu, X. Hou, H.B. Park, H. Lin, High-Performance Polymers for Membrane CO_2/N_2 Separation, Chem. - A Eur. J. 22 (2016) 15980–15990. https://doi.org/10.1002/chem.201603002.

[60] S.J. Metz, M.H. V Mulder, M. Wessling, Gas-Permeation Properties of Poly(ethylene oxide) Poly(butylene terephthalate) Block Copolymers, (2004) 4590–4597.

[61] L. Huang, J. Liu, H. Lin, Thermally stable, homogeneous blends of cross-linked poly(ethylene oxide) and crown ethers with enhanced CO_2 permeability, J. Memb. Sci. 610 (2020) 118253. https://doi.org/10.1016/j.memsci.2020.118253.

[62] W. Yave, A. Car, K.V. Peinemann, Nanostructured membrane material designed for carbon dioxide separation, J. Memb. Sci. 350 (2010) 124–129. https://doi.org/10.1016/j.memsci.2009.12.019.

[63] P.M. Budd, N.B. McKeown, B.S. Ghanem, K.J. Msayib, D. Fritsch, L. Starannikova, N. Belov, O. Sanfirova, Y. Yampolskii, V. Shantarovich, Gas permeation parameters and other physicochemical properties of a polymer of intrinsic microporosity: Polybenzodioxane PIM-1, J. Memb. Sci. 325 (2008) 851–860. https://doi.org/10.1016/j.memsci.2008.09.010.

[64] S. Mashhadikhan, A. Moghadassi, A.E. Amooghin, H. Sanaeepur, Interlocking a synthesized polymer and bifunctional filler containing the same polymer's monomer for conformable hybrid membrane systems, J. Mater. Chem. A. 8 (2020) 3942–3955. https://doi.org/10.1039/C9TA13375E.

[65] R. Kardani, M. Asghari, N.F. Hamedani, M. Afsari, Mesoporous copper zinc bimetallic imidazolate MOF as nanofiller to improve gas separation performance of PEBA-based

membranes, J. Ind. Eng. Chem. 83 (2020) 100–110. https://doi.org/10.1016/j.jiec.2019.11.018.

[66] Y. Wang, L. Li, X. Zhang, J. Li, C. Liu, N. Li, Z. Xie, Polyvinylamine/graphene oxide/PANI@CNTs mixed matrix composite membranes with enhanced CO_2/N_2 separation performance, J. Memb. Sci. 589 (2019) 117246. https://doi.org/10.1016/j.memsci.2019.117246.

[67] M. Mosadegh, F. Amirkhani, H. Riasat Harami, M. Asghari, M.J. Parnian, Effect of Nafion and APTEOS functionalization on mixed gas separation of PEBA-FAU membranes: Experimental study and MD and GCMC simulations, Sep. Purif. Technol. 247 (2020). https://doi.org/10.1016/j.seppur.2020.116981.

[68] S. Meshkat, S. Kaliaguine, D. Rodrigue, Comparison between ZIF-67 and ZIF-8 in Pebax® MH-1657 mixed matrix membranes for CO_2 separation, Sep. Purif. Technol. 235 (2020) 116150. https://doi.org/10.1016/j.seppur.2019.116150.

[69] D. Wang, D. Yao, Y. Wang, F. Wang, Y. Xin, S. Song, Z. Zhang, F. Su, Y. Zheng, Carbon nanotubes and graphene oxide-based solvent-free hybrid nanofluids functionalized mixed-matrix membranes for efficient CO_2/N_2 separation, Sep. Purif. Technol. 221 (2019) 421–432. https://doi.org/10.1016/j.seppur.2019.04.005.

[70] C. Wang, F. Guo, H. Li, J. Xu, J. Hu, H. Liu, M. Wang, A porous ionic polymer bionic carrier in a mixed matrix membrane for facilitating selective CO_2 permeability, J. Memb. Sci. 598 (2020). https://doi.org/10.1016/j.memsci.2019.117677.

[71] J. Liu, C.R.P. Fulong, L. Hu, L. Huang, G. Zhang, T.R. Cook, H. Lin, Interpenetrating networks of mixed matrix materials comprising metal-organic polyhedra for membrane CO_2 capture, J. Memb. Sci. 606 (2020) 118122.

https://doi.org/10.1016/j.memsci.2020.118122.

[72] S. Bano, S.R. Tariq, A. Ilyas, M. Aslam, M.R. Bilad, A.S. Nizami, A.L. Khan, Synergistic solution of CO_2 capture by novel lanthanide-based MOF-76 yttrium nanocrystals in mixed-matrix membranes, Energy Environ. 31 (2020) 692–712. https://doi.org/10.1177/0958305X19882413.

[73] M. Asghari, M. Mosadegh, H. Riasat Harami, Supported PEBA-zeolite 13X nano-composite membranes for gas separation: Preparation, characterization and molecular dynamics simulation, Chem. Eng. Sci. 187 (2018) 67–78. https://doi.org/10.1016/j.ces.2018.04.067.

[74] M. Rostamizadeh, B. Sadatnia, S. Norouzbahari, A. Ghadimi, Enhancing the gas separation properties of mixed matrix membranes via impregnation of sieve phases with metal and nonmetal promoters, Sep. Purif. Technol. 245 (2020) 116859. https://doi.org/10.1016/j.seppur.2020.116859.

[75] X. Wang, X. Ding, H. Zhao, J. Fu, Q. Xin, Y. Zhang, Pebax-based mixed matrix membranes containing hollow polypyrrole nanospheres with mesoporous shells for enhanced gas permeation performance, J. Memb. Sci. 602 (2020) 117968. https://doi.org/10.1016/j.memsci.2020.117968.

[76] R. Rong, Y. Sun, T. Ji, Y. Liu, Fabrication of highly CO_2/N_2 selective polycrystalline UiO-66 membrane with two-dimensional transition metal dichalcogenides as zirconium source via tertiary solvothermal growth, J. Memb. Sci. 610 (2020) 118275. https://doi.org/10.1016/j.memsci.2020.118275.

[77] H. Yin, A. Alkaş, Y. Zhang, Y. Zhang, S.G. Telfer, Mixed matrix membranes (MMMs) using an emerging metal-organic framework (MUF-15) for CO_2 separation, J. Memb. Sci.

609 (2020). https://doi.org/10.1016/j.memsci.2020.118245.

[78] S.A. Alavi, A. Kargari, H. Sanaeepur, M. Karimi, Preparation and characterization of PDMS/zeolite 4A/PAN mixed matrix thin film composite membrane for CO_2/N_2 and CO_2/CH_4 separations, Res. Chem. Intermed. 43 (2017) 2959–2984. https://doi.org/10.1007/s11164-016-2806-2.

[79] H.T. Afarani, M. Sadeghi, A. Moheb, The Gas Separation Performance of Polyurethane–Zeolite Mixed Matrix Membranes, Adv. Polym. Technol. 37 (2018) 339–348. https://doi.org/10.1002/adv.21672.

[80] A.S. Ghanem, M. Ba-Shammakh, M. Usman, M.F. Khan, H. Dafallah, M.A.M. Habib, B.A. Al-Maythalony, High gas permselectivity in ZIF-302/polyimide self-consistent mixed-matrix membrane, J. Appl. Polym. Sci. 137 (2020) 1–11. https://doi.org/10.1002/app.48513.

[81] B. Haider, M.R. Dilshad, M. Atiq Ur Rehman, J. Vargas Schmitz, M. Kaspereit, Highly permeable novel PDMS coated asymmetric polyethersulfone membranes loaded with SAPO-34 zeoilte for carbon dioxide separation, Sep. Purif. Technol. 248 (2020) 116899. https://doi.org/10.1016/j.seppur.2020.116899.

[82] J. Shen, G. Liu, K. Huang, Q. Li, K. Guan, Y. Li, W. Jin, UiO-66-polyether block amide mixed matrix membranes for CO_2 separation, J. Memb. Sci. 513 (2016) 155–165. https://doi.org/10.1016/j.memsci.2016.04.045.

[83] G. Onyestyák, J. Valyon, L.V.C. Rees, The sorption dynamics of N_2 and O_2 in zeolite particles, Stud. Surf. Sci. Catal. 158 B (2005) 1019–1026. https://doi.org/10.1016/s0167-2991(05)80443-4.

[84] W. Chen, Z. Zhang, L. Hou, C. Yang, H. Shen, K. Yang, Z. Wang, Metal-organic

framework MOF-801/PIM-1 mixed-matrix membranes for enhanced CO_2/N_2 separation performance, Sep. Purif. Technol. 250 (2020) 117198. https://doi.org/10.1016/j.seppur.2020.117198.

[85] J. Cheng, Y. Wang, N. Liu, W. Hou, J. Zhou, Enhanced CO_2 selectivity of mixed matrix membranes with carbonized Zn/Co zeolitic imidazolate frameworks, Appl. Energy. 272 (2020) 115179. https://doi.org/10.1016/j.apenergy.2020.115179.

[86] V. Nafisi, M.B. Hägg, Development of dual layer of ZIF-8/PEBAX-2533 mixed matrix membrane for CO_2 capture, J. Memb. Sci. 459 (2014) 244–255. https://doi.org/10.1016/j.memsci.2014.02.002.

[87] H. Gong, T.H. Nguyen, R. Wang, T.H. Bae, Separations of binary mixtures of CO_2/CH_4 and CO_2/N_2 with mixed-matrix membranes containing Zn(pyrz)2(SiF6) metal-organic framework, J. Memb. Sci. 495 (2015) 169–175. https://doi.org/10.1016/j.memsci.2015.08.018.

[88] B. Haider, M.R. Dilshad, M. Atiq Ur Rehman, J. Vargas Schmitz, M. Kaspereit, Highly permeable novel PDMS coated asymmetric polyethersulfone membranes loaded with SAPO-34 zeoilte for carbon dioxide separation, Sep. Purif. Technol. 248 (2020). https://doi.org/10.1016/j.seppur.2020.116899.

[89] S.A. Alavi, A. Kargari, H. Sanaeepur, M. Karimi, Preparation and characterization of PDMS/zeolite 4A/PAN mixed matrix thin film composite membrane for CO_2/N_2 and CO_2/CH_4 separations, Res. Chem. Intermed. 43 (2017) 2959–2984. https://doi.org/10.1007/s11164-016-2806-2.

[90] G. Castruita-de León, C.Y. Yeverino-Miranda, A. de J. Montes-Luna, H.I. Meléndez-Ortiz, G. Alvarado-Tenorio, L.A. García-Cerda, Amine-impregnated natural zeolite as

filler in mixed matrix membranes for CO_2/CH_4 separation, J. Appl. Polym. Sci. 137 (2020) 3. https://doi.org/10.1002/app.48286.

[91] J. Cheng, Y. Wang, N. Liu, W. Hou, J. Zhou, Enhanced CO_2 selectivity of mixed matrix membranes with carbonized Zn/Co zeolitic imidazolate frameworks, Appl. Energy. 272 (2020) 115179. https://doi.org/10.1016/J.APENERGY.2020.115179.

[92] N. Habib, Z. Shamair, N. Tara, A.S. Nizami, F.H. Akhtar, N.M. Ahmad, M.A. Gilani, M.R. Bilad, A.L. Khan, Development of highly permeable and selective mixed matrix membranes based on Pebax®1657 and NOTT-300 for CO_2 capture, Sep. Purif. Technol. 234 (2020). https://doi.org/10.1016/j.seppur.2019.116101.

[93] R. Kardani, M. Asghari, N.F. Hamedani, M. Afsari, Mesoporous copper zinc bimetallic imidazolate MOF as nanofiller to improve gas separation performance of PEBA-based membranes, J. Ind. Eng. Chem. 83 (2020) 100–110. https://doi.org/10.1016/j.jiec.2019.11.018.

[94] Y. Zhang, J. Sunarso, S. Liu, R. Wang, Current status and development of membranes for CO2/CH4 separation: A review, Int. J. Greenh. Gas Control. 12 (2013) 84–107.

[95] S.K. Pavelić, J.S. Medica, D. Gumbarević, A. Filošević, N. Pržulj, K. Pavelić, Critical review on zeolite clinoptilolite safety and medical applications in vivo, Front. Pharmacol. 9 (2018) 1350. https://doi.org/10.3389/fphar.2018.01350.

[96] M. Asghari, M. Mosadegh, H. Riasat Harami, Supported PEBA-zeolite 13X nano-composite membranes for gas separation: Preparation, characterization and molecular dynamics simulation, Chem. Eng. Sci. 187 (2018) 67–78. https://doi.org/10.1016/j.ces.2018.04.067.

[97] M. Vinoba, M. Bhagiyalakshmi, Y. Alqaheem, A.A. Alomair, A. Pérez, M.S. Rana,

Recent progress of fillers in mixed matrix membranes for CO_2 separation: A review, Sep. Purif. Technol. 188 (2017) 431–450. https://doi.org/10.1016/j.seppur.2017.07.051.

[98] M. Chawla, H. Saulat, M. Masood Khan, M. Mahmood Khan, S. Rafiq, L. Cheng, T. Iqbal, M.I. Rasheed, M.Z. Farooq, M. Saeed, N.M. Ahmad, M.B. Khan Niazi, S. Saqib, F. Jamil, A. Mukhtar, N. Muhammad, Membranes for CO_2 /CH_4 and CO_2/N_2 Gas Separation, Chem. Eng. Technol. 43 (2020) 184–199. https://doi.org/10.1002/ceat.201900375.

[99] S. Yang, J. Sun, A.J. Ramirez-Cuesta, S.K. Callear, W.I.F. David, D.P. Anderson, R. Newby, A.J. Blake, J.E. Parker, C.C. Tang, M. Schröder, Selectivity and direct visualization of carbon dioxide and sulfur dioxide in a decorated porous host, Nat. Chem. 4 (2012) 887–894. https://doi.org/10.1038/nchem.1457.

CHAPTER 3: APPLICATION OF A 2^6-FACTORIAL DESIGN OPTIMIZATION FOR POLY (VINYL ALCOHOL) BASED MEMBRANE SYNTHESIS FOR CO_2 /N_2 AND CO_2/CH_4 SEPARATION

3.1 ABSTRACT

The consumption of hydrocarbons and therefore the rise in global temperatures is predicted to continue increasing with the increase in globalization and the industrialization of third world countries. Separation of carbon dioxide (CO_2), the main global warming causing greenhouse gas, from biogas so that it can be upgraded to a renewable source of natural gas and from other flue gases have therefore became of great interest. This research focuses on the separation of CO_2 from methane (CH_4) and nitrogen (N_2) gases using membranes. Amine-based Poly vinyl alcohol (PVA) polymeric membranes that had previously shown good gas separation results were adapted for use in this research. The adapted membrane was then optimized using a 2^6 factorial design to optimize the membranes' performance with respect to CO_2/N_2 and CO_2/CH_4 selectivities when tested at near atmospheric conditions. The factorial design was also done to optimize the membrane's mechanical stability. It was established that the highest selectivity of 2.45 was achieved with the CO_2/CH_4 pair where the combination of PVA, formaldehyde and Poly (allylamine hydroxide) most positively affected CO_2 selectivity over CH_4.. The most optimized CO_2/N_2 selectivity obtained was lower at a maximum selectivity of 1.83 with PVA being the sole component that most positively affected CO_2 selectivity over N_2.

Key words: CO_2/N_2 separation, CO_2/CH_4 separation, CH_4/N_2 separation, polymeric membranes, PVA membranes, factorial design.

3.2 INTRODUCTION

Continual global warming has become a serious concern with policy makers, and particularly the Intergovernmental Panel on Climate Change (IPCC) warning that the earth should not warm more than 2°C higher than pre-industrial revolution temperatures. The average global temperatures have already increased by a little over 1°C since 1880[1]. To avoid any further increase, the cumulative carbon emissions released between 2011 and 2050 need to be limited to around 1,100 gigatonnes of carbon dioxide[2]. Consequently, various international multilateral environmental agreements have been organized to synchronize the reduction of greenhouse gas emissions between international countries such as the Montreal Protocol in 1999 and more recently the Paris agreement of 2015[3,4]. The synchronized reduction is needed. As stated by IPCC, the effects of climate change over the past two decades included shrinkage of glaciers, thawing of permafrost, later freezing and earlier breakup of ice on rivers and lakes. This is all in addition to the lengthening of mid to high latitude growing seasons, declines in plant and animal populations and earlier emergence of insects, flowering of trees and egg-laying in birds[5]. Other predicted effects of global warming as the earth continues to warm include floods, insect infestations, spread of disease, wildfire and drought, which are predicted to affect a lot of the biodiversity on earth from plants to all animals alike[6]. For these reasons, there has been a real effort to decrease the amount of greenhouse gas emissions from fossil fuel combustion, the major contributor to global warming.

The main greenhouse gases in the earth's atmosphere are water vapor (H_2O), carbon dioxide (CO_2), methane (CH_4), nitrous oxide (N_2O) and ozone (O_3). Most of the greenhouse gas emissions leading to the climate change experienced on earth are from CO_2. In fact, the atmospheric CO_2 concentration has increased by 35% since preindustrial times. This has been especially brought about by the emission from fossil fuel combustion and to a lesser extent by land conversion and

cement production[7,8]. Approximately 50% of world's CO_2 emissions are from power generated by fossil fuel combustion[13]. Although fossil fuels are being phased out in an attempt to use more environmentally friendly energy sources, the International Energy Agency World Energy Outlook predicts that fossil fuels will remain significant for many decades to come[9]. Thus, it is necessary to find a way to reduce the net CO_2 emitted into the atmosphere. Carbon Capture and Storage (CCS) is a growing method of doing this where it involves the removal of CO_2 from streams where it is produced, such as at a power plant. This is followed by the transport of CO_2 to a safe location for long-time storage[10]. This paper focuses on post-combustion CO_2 capture that is separation of CO_2 from N_2.

Separation of CO_2 from CH_4 was also explored for application in natural gas sweetening. Natural gas sweetening is necessary as CO_2 lowers the Btu content of natural gas and it makes the natural gas corrosive, which prevents the transportation of natural gas[11]. Other methods currently used for natural gas sweetening are absorption and adsorption that have fouling and corrosion issues. This has prompted the exploration of the use of membranes for CO_2/CH_4 separation. Hence, CO_2 separation from CH_4 was also studied as a method of lowering the environmental footprint in the process of harnessing energy from the biogas power generating sector[11]. Other applications for the separation of CO_2 from CH_4 are in the enhancement of the oil recovery process and in the upgrading of biogas[12].

The CO_2, CH_4 and N_2 properties that allow for their separation include the kinetic diameter, polarizability and quadrupole moment as shown in Table 3.1. The quadrupole moment of carbon dioxide, as well as its polarizability are higher than that of nitrogen and methane [11]. Different polymeric, inorganic and mixed matrix membranes have been explored for CO_2/N_2 and CO_2/CH_4 separation as they offer an environmentally friendly and cheaper method of gas separation[11,14].

Among polymeric membranes, PVA based membranes have shown a lot of promise when incorporated into gas separation membranes due to their hydrophilic nature as well as their good mechanical stability[15]. When combined with amines, PVA membranes have shown high CO_2/N_2 and CO_2/CH_4 selectivity values. Zou and Ho observed a high CO_2/N_2 selectivity of 280 with other research papers reporting similar high CO_2/N_2 and CO_2/CH_4 selectivity values above 50 with different amine based PVA membranes[15,16]. Unfortunately, polymeric membranes have been associated with the trade-off between the permeabilities and the selectivities as illustrated by Robeson's curve[18,19]. Facilitated transport membranes make use of the quadruple moment of CO_2 to selectively transport CO_2. This is done by incorporating amines and carboxylic groups which act as carriers and selectively interact with the CO_2 reversibly thus transporting it across the membrane [20]. This mode of transportation is facilitated transport. The other mode of transportation is through a concentration or pressure difference. As CO_2 is able to be transported by both means, whereas the uncharged N_2 and CH_4 are not, the permeability and therefore selectivity of CO_2 is higher. With facilitated transport membranes there can be transportation through the use of fixed carriers and through the use of mobile carriers. Mobile carriers can move freely within the membrane and are usually seen with supported liquid membranes whereas fixed carriers have limited mobility. The membrane fabricated in this study used fixed amine carriers to enhance facilitated transport [16].

It is usually very difficult to develop defect-free membranes and as such it is important to characterize the transport through the defects. There are two mechanisms of transport through these defect pores: Knudsen flow and viscous flow. Knudsen flow describes flow through smaller pores whereas viscous flow describes flow through larger pores. In Knudsen flow the mean free

path is greater than the pore diameter whereas for viscous flow, the mean free path is less than the pore diameter. In Knudsen flow there is collision between the permeant and the walls of the membrane and therefore there can be some selectivity with this kind of flow. With viscous flow the main interaction is between the permeating molecules [17].

Table 3.1: Summary of important CO_2, CH_4 and N_2 properties[11].

	Property		
Molecule	**Kinetic diameter (Å)**	**Polarizability (Å^3)**	**Quadrupole moment (DÅ)**
CO_2	3.30	2.507	4.30
CH_4	3.80	2.448	0.02
N_2	3.64	1.710	1.54

3.3 EXPERIMENTAL

3.3.1 Factorial design

Membranes with both high permeability and selectivity are desired due to their cost-effective nature (definitions of permeability and selectivity used are given in section 2.3). However, it is observed that polymeric membranes that are more permeable are usually less selective towards the desired gas. Polymers that achieve both high permeability and selectivity are extremely rare and therefore, a trade-off between the two characteristics is often accepted[21]. To achieve the best possible trade-off, a working adapted membrane was prepared using the procedure similar to the one used by Zou and Ho and then optimized using a factorial design technique[16].

The factorial design allows for the analysis of the weight factor of individual component factors as well as the combination of the component factors that could affect the performance of the membrane[22]. Factorial designs have been used widely to optimize membrane gas separation performance, specifically for CO_2 capture by varying the membrane components used[23–26]. In factorial design, the heaviest factor corresponds to the most important component or components as the design examines each component's upper and lower limit. The optimization study was done using a 2^k-level full factorial design where k represents number of component factors (k in this case was 6), representing each of the 6 components. Thus, a 2^6-level factorial experiment was designed which resulted in 64 experiments to be conducted with additional three error experiments. The effects of these component factors known as beta weight factors were calculated using Equations 1 and 2. The equations used in the factorial design and its analysis were adapted from the Wiley published book on 'Design and Analysis of experiments' by Dean et al. and paper on 'Factorial Experiments in Completely Randomized Designs' by Mason et al. [27,28].

$$\hat{\beta}_0 = \frac{\sum Responses}{n} \tag{1}$$

$$\hat{\beta}_i = \frac{\sum(Responses * x_i)}{m} \tag{2}$$

Here $\hat{\beta}_i$ represents the weight factors, *n* is the total number of experiments including the three error experiments (2^6 + 3 =67), *m* corresponds to the total number of experiments excluding the repeats (2^6 = 64) and x_i represents the component factors being studied. For this project, selectivity values of the pairs CO_2/N_2, CH_4/N_2 and CO_2/CH_4 were chosen to be the responses studied. Once all the beta weight factors were determined, the design was modelled using a mathematical relation between the response, weight factor values, and the component factors themselves as shown in Equation 3.

$$\begin{aligned} y = \hat{\beta}_0 + \hat{\beta}_A x_A + \cdots + \hat{\beta}_F x_F + \hat{\beta}_{AB} x_A x_B + \cdots + \hat{\beta}_{EF} x_E x_F + \hat{\beta}_{ABC} x_A x_B x_C + \cdots \\ + \hat{\beta}_{DEF} x_D x_E x_F \\ + \hat{\beta}_{ABCD} x_A x_B x_C x_D + \cdots + \hat{\beta}_{CDEF} x_C x_D x_E x_F + \hat{\beta}_{ABCDE} x_A x_B x_C x_D x_E + \cdots \\ + \hat{\beta}_{BCDEF} x_B x_C x_D x_E x_F + \hat{\beta}_{ABCDEF} x_A x_B x_C x_D x_E x_F \end{aligned} \tag{3}$$

Here *y* represents the response used to create the model and since it was 2^6-level factorial design the equation contained 64 terms showing the weight of all the individual as well as combined factors. This factorial design was used to see the relative effects of different components in the membrane on the selectivity of the gases to be separated. The higher is the individual or combined weight factor obtained, the higher would be the effect on the selectivity values.

3.3.2 Membrane development procedure

The procedure for the membrane preparation has been adapted from Zou and Ho with changes that ensured a working membrane was made[16]. The base working membrane made as described in the procedure below contained 2.06wt% Polyvinyl alcohol (PVA), 0.72wt% Formaldehyde, 94.74 wt% deionized water, 0.45 wt% Poly (allylamine hydroxide) (Pam-OH), 1.17 wt % potassium hydroxide (KOH) and 0.85wt% 2-Aminoisobutyric acid (AIBA). This was then optimized using a factorial design where the upper and lower limits of each factor are mentioned in Table 3.2. The water that was added after cross-linking was used to bring the weight to 100g and therefore water weight was variable depending on the amounts of each component used. This was done as the water was eventually all dried off the membrane in the last step of the procedure.

Table 3.2: Upper and lower limits for components used in the optimization study. Each of these components were taken as different factors in preparing the membranes. These factors were labelled from A to F, as shown in this table.

Component-Factor	Upper limit (wt%)	Lower limit (wt%)
Polyvinyl alcohol (PVA)-A	3.6	0.21
Formaldehyde-B	2.07	0.30
Water-C	90.64	82.65
Poly (allylamine hydroxide) (Pam-OH)-D	0.70	0.30
Potassium hydroxide (KOH)-E	2.00	0.30
2-Aminoisobutyric acid (AIBA)-F	2.00	0.30

The upper bound of PVA and water that was added before cross-linking were determined from the solubility of PVA in water and the lower bounds were determined from results observed in the

literature to allow a physically stable membrane[29]. The amount of formaldehyde was determined from our own previous experiments where only formaldehyde was varied. The amount of AIBA and KOH were dependent on each other since they interacted with each other to form AIBA-K and $KHCO_3$-K_2CO_3 and therefore their limits were determined from experimentation with one as them[16]. The amount of Poly (allylamine hydroxide) was determined from our previous experiments as well as other components already presented, particularly KOH. The amount of water added after cross-linking, that contained the AIBA and the Poly (allylamine hydroxide) that had been synthesized was variable as the membranes would be dried both overnight and in the oven at 120°C as described in the procedure. The procedure below describes how the adapted base membrane was prepared. The other 67 membranes were prepared similarly with all possible permutations of the upper and lower limits of each factor. All the other 67 membranes were also made from a batch amount so that the 3 hours 35 minute mixing for cross-linking was done on similar total fixed weight of 100 grams.

3.3.2.1 Materials

- Deionized water used was available at University of Ottawa campus.
- Polyacrylonitrile (PAN) I flat sheet support with a molecular weight cut-off of 30kDa and a thickness of 150µM was purchased from Synder Filtration (Vacaville, CA, USA). Catalogue number: 500-06-9095.

The following chemicals were obtained from Sigma-Aldrich® (Oakville ON, Canada) at the highest purity available:

- Polyvinyl alcohol (PVA) (99% hydrolyzed powder)
- Poly (allylamine hydrochloride) (Pam-HCl)
- 2-Aminoisobutyric acid (AIBA)

- Formaldehyde solution (37 wt.% aqueous solution)
- Potassium hydroxide (KOH)
- Methanol

3.3.2.2 Procedure

Three separate mixtures were prepared:

- The first mixture was poly(allymine) hydroxide which was obtained by mixing Pam-HCl with KOH in methanol overnight (0.44g Pam-HCl in 0.528g KOH mixed with 60ml of methanol). This mixture was stirred overnight in a flask covered with parafilm. The resulting KCl was precipitated after the 24 hours leaving a mixture of poly(allymine) solution. 20ml of deionized water was added as the solvent and then the mixture was placed in the fume hood for the methanol to evaporate.
- The second mixture was prepared by first dissolving 2g of PVA in 50g of deionized water at 80℃ with stirring until the solution turned colourless. Separately, 0.6977g of the 37wt% formaldehyde solution was dissolved in 1.8856g of deionized water and 0.732g of KOH was added. These 2 separate solutions were mixed, and the resulting mixture was then heated at 80℃ with stirring at level of 500 rpm for 3h 35 min. This was changed from the original 16 hours as with 16 hours a solid was formed. The solution turned from colourless to yellow to orange while thickening up all through the 3h 35min heating. The solution was thickening up due to crosslinking. As mentioned earlier a batch solution of 100g total was prepared so that an equal total weight was being heated and therefore cross-linked each time.
- The third mixture was prepared by mixing a 1:1 molar ratio of KOH and AIBA; 0.405g KOH into an aqueous solution of AIBA (0.828g AIBA in 20 ml of deionized water).

After the 3 hour 35 minute heating of the second solution, the third mixture was added to the second solution with mixing for 30 minutes. Thereafter, the first mixture was added to the second and third mixture with mixing again for another 30 minutes. This mixture is the polymeric membrane mixture. The weight % were kept constant for the adapted membrane for a total weight of 100 grams where the amount of water in the third mixture was varied to maintain this total constant weight. This is because the total amount of water added after cross linking was all later evaporated during drying.

To cast the membrane, the PAN support was flattened and taped on the sides on top of a glass to prevent it from moving during the casting of the membrane. Then, using the thickness measurer, a dropper was used to apply the solution mixture on the support. The casting knife was then used to spread the PVA blend on the PAN support. This PAN coated membrane solution was then dried overnight for about 16h. The formed membrane was thereafter dried further at 120℃ for 4 hours. The membrane was then cut into a circle of diameter 6.8 cm to fit in the gas permeation device. The mechanical stability of the base membrane as well as membranes 13 and 61 was also analyzed to see whether a mechanically stable membrane film that did not need the PAN support was able to be formed.

3.3.3 Aging test procedure

In order to determine how stable the fabricated membranes were before carrying out the factorial design, a batch of membranes were prepared following the adapted procedure. They were then tested over a duration of 37 days. They were tested on the first day after making the membrane and then every 7 days using the single gas permeation procedure outlined below for 60 minutes until steady state was achieved. These membranes were stored in a desiccator when not being

tested. The results from this aging test procedure were then used in testing of the 67 membranes made for the 2^6 factorial design.

3.3.4 Single gas permeation experiment procedure

All gases used were purchased from Messer Canada Ltd. (Mississauga, ON, Canada) and their grades and purities are displayed in Table 3.3.

Table 3.3: Gases used for the experiments in this study and their grades and purities.

Species	Grade	Purity (%)
CO_2	4.0	99.99
CH_4	4.0	99.99
N_2	4.0	99.99

The results of the aging tests indicated that the PVA membrane took 21 days to stabilize. This is because of the excess free volume associated with glassy polymers decreasing with increase in time[30]. Therefore, all membranes were tested 21 days after being prepared. To test the membranes, a single gas flow of N_2, CO_2 or CH_4 gas passed through the membrane and the permeate and retentate flow rates were measured. The membranes were tested using the set up shown in Figure 3.1 at 2.5atm feed pressure to compare results with previous tests done. The membrane was placed in the membrane module shown in Figure 3.1. The feed pressure was set and the retentate and permeate flow rates were measured using the bubble flow meters. The measurement was done every 5 minutes for 60 minutes (until values stabilized) and the last couple of readings were averaged to give the steady state retentate and permeate flow rates for each of the individual gases. The permeability and ideal selectivity values were then calculated as explained below.

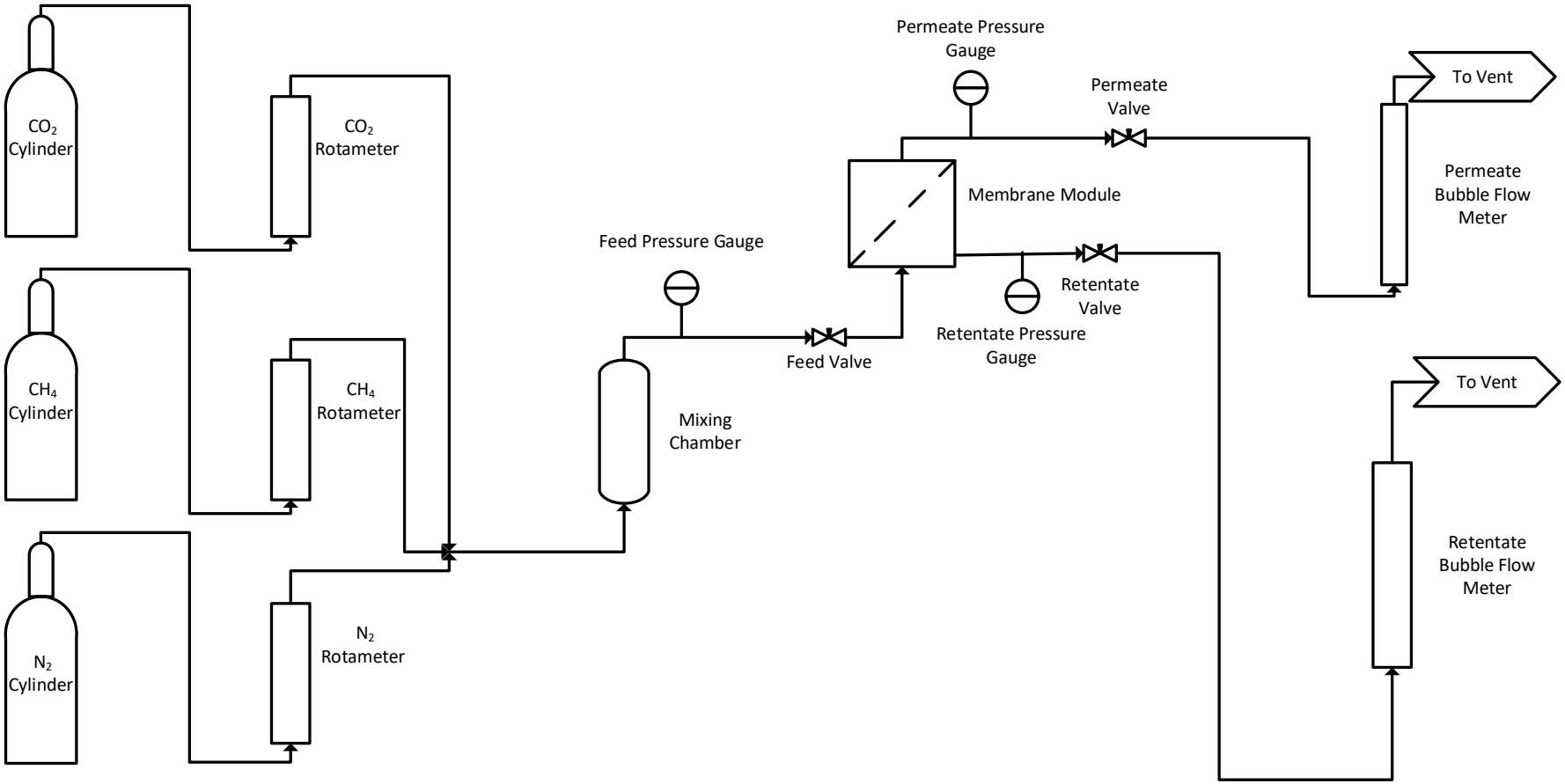

Figure 3.1: Schematic diagram of single gas permeation setup used in this study

The gas permeability for the membrane for component i, P_i, was calculated in Barrer using Equation 4:

$$P_i = F_i \frac{T_{STP}}{T_{feed} \times p_{STP}} \frac{L\,\Delta p}{A\,p_{feed}} \times 10^{10} \quad (4)$$

Where F_i is the volumetric flow rate [cm^3/s] taken at STP conditions for component *i* and *A* is the surface area of the membrane[cm^3], T_{STP} is the temperature of gas at STP conditions in K, 273.15K was used. p_{STP} is the pressure of 1 mol of gas at STP conditions in cmHg, 76cmHg was used. T_{feed} is the temperature of the feed and p_{feed} is the pressure of the feed. Δp is the difference between the upstream and downstream pressure and *L* is the thickness of the active layer of the membrane measured in cm. The 10^{10} converts the permeability from {cm^3 (STP)cm/s cm^2 cmHg} units to Barrer. The permeability of gases is dependent on the solubility, size and diffusivity of the gases[31].

The membrane selectivity is defined as the ratio of the permeability values for the membrane for different components.(For example, for the selectivity of gas 1 over gas 2, Equation 5 is used.

$$\alpha^*_{1/2} = \frac{P_1}{P_2} \quad (5)$$

Where $\alpha^*_{1/2}$, is the selectivity of the membrane for component 1 over component 2 and P_i is the permeability of gas i where i is either 1 or 2[32].

3.3.5 Characterization of synthesized membranes

A selection of the good performing membranes were characterized using a Scanning Electron Microscope (SEM) which was used to verify the thickness of the active layer of the membrane. This was done using JEOL JSM-7500F FESEM series operated with 30kV electron beams under 30Pa of vacuum. The cross-sectional images were taken at X100 and X800 magnification on top

surface of the membrane coated with 10nm of gold. Imaging of the top surface of the membrane was also done by SEM imaging at X1,000, X5,000 and X10,000 magnification levels on samples coated with 7nm of gold. Fourier Transform Infrared (FTIR) Spectroscopy was also carried out with wave numbers in the ranges of (4000- 650) cm^{-1} to determine the functional groups of the best performing membranes. This was done using a Cary 630 FTIR spectrometer by Agilent. Lastly, the hydrophobicity of the membranes was established through contact angle measurements using a goniometer. 7 measurements were taken at different locations on the membrane surface and an average of those 7 determined the contact angles was reported. The goniometer used was the Video Contact Angle System (VCA) Optima XE from AST products.

3.4 RESULTS AND DISCUSSION

3.4.1 Physical aging study

PVA amine based cross-linked membranes have shown promise when used in the separation of CO_2 from N_2 as shown by the work of Zou and Ho[16]. When compared to other polymeric membranes, they showed a lot of promise when used in the separation of CO_2 from N_2 with a CO_2 permeability of 1800 Barrer and a CO_2/N_2 selectivity of 280, higher than that of most polymeric membranes. This was observed when tested at 150°C and 2 atm pressure in the presence of water with water rates of 0.03/0.03 cm^3/min (feed/sweep) and when Argon was used as a sweep gas[16]. The goal of this research was to replicate the membrane tested and optimize the membrane's performance where the membrane was tested in near atmospheric conditions. In doing this, the inconsistent results initially obtained necessitated the need to study the physical aging of the membrane with time. This was done by measuring the permeability of the membrane for the 3 gases CO_2, CH_4 and N_2 every seven days from the first day after making the membrane to the 37^{th} day. This was done with the concentrations of the adapted working procedure (outlined in section 3.3.2) with the assumption that the different membranes resulting from the different concentrations used in the factorial design would age similarly. The results are shown in Figure 3.2. These results show that the membrane permeability for all the gases decreased significantly until the 21^{st} day after which the membrane's permeability seemed to be constant until the 37^{th} day. Physical aging has been observed with glassy polymers and polymers with glassy components. This has been attributed to the non- equilibrium excess free volume which is time dependent and causes a decrease in the permeability of the membrane over time [33]. Similar results have been reported in literature where there is initially a rapid permeance decrease for the first 15 days followed by slowed down aging which can be accurately extrapolated for up to 2 years for industrially used

membranes [33,34]. Therefore, all subsequent membranes were tested after 21 days and within a 1-2 day time period for consistency.

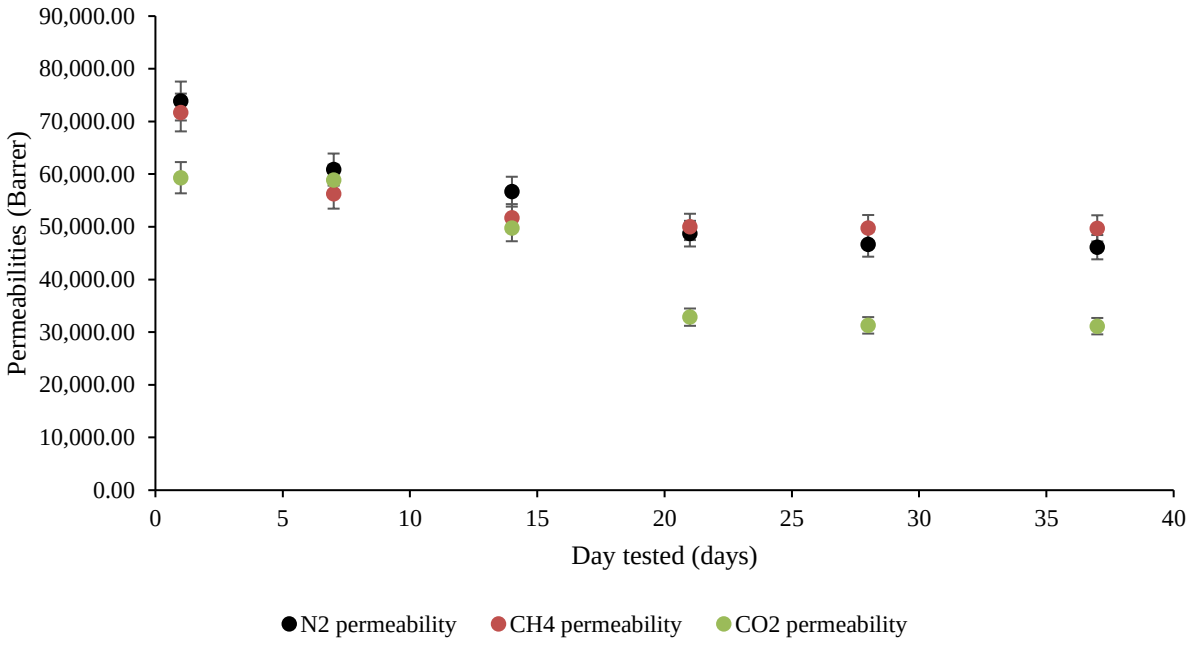

Figure 3.2: CO_2, N_2 and CH_4 permeabilities as a function of day tested from day 1 to day 37.

3.4.2 Membrane characterization

The best performing membranes out of the factorial design, the concentration of their components, CO_2 permeability as well as the CO_2/N_2 and CO_2/CH_4 selectivities are shown in Table 3.4. It is important to note that these membranes did not produce mechanically stable membrane films and required the use of the PAN support. Membrane 13 was chosen as it showed the highest selectivity for CO_2 over N_2. Membrane 61 was chosen as it showed the highest selectivity for CO_2 over CH_4. The term "base membrane" was used to describe the membranes in experiments 65, 66 and 67, which were the error experiments as described in the factorial design section. Membrane 66 was used in Table 3.4, but membranes 65 and 67 showed very similar results. Moreover, these

membranes (65-67) had the same ratios of components as the adapted procedure from which the factorial design was based. The characterization section that follows also focuses on these three membranes.

Table 3.4: Material development concentrations, CO_2 permeability, CO_2/N_2 and CO_2/CH_4 selectivity values for the base membrane, membrane 13 and membrane 61. Permeability values were based on active layer thickness.

Property	Base membrane 66	Membrane 13	Membrane 61
% PVA	1.905	3.6	0.21
% Formaldehyde	1.185	0.3	0.3
% H20	86.645	82.65	82.65
% Pam-OH	0.5	0.7	0.7
% KOH	1.15	2	2
%AIBA	1.15	0.3	2
CO_2 permeability (Barrer)	76,501	20,114	32,405
CO_2/N_2	1.03	1.83	1.10
CO_2/CH_4	1.01	0.94	2.45

The SEM imaging was done to view the morphology of the membrane surface. As can be seen in Figure 3.3, the SEM imaging showed a neat flat even membrane surface. Only the membrane surface of membrane 13 and membrane 61 are shown in this figure, but SEM images for other experiments showed a similar flat neat surface. Cross-sectional images of the membranes were also taken to determine the thickness of the active layer of the membrane. There is a clear void separating the active layer from the support material, PAN as shown in Figure 3.4, on the left image. As shown by the white arrow on the right image in Figure 3.4, the thickness of the active layer is about 25µm. All membranes were assumed to have the same average active layer thickness of 25 µm and this active layer thickness was used in the calculation of the permeabilities. The total thickness of the active layer and support was maintained at 160 µm- 165 µm.

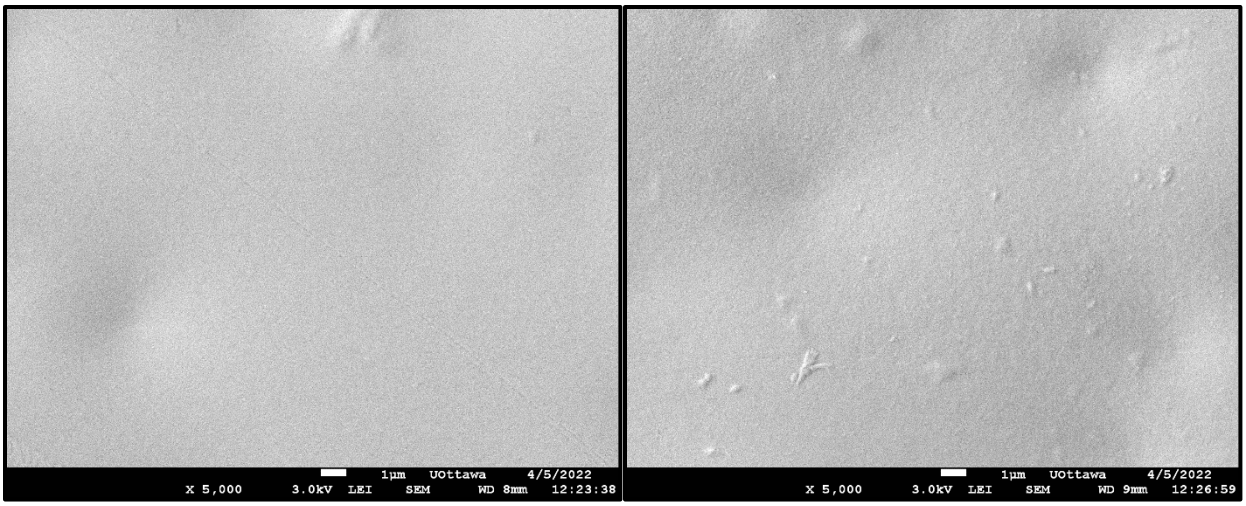

Figure 3.3: Top membrane surface area SEM images of membrane 13 (left) and 61 (right) at X5000 magnification

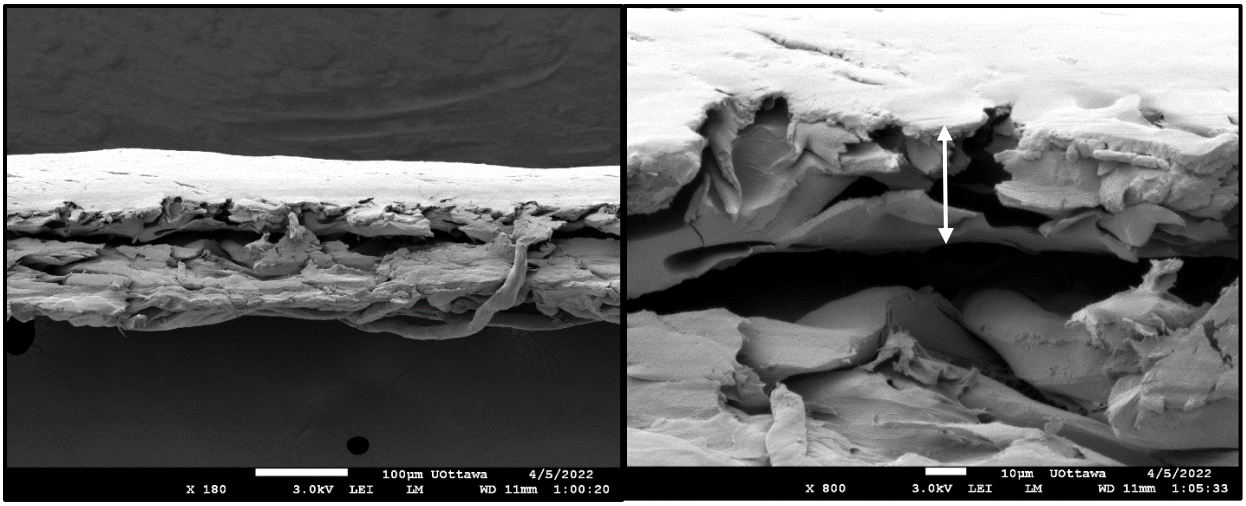

Figure 3.4: Cross- sectional images of base membrane at X100 magnification (left) and X800 magnification (right)

FTIR imaging was also done to observe the functional groups of the base membrane and the 2 best performing membranes in terms of CO_2/N_2 and CO_2/CH_4 separation. The results with the most conspicuous functional groups are seen in Figure 3.5. The characterization of the peaks was done using "Interpretation of infrared spectra, a practical approach" by John Coates, 2000 [35]. The acetal linkage associated with the cross-linking between PVA and formaldehyde as mentioned by

Zou and Ho with the wavenumber of 1144cm^{-1} was noted with the base membrane and membrane 13 but not with membrane 61. This is because of the lower concentration of PVA in membrane 61 compared to the concentration of formaldehyde resulting in the most prominent peak with membrane 13 followed by the base membrane [16,35]. Figure 3.5 also shows a broad peak at a wavenumber of 3000 cm^{-1} to about 3500 cm^{-1} with membrane 13 the base membrane and membrane 61. This peak indicates the presence of hydrogen bonded hydroxyl (O-H) and amine (N-H) groups. The presence of the nitrile peak at a wavenumber of 2240cm^{-1} with only membrane 61 is due to the higher concentration of AIBA in membrane 61 compared to membrane 13 and the base membrane [35,36]. The higher degree of hydrophilicity of membrane 13 followed by the base membrane and membrane 61 was the consequence of the hydroxyl peak at 3280 cm^{-1} present with membrane 13. Moreover, the hydrophilicity could be attributed to the epoxy (C-O-C) functional group at a wavenumber of around 1240 cm^{-1} for both membranes 13 and 61 [35]. Other highlighted functional groups include the aromatic C-H bends with wavenumbers in between 670-1225 cm^{-1}. The FTIR confirmed the effects of the applied factorial design.

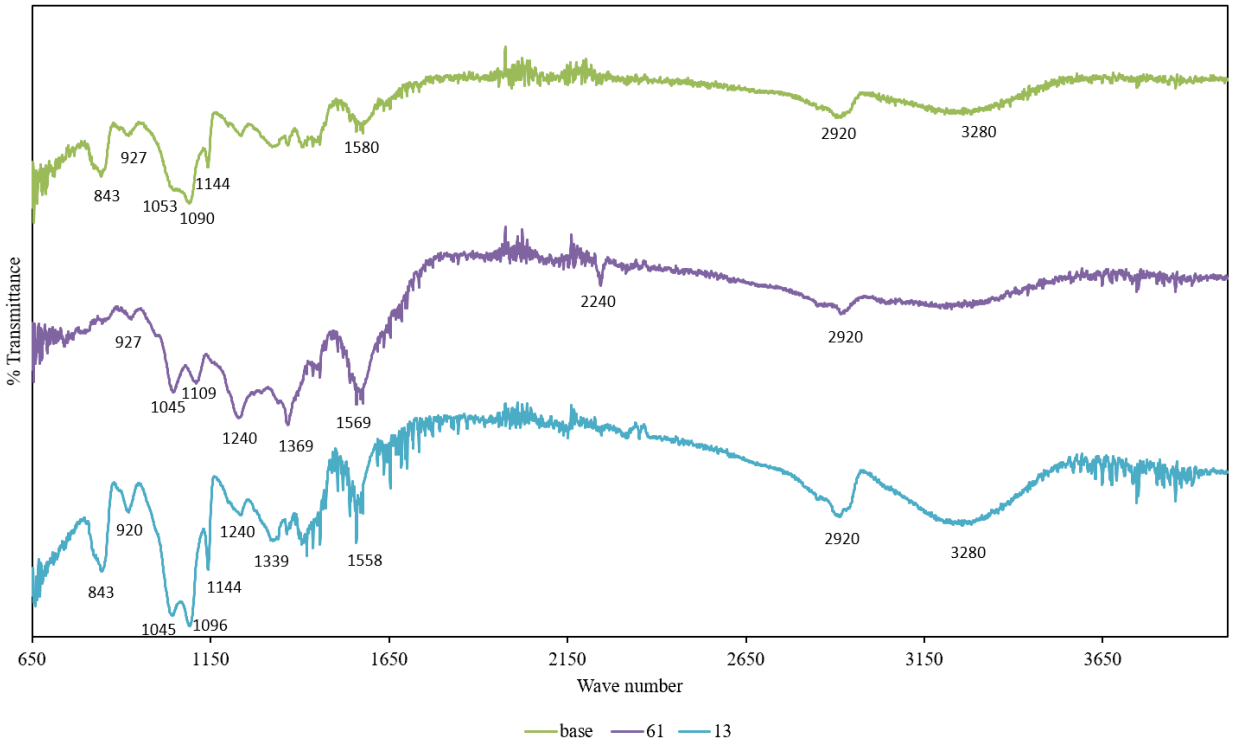

Figure 3.5: FTIR spectroscopy image of the base membrane, membrane 13 and membrane 61

The results of the contact angle measurements are shown in Figure 3.6. They showed that the base membrane had the highest average contact angle of about 53° followed by membrane 61 with 44° and finally the membrane 13 with 32°. Contact angles are known to decrease with the increase in hydrophilic groups which include carboxylic groups (C=O), hydroxyl groups, (C-OH) and epoxy groups (C-O-C) [37,38]. This is because membrane 13 had the highest concentration of PVA compared to membrane 61 and the base membrane, which introduced hydrophilic groups, which in turn decreased the contact angle of the membrane. This increase in the hydrophilicity of the membrane with increase in concentration of PVA has been observed by Li et al. in their PVDF/PVA hollow fibre membrane [37]. The base membrane likely had the highest contact angle as it had the least amount of hydrophilic groups introduced from the PVA, KOH, Pam-OH components present in higher concentrations in membranes 13 and 61 compared to the base

membrane. These components all contributed to the lowering of the contact angles in these 2 membranes by introducing hydrophilic groups. These results align with the results observed from the FTIR imaging results from Figure 3.5.

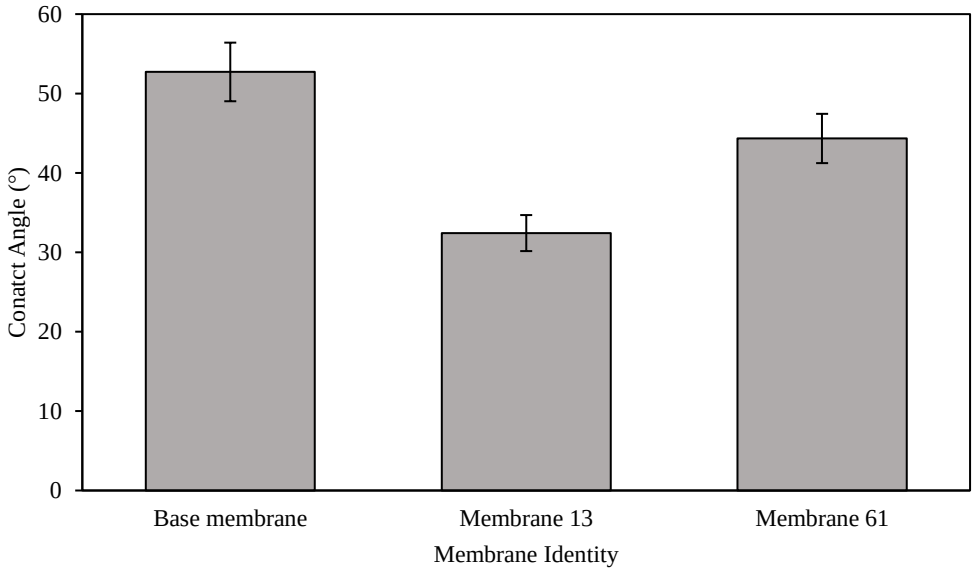

Figure 3.6: Contact angle measurements of the base membrane, membrane 13 and membrane 61.

3.4.3 Factorial design study for CO_2/N_2 and CO_2/CH_4 selectivity

As mentioned earlier, for the optimization study, a 2^6-level factorial design was used which led to 64 experiments with additional three error (base) experiments. Table 3.5 shows the maximum and minimum permeability and selectivity values out of the 64 experiments observed for each gas pair.

Table 3.5: Maximum and minimum permeability and selectivity data observed in this study. Permeability values were based on active layer thickness.

Category	Maximum	Minimum
CO_2 Permeability (Barrer)	81,552	884
N_2 Permeability (Barrer)	81,544	690
CH_4 Permeability (Barrer)	80,111	622
CO_2/CH_4 (-)	2.45	0.51
CO_2/N_2 (-)	1.83	0.77
N_2/CH_4 (-)	2.22	0.52

The highest permeability for each of the gas shown in Table 3.5 and membrane 40 in Table 3.7 in the appendix was achieved with lower limits of PVA (0.21 wt%), KOH (0.3 wt%) and AIBA (0.3 wt%) whereas with upper limits of formaldehyde (2.07wt%) water (86.65 wt%), and Pam-OH's (0.7 wt%). Here, Pam-OH is used instead of Pam-HCl as Pam-OH was the component of interest made from Pam-HCl and KOH as described in the procedure above. Contrastingly, the lowest permeability for each gas as shown in Table 3.5 and membrane 8 in Table 3.7 in the appendix was noted with upper limits of PVA (3.6 wt%), formaldehyde (2.07 wt%), water (86.65 wt%) and Pam-OH (0.7 wt%) and with lower limits for KOH (0.3 wt%) and AIBA (0.3 wt%). The membrane mixtures were observed to have a high viscosity when both the PVA and formaldehyde concentrations were higher as this allowed for more cross-linking during the 3 hour 35 minute heating time. These results show that the permeability of the membranes was determined mostly by the amount of cross-linking between the PVA and the formaldehyde as the membranes with the lowest permeabilities had high PVA and formaldehyde concentrations and the membranes with the higher permeabilities had the lower PVA and formaldehyde concentrations. With a decrease in the permeability of the membrane with higher PVA and formaldehyde concentrations there is an increase in the selectivity for CO_2 over N_2 due to the trade-off between selectivity and permeability[21]. This can be seen from Table 3.7 in the appendix. The membranes with higher PVA and formaldehyde concentrations generally have the higher CO_2/N_2 selectivities as shown by membranes 8 and 13. All the experiments with the lower especially PVA concentrations generally had a lower CO_2/N_2 selectivity of about 1 as shown by membranes 33-64. This observation is also seen in Figure 3.9 where PVA had the most impact on CO_2/N_2 selectivity. It could therefore be hypothesized that a longer cross-linking duration at the 80°C would lead to more water evaporation and therefore have the same effect as increasing the concentration of both PVA and formaldehyde.

Overall, according to the data displayed by membrane 61 in Table 3.4, PVA amine based polymeric membranes developed for this research project were optimized to have the highest selectivity for CO_2 over CH_4 when the upper concentrations of Pam-OH, KOH and AIBA and lower concentrations of PVA, formaldehyde and water were used. This could be because of the membrane defects, specifically small pore membrane defects characterized by Knudsen flow. This Knudsen flow could be responsible for the higher CO_2/CH_4 selectivity and the lower CO_2/N_2 selectivity shown by membrane 61 as there is some selectivity with this type of flow brought about by the interaction between the permeant and the membrane pore walls. The low CO_2/N_2 selectivity could be because of the comparable interaction of both CO_2 and N_2 with the membrane walls. There could also be competing transport through the defects and through the membrane causing a high CO_2 and N_2 permeability but causing low CH_4 permeability[17].

On the other hand, with membrane 13, there was an increased PVA concentration leading to an increase in cross-linking of the membrane. The increase in PVA concentration also resulted in the primary amines as seen from the FTIR spectra. This is because a higher concentration of PVA means a higher concentration of carbonyl groups which come from the interaction between PVA and AIBA. The higher degree of cross-linking in membrane 13 likely caused facilitated transport to be the main form of transport through the membrane hence leading to CO_2 having a much higher permeability than N_2[39].

The permeability of CH_4 was slightly higher than that of CO_2 where the inverse was expected to be true. This inverse selectivity could be explained once more through the small pore defects causing Knudsen flow through the membrane. Membrane 13 had defects which caused it to have a similar selectivity for CO_2 and CH_4 as the defects likely affected the transport of the more

selective permeant, CO_2 more than that of CH_4 as facilitated transport was likely the major form of transport through this membrane 13. Similar observations have been seen in literature with the direct relationship between membrane defects and decrease in selectivity for the selective penetrant transported through facilitated transport[40,41]. The defects were presumed to affect the CO_2 more than the CH_4 as it was interacting with the membrane unlike the uncharged CH_4 and N_2.

3.4.3.1 Factorial design

The figures shown in this section use the notation of A, B, C, D, E, and F to represent the component factors manipulated where A corresponds to PVA, B is formaldehyde, C is water, D is PAM-OH, E is KOH and F represents AIBA. This was done for easy data representation. All charts have component factor definition displayed on the x-axis and $\hat{\beta}_i$ weight factor value from each individual or combined component factor shown on the y-axis. The most and least heavy individual as well as combined factors for CH_4/N_2 selectivity are shown in Figure 3.7. The higher the weight factor, the higher would be its effect on the selectivity value.

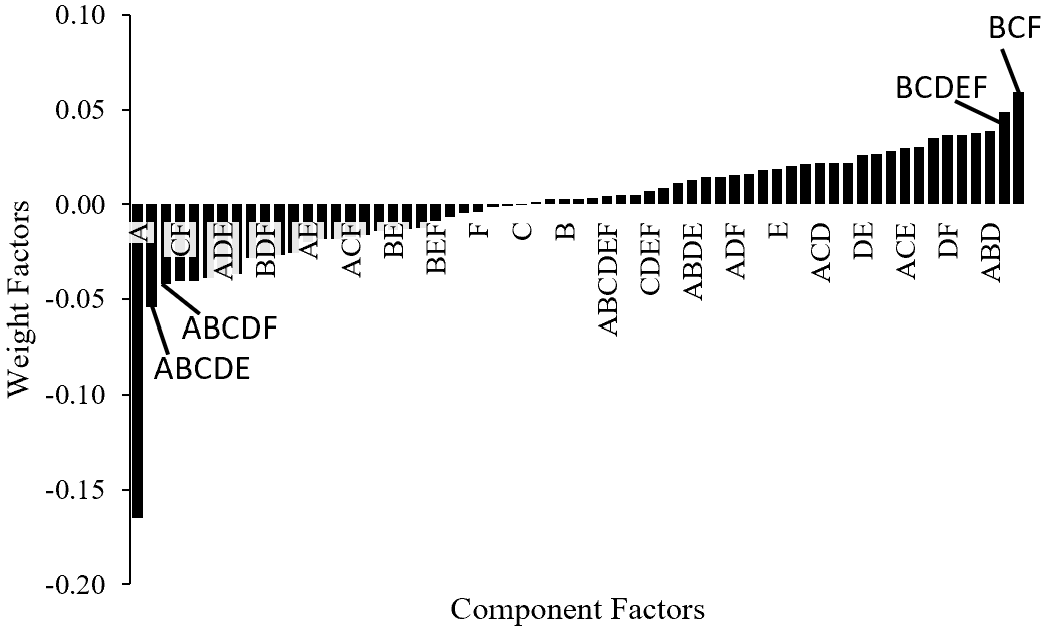

Figure 3.7: Weight factors of individual and combined component factors for CH_4/N_2 selectivity.

Figure 3.7 relays that E or KOH, most positively affects the selectivity of methane over nitrogen since it had the highest weight factor as an individual component. A or PVA on the other hand, most negatively affects methane to nitrogen selectivity as an individual component factor, since it had the most negative weight factor. Overall, the combined effect of BCF formaldehyde, water and AIBA positively affects methane's selectivity over nitrogen the most whereas A, PVA alone negatively affects methane's selectivity over nitrogen the most. From these results it can be inferred that the selectivity of methane over nitrogen is favored when there is the least amount of cross-linking and more hydroxyl and amine groups.

The most and least heavy individual as well as combined factors for CO_2/CH_4 selectivity are shown in Figure 3.8.

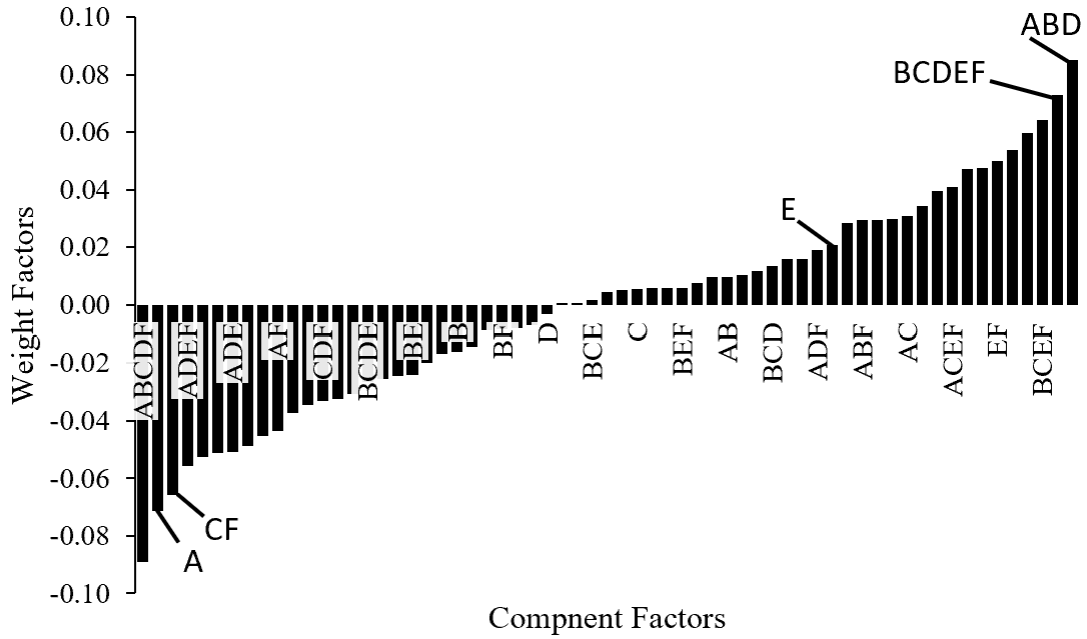

Figure 3.8: Weight factors of individual and combined component factors for CO_2/CH_4 selectivity.

According to Figure 3.8, for CO_2/CH_4 selectivity factor E or KOH positively affects the selectivity of methane the most as an individual component factor, whereas A or PVA has the most negative effect as an individual component factor. Alternatively, overall and in terms of combined factors ABD or combination of PVA, formaldehyde and Pam-OH positively affects CO_2/CH_4 selectivity the most, whereas ABCDF or PVA, formaldehyde, water, Pam-OH and AIBA combined had the most negative effect on the CO_2/CH_4 selectivity. These results show that for the separation of CO_2 from CH_4, as shown by membrane 61, the amount of cross-linking between PVA and formaldehyde is not as important rather what could be more important for CO_2/CH_4 selectivity is the formation of nitrile/ amine groups imparted by the Pam-OH, the amine carrier.

The most and least heavy individual as well as combined factors for CO_2/N_2 selectivity are shown in Figure 3.9.

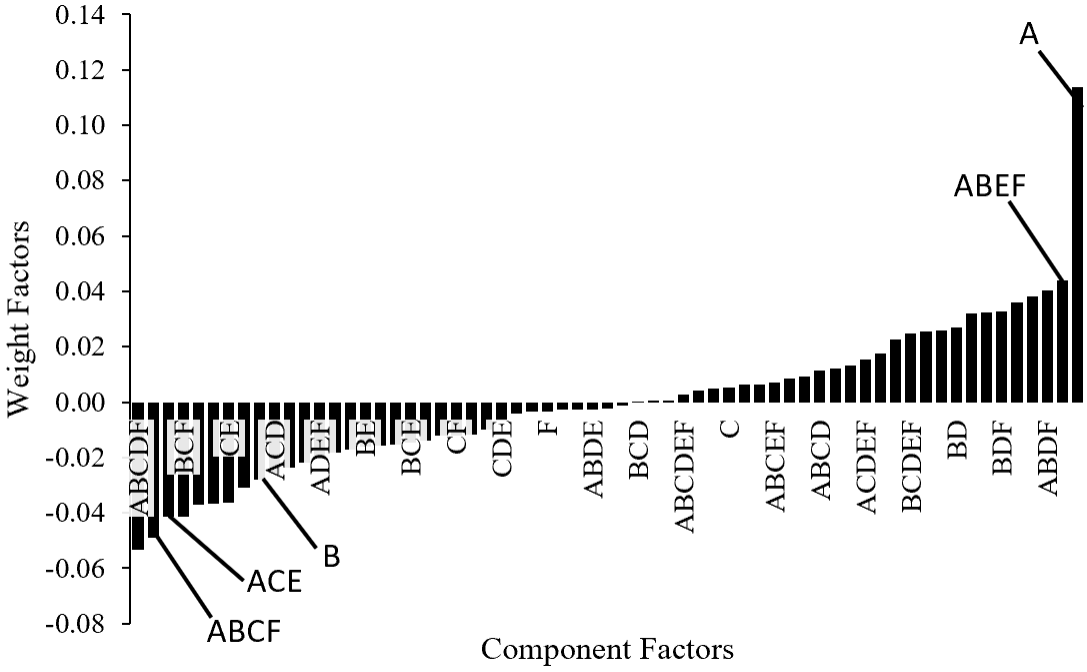

Figure 3.9: Weight factors of individual and combined component factors for CO_2/N_2 selectivity

Figure 3.9 portrays that individual component factor A or PVA positively affects the selectivity of carbon dioxide over nitrogen the most, whereas individual factor B or formaldehyde most negatively affects it. In terms of overall effects, A most positively affects CO_2 permeation over N_2 while a combination of PVA, formaldehyde, water, Pam-OH and AIBA; ABCDF together have the most negative effect on CO_2 permeation over N_2. The positive effect of PVA on CO_2 permeation over N_2 permeation was also observed by many researchers[42–45]. Yet PVA alone cannot positively aid CO_2 permeation, it requires cross-linking from compounds such as formaldehyde[16]. As previously described, with increase in PVA concentration and increase in cross-linking CO_2 becomes mainly transported through facilitated transport and because CO_2 is

able to interact with the membrane due to its electrostatic properties, its permeability dominates over the uncharged N_2.

3.4.4 Literature Comparison

The better performing CO_2/CH_4 optimized membrane, membrane 61, was compared to the Robeson plot and other polymeric membranes found in literature as shown in Table 3.6 and Figure 3.10.

Table 3.6: Comparison with membranes from literature

Membrane	CO_2 permeability (Barrers)	CO_2/CH_4	Temperature (°C)	Feed Pressure absolute (atm)	Reference
PEBAX	150	7.5	55	15.8	[46]
PAAm-PVA	$2.4 X10^5$	58	25	1	[15]
$PTMEG_{0.8}$+PEBAX	325	22.5	25	15.8	[46]
XL-PEGDA	145	19.86	35	2.2	[47]
PEBAX/PA-PPG	79.7	14.0	25	1	[48]
TZPIM	3076	24	25	-	[49]
PIM-7	1100	17.74	30	1.3	[50]
PIM-1	2300	18.5	30	1.2	[50]
PIM-CO15	2000	15.38	30	1.5	[51]
Bio-PITB-2 (air-100)	1161	26	35	1	[52]
Bio-PITB-1 (vac)	1123	23	35	1	[52]
Bio-PITB-1(vac-100)	1008	25	35	1	[52]
Bio-PITB-1 (air-100)	1076	25	35	1	[52]
Bio-PITB-2 (vac)	1201	24	35	1	[52]
Bio-PITB-2 (vac-100)	1087	27	35	1	[52]
Bio-PITB-2 (air)	1384	23	35	1	[52]
Bio-PITB-1 (air)	1352	23	35	1	[52]
PIM-CO19	6100	10.52	30	1.5	[51]
PDMS	3800	28	35	1	[53]
This work-61	$3.24X10^4$	2.45	23	2.5	-
PTMSP	28010	2.2	20-25	-	[54]

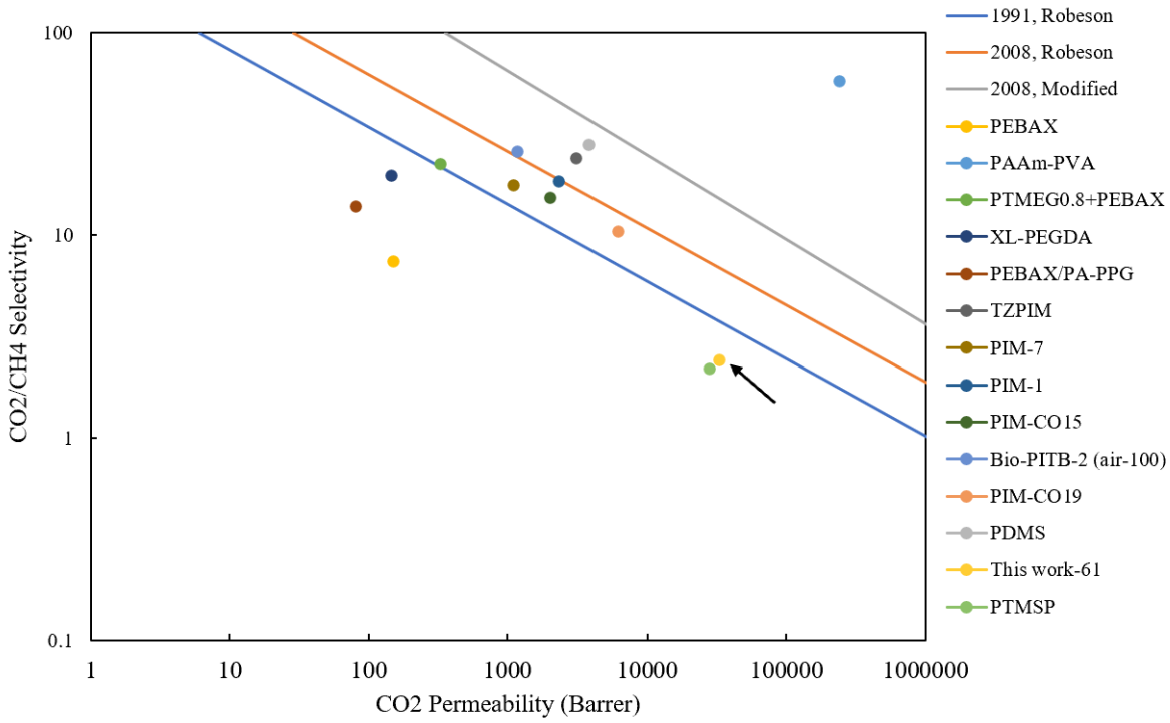

Figure 3.10: Comparison with membranes from literature and Robeson plot.

When compared to other membranes in the literature, the membrane optimized in this study has much higher permeability but much lower CO_2/CH_4 selectivity, a common trade-off noted by Robeson[55]. This shows that the membrane's performance could potentially be improved by lowering its permeability by making thicker membranes. This would increase the resistance of the membrane to the penetrants thereby lowering their permeabilities. They could also be improved further by incorporating adsorbents in the making of mixed matrix membranes[36]. When compared to the 1991 upper Robeson line, the optimized membrane fairs well but doesn't fair well when compared to the 2008 Robeson and the modified 2008 Robeson upper bound line as shown in Figure 3.10.

3.5 CONCLUSIONS

PVA based polymer membranes were chosen to work with as they provide a cost effective, environmentally friendly, are adaptable, and energy efficient solution to gas separation. Furthermore, membranes can be easily retrofitted for post combustion and biogas applications. In this project, an adapted membranes from Zou and Ho's procedure were prepared and tested at atmospheric conditions and their performance was optimized at these conditions. Aging tests were done first to determine the appropriate membrane testing/ use time which was established to be 21 days after which the physical aging of the membrane had slowed down. The optimization was done through a 2^6 factorial design using the membrane forming components PVA, formaldehyde, water, AIBA, KOH and Pam-OH. This design used the CO_2/N_2 and CO_2/CH_4 selectivities to optimize the membrane. The experiments were conducted at room temperature and 2.5 atm operating pressure.

Out of 64 experiments and 3 error experiments it was established that the maximum permeability was achieved by CO_2 at 81,552 Barrer followed by N_2 and CH_4 at 81.544 Barrer and 80,111Barrer, respectively. The highest membrane separation selectivity of 2.45 was achieved with the CO_2/CH_4 pair where the combination of PVA, formaldehyde and Poly (allylamine hydroxide) most positively affected CO_2 selectivity over CH_4.. The most optimized CO_2/N_2 selective membrane obtained a lower maximum selectivity of 1.83, with PVA being the sole component that most positively affected CO_2 selectivity over N_2. CO_2/N_2 separation was most positively affected by the PVA concentration and CO_2/CH_4 separation was most positively affected by a combination of PVA, formaldehyde and Pam-OH components. Although the selectivities didn't drastically vary with optimization, the wide range in the permeabilities observed (from 600 to 80,000 Barrer) did

foreshadow the potential of the membrane when used with a filler in making mixed-matrix membrane.

3.6 APPENDIX

Table 3.7: Summary of results from factorial design

Experiment number	A	B	C	D	E	F	N_2 permeability	CH_4 Permeability	CO_2 Permeability	CO_2/CH4	CO_2/N_2
1	1	-1	-1	-1	-1	-1	2,648	3,974	3,051	0.77	1.15
2	1	1	-1	-1	-1	-1	1,144	1,089	1,201	1.10	1.05
3	1	-1	1	-1	-1	-1	1,603	1,334	2,153	1.61	1.34
4	1	1	1	-1	-1	-1	5,109	6,481	6,786	1.05	1.33
5	1	-1	-1	1	-1	-1	2,669	4,083	3,238	0.79	1.21
6	1	1	-1	1	-1	-1	1,419	2,353	1,189	0.51	0.84
7	1	-1	1	1	-1	-1	24,699	43,709	24,391	0.56	0.99
8	1	1	1	1	-1	-1	690	622	1,215	1.95	1.76
9	1	-1	-1	-1	1	-1	4,245	6,248	6,216	0.99	1.46
10	1	1	-1	-1	1	-1	10,848	18,218	13,475	0.74	1.24
11	1	-1	1	-1	1	-1	2,192	2,018	2,774	1.37	1.27
12	1	1	1	-1	1	-1	2,743	2,924	3,026	1.03	1.10
13	1	-1	-1	1	1	-1	10,994	21,354	20,114	0.94	1.83
14	1	1	-1	1	1	-1	881	943	884	0.94	1.00
15	1	-1	1	1	1	-1	3,992	5,042	4,709	0.93	1.18
16	1	1	1	1	1	-1	4,971	8,078	4,872	0.60	0.98
17	1	-1	-1	-1	-1	1	2,612	3,652	3,283	0.90	1.26
18	1	1	-1	-1	-1	1	1,840	2,657	1,446	0.54	0.79
19	1	-1	1	-1	-1	1	4,978	9,501	6,873	0.72	1.38
20	1	1	1	-1	-1	1	4,474	7,160	4,706	0.66	1.05
21	1	-1	-1	1	-1	1	4,726	6,178	5,395	0.87	1.14
22	1	1	-1	1	-1	1	2,208	2,817	3,219	1.14	1.46
23	1	-1	1	1	-1	1	2,678	3,868	3,597	0.93	1.34

Experiment number	A	B	C	D	E	F	N_2 permeability	CH_4 Permeability	CO_2 Permeability	$CO_2/CH4$	CO_2/N_2
24	1	1	1	1	-1	1	5,298	6,043	5,203	0.86	0.98
25	1	-1	-1	-1	1	1	7,203	7,836	10,664	1.36	1.48
26	1	1	-1	-1	1	1	5,591	7,363	6,101	0.83	1.09
27	1	-1	1	-1	1	1	2,751	5,017	4,496	0.90	1.63
28	1	1	1	-1	1	1	1,457	1,617	1,818	1.12	1.25
29	1	-1	-1	1	1	1	4,002	5,204	4,066	0.78	1.02
30	1	1	-1	1	1	1	13,195	18,198	20,735	1.14	1.57
31	1	-1	1	1	1	1	6,070	10,023	5,971	0.60	0.98
32	1	1	1	1	1	1	6,193	6,838	6,822	1.00	1.10
33	-1	-1	-1	-1	-1	-1	76,059	70,993	73,897	1.04	0.97
34	-1	1	-1	-1	-1	-1	75,216	73,275	75,168	1.03	1.00
35	-1	-1	1	-1	-1	-1	74,986	71,957	75,013	1.04	1.00
36	-1	1	1	-1	-1	-1	74,824	71,319	76,211	1.07	1.02
37	-1	-1	-1	1	-1	-1	81,267	79,442	79,732	1.00	0.98
38	-1	1	-1	1	-1	-1	72,554	70,325	69,851	0.99	0.96
39	-1	-1	1	1	-1	-1	68,069	55,591	64,339	1.16	0.95
40	-1	1	1	1	-1	-1	81,544	79,886	81,552	1.02	1.00
41	-1	-1	-1	-1	1	-1	72,369	69,914	75,145	1.07	1.04
42	-1	1	-1	-1	1	-1	61,992	60,520	64,980	1.07	1.05
43	-1	-1	1	-1	1	-1	69,465	68,799	67,228	0.98	0.97
44	-1	1	1	-1	1	-1	48,614	45,532	53,627	1.18	1.10
45	-1	-1	-1	1	1	-1	30,858	26,552	23,818	0.90	0.77
46	-1	1	-1	1	1	-1	38,370	29,777	39,185	1.32	1.02
47	-1	-1	1	1	1	-1	37,635	33,473	43,501	1.30	1.16
48	-1	1	1	1	1	-1	70,202	69,525	70,443	1.01	1.00
49	-1	-1	-1	-1	-1	1	73,343	69,936	72,065	1.03	0.98

Experiment number	A	B	C	D	E	F	N_2 permeability	CH_4 Permeability	CO_2 Permeability	CO_2/CH4	CO_2/N_2
50	-1	1	-1	-1	-1	1	80,803	80,111	79,756	1.00	0.99
51	-1	-1	1	-1	-1	1	71,529	64,227	69,475	1.08	0.97
52	-1	1	1	-1	-1	1	69,967	59,744	71,682	1.20	1.02
53	-1	-1	-1	1	-1	1	75,968	74,563	74,529	1.00	0.98
54	-1	1	-1	1	-1	1	78,013	75,965	76,187	1.00	0.98
55	-1	-1	1	1	-1	1	74,254	70,909	69,964	0.99	0.94
56	-1	1	1	1	-1	1	76,405	74,018	75,238	1.02	0.98
57	-1	-1	-1	-1	1	1	60,364	61,206	59,685	0.98	0.99
58	-1	1	-1	-1	1	1	70,237	69,835	74,640	1.07	1.06
59	-1	-1	1	-1	1	1	50,490	52,177	52,657	1.01	1.04
60	-1	1	1	-1	1	1	63,761	60,683	66,473	1.10	1.04
61	-1	-1	-1	1	1	1	29,442	13,242	32,405	2.45	1.10
62	-1	1	-1	1	1	1	66,420	61,405	65,661	1.07	0.99
63	-1	-1	1	1	1	1	44,479	44,841	44,778	1.00	1.01
64	-1	1	1	1	1	1	69,148	59,480	63,067	1.06	0.91
65	0	0	0	0	0	0	80,459	80,318	80,456	1.00	1.00
66	0	0	0	0	0	0	75,374	74,599	76,501	1.03	1.01
67	0	0	0	0	0	0	73,958	72,191	72,809	1.01	0.98

3.7 NOMENCLATURE

A	Area of membrane (cm^2)
Barrer	10^{-10} cm^3(STP)cm/scm^2cmHg
F_i	Volumetric flow rate of component i at STP conditions (cm^3/s)
P_i	Permeability of the membrane for component i where i can be either CO_2, CH_4 or N_2 (Barrer)
p_{STP}	Pressure of 1 mol of gas at STP, 760cmHg was used (cmHg)
p_{feed}	Pressure of feed gas (psi)
T_{STP}	Temperature of 1 mol of gas at STP conditions, 273.15K was used (Kelvin)
T_{feed}	Temperature of feed gas (Kelvin)

3.8 GREEK SYMBOLS

$\alpha^*_{1/2}$	Ideal selectivity based on pure component data
Δp	Pressure difference measured at feed and permeate side (psi)

3.9 ABBREVIATIONS

AIBA	2-Aminoisobutyric acid, also referred to as F
Bio-PITB-1	Polyimide incorporating Tröger's Base
Btu	British Thermal Unit
C=O	Carboxyl
CCS	Carbon Capture and Storage
C-O-C	Epoxy
FTIR	Fourier Transform Infrared
IPCC	Intergovernmental Panel on Climate Change
KOH	Potassium hydroxide, also referred to as E
N-H	Amine
O-H	Hydroxyl
PAAm-PVA	Polyallylamine-poly(vinyl alcohol)
Pam-OH	Poly (allylamine hydroxide) also referred to as D
PAN	Polyacrilonitrile
PDMS	Poly(dimethylsiloxane)
PEBAX	Polyether block amine
PEBAX/ PA-PPG	Polyether block amine / Poly(amide-c-poly(propylene glycol))
PIM-1	Polymers of intrinsic microporosity-1
PIM-7	Polymers of intrinsic microporosity-2
PIM-CO-15	Polymers of intrinsic microporosity-CO-15
PIM-CO-19	Polymers of intrinsic microporosity-CO-19
PTMEG+PEBAX	Poly(tetramethylene ether) glycol + Polyether block amine
PTMSP	poly[1-(trimethylsilyl)-1-propyne]
PVA	Polyvinyl alcohol, also referred to as A
PVDF	Polyvinylidene difluoride
SEM	Scanning Electron Microscope
STP	Standard Temperature Pressure conditions, 1 atmosphere, 76cmHg and 273.15K
TZPIM	Tetrazole-modified polymers of intrinsic microporosity
VCA	Video Contact Angle
XL-PEGDA	Cross linked poly(ethylene glycil) diacrylate

3.10 REFERENCES

[1] IPCC News from Policy and Legislation News from Policy and Legislation Intergovernmental Panel on Climate Change IPCC Second Assessment Synthesis of Scientific-Technical Information Relevant to Interpreting Article 2 of the UN Framework Convention on Climate Change 1995', n.d.

[2] C. McGlade, P. Ekins, The geographical distribution of fossil fuels unused when limiting global warming to 2°C, Nature. 517 (2015) 187–190. https://doi.org/10.1038/nature14016.

[3] UNEP, Handbook on data reporting under the Montreal Protocol, 1999.

[4] V. Popovski, The Implementation of the Paris Agreement on Climate Change, First edit, Routledge, London, 2018.

[5] Intergovernmental Panel on Climate Change (IPCC) third assessment report : hearing before the Committee on Commerce, Science, and Transportation, United States Senate, One Hundred Seventh Congress, first session, May 1, 2001., Intergov. Panel Clim. Chang. Third Assess. Rep. Hear. before Comm. Commer. Sci. Transp. United States Senat. One Hundred Seventh Congr. First Sess. May 1, 2001. . (2004). https://heinonline.org/HOL/Page?handle=hein.cbhear/cbhearings71893&id=1&div=&collection=congrec (accessed June 16, 2021).

[6] J. Kerr, Changing Ecosystems: Effects of global warming, Facts on File, Inc., New York, 2010.

[7] N.R. Table, N.R. Table, I. Isbn, P. Downloaded, S.P. Books, S.P. Books, Canada ' s options for a domestic greenhouse gas emissions trading program, 2020.

[8] J.A. Dunne, S.C. Jackson, J. Harte, Greenhouse Effect, Encycl. Biodivers. Second Ed. 4

(2013) 18–32. https://doi.org/10.1016/B978-0-12-384719-5.00068-X.

[9] International Energy Agency (IEA), World Energy Outlook 2019, OECD, 2019. https://doi.org/10.1787/caf32f3b-en.

[10] J. Gibbins, H. Chalmers, Chapter 2. Fossil Power Generation with Carbon Capture and Storage (CCS): Policy Development for Technology Deployment, Carbon Capture. (2010) 41–64. https://doi.org/10.1039/9781847559715-00041.

[11] M. Stewart, K. Arnold, Gas Sweetening and Processing Field Manual, Gas Sweeten. Process. F. Man. (2011).

[12] N. Norahim, P. Yaisanga, K. Faungnawakij, T. Charinpanitkul, C. Klaysom, Recent Membrane Developments for CO2 Separation and Capture, Chem. Eng. Technol. 41 (2018) 211–223. https://doi.org/10.1002/CEAT.201700406.

[13] A. Lowe, B. Beasley, T. Berly, Chapter 3. Carbon Capture and Storage (CCS) in Australia, Carbon Capture. (2010) 65–101. https://doi.org/10.1039/9781847559715-00065.

[14] H. Liu, R. Idem, P. Tontiwachwuthikul, Post-combustion CO_2 Capture Technology, Springer International Publishing, Regina, 2019. https://doi.org/10.1007/978-3-030-00922-9.

[15] Y. Cai, Z. Wang, C. Yi, Y. Bai, J. Wang, S. Wang, Gas transport property of polyallylamine-poly(vinyl alcohol)/polysulfone composite membranes, J. Memb. Sci. 310 (2008) 184–196. https://doi.org/10.1016/j.memsci.2007.10.052.

[16] J. Zou, W.S.W. Ho, CO2-selective polymeric membranes containing amines in crosslinked poly(vinyl alcohol), J. Memb. Sci. 286 (2006) 310–321. https://doi.org/10.1016/j.memsci.2006.10.013.

[17] J.D. Seader, E.J. Henley, Separation process principles, Choice Rev. Online. 36 (1999) 36-

5112-36–5112. https://doi.org/10.5860/choice.36-5112.

[18] L.M. Robeson, The upper bound revisited, J. Memb. Sci. 320 (2008) 390–400. https://doi.org/10.1016/j.memsci.2008.04.030.

[19] E.P. Favvas, A. Figoli, R. Castro-Muñoz, V. Fíla, X. He, Polymeric membrane materials for CO_2 separations, 2018. https://doi.org/10.1016/B978-0-12-813645-4.00001-5.

[20] T.E. Rufford, S. Smart, G.C.Y. Watson, B.F. Graham, J. Boxall, J.C. Diniz da Costa, E.F. May, The removal of CO_2 and N_2 from natural gas: A review of conventional and emerging process technologies, J. Pet. Sci. Eng. 94–95 (2012) 123–154. https://doi.org/10.1016/j.petrol.2012.06.016.

[21] B.D. Freeman, Basis of Permeability/Selectivity Tradeoff Relations in Polymeric Gas Separation Membranes, Macromolecules. 32 (1999) 375–380. https://doi.org/10.1021/MA9814548.

[22] K. Hinkelmann, O. Kempthorne, Design and Analysis of Experiments: Second Edition, Des. Anal. Exp. Second Ed. 1 (2007) 1–641. https://doi.org/10.1002/9780470191750.

[23] M.S. Abdul Wahab, A.R. Sunarti, N.H. Ramli, A.L. Ahmad, 24 fractional factorial design for PVDF/Pebax film composite synthesis on gas selectivity study, IOP Conf. Ser. Mater. Sci. Eng. 702 (2019) 012046. https://doi.org/10.1088/1757-899X/702/1/012046.

[24] S. Gagné, G. Chowdhury, T. Matsuura, B. Laverty, Optimization of CO_2-CH_4 Separation Performance of Integrally Skinned Asymmetric Membranes Prepared from Poly(2,6-dimethyl-1,4-phenylene oxide) by Factorial Design, J Appl Polym Sci. 72 (1999) 1601–1610. https://doi.org/10.1002/(SICI)1097-4628(19990620)72:12.

[25] D. Wu, H. Cao, N. Lv, al -, K.R. Raj, A.R. Sunarti, Preliminary Fractional Factorial Design (FFD) study using incorporation of Graphene Oxide in PVC in mixed matrix membrane to

enhance CO_2/CH_4 separation, IOP Conf. Ser. Mater. Sci. Eng. 702 (2019) 012041. https://doi.org/10.1088/1757-899X/702/1/012041.

[26] A.A. Ghazali, R.K. Roshan, S. Abd Rahman, M.S. Abdul Wahab, N.S. Hazleen, N. Mandayar, 23 fractional factorial design for polymer based thin film composite (TFC) membrane synthesis for CO_2/CH_4 separation, IOP Conf. Ser. Mater. Sci. Eng. 702 (2019) 012049. https://doi.org/10.1088/1757-899X/702/1/012049.

[27] A. Dean, D. Voss, D. Draguljić, Design and Analysis of Experiments, (2017). https://doi.org/10.1007/978-3-319-52250-0.

[28] R.L. Mason, R.F. Gunst, J.L. Hess, Factorial Experiments in Completely Randomized Designs, Stat. Des. Anal. Exp. (2003) 140–169. https://doi.org/10.1002/0471458503.CH5.

[29] Y. Li, J. Deng, J. Zhang, Porous poly(vinyl formal) foam prepared using poly(vinyl alcohol) of low degree of polymerization, Polym. Int. 67 (2018) 1438–1444. https://doi.org/10.1002/PI.5666.

[30] P. Bernardo, F. Bazzarelli, F. Tasselli, G. Clarizia, C.R. Mason, L. Maynard-Atem, P.M. Budd, M. Lanč, K. Pilnáček, O. Vopička, K. Friess, D. Fritsch, Y.P. Yampolskii, V. Shantarovich, J.C. Jansen, Effect of physical aging on the gas transport and sorption in PIM-1 membranes, Polymer (Guildf). 113 (2017) 283–294. https://doi.org/10.1016/J.POLYMER.2016.10.040.

[31] Y. Kudo, H. Mikami, M. Tanaka, T. Isaji, K. Odaka, M. Yamato, H. Kawakami, Mixed matrix membranes comprising a polymer of intrinsic microporosity loaded with surface-modified non-porous pearl-necklace nanoparticles, J. Memb. Sci. 597 (2020) 117627. https://doi.org/10.1016/j.memsci.2019.117627.

[32] R. Singh, Introduction to Membrane Technology, Elsevier Ltd., Colorado Springs, 2015.

[33] M.M. Merrick, R. Sujanani, B.D. Freeman, Glassy polymers: Historical findings, membrane applications, and unresolved questions regarding physical aging, Polymer (Guildf). 211 (2020) 123176. https://doi.org/10.1016/J.POLYMER.2020.123176.

[34] Y. Huang, X. Wang, D.R. Paul, Physical aging of thin glassy polymer films: Free volume interpretation, J. Memb. Sci. 277 (2006) 219–229. https://doi.org/10.1016/J.MEMSCI.2005.10.032.

[35] J. Coates, Interpretation of Infrared Spectra, A Practical Approach, (n.d.) 10815–10837.

[36] M. Barooah, B. Mandal, Synthesis, characterization and CO_2 separation performance of novel PVA/PG/ZIF-8 mixed matrix membrane, J. Memb. Sci. 572 (2019) 198–209. https://doi.org/10.1016/J.MEMSCI.2018.11.001.

[37] N. Li, C. Xiao, S. An, X. Hu, Preparation and properties of PVDF/PVA hollow fiber membranes, Desalination. 250 (2010) 530–537. https://doi.org/10.1016/J.DESAL.2008.10.027.

[38] G. Hurwitz, G.R. Guillen, E.M.V. Hoek, Probing polyamide membrane surface charge, zeta potential, wettability, and hydrophilicity with contact angle measurements, J. Memb. Sci. 349 (2010) 349–357. https://doi.org/10.1016/J.MEMSCI.2009.11.063.

[39] Y. Han, W.S.W. Ho, Recent developments on polymeric membranes for CO_2 capture from flue gas, J. Polym. Eng. 40 (2020) 529–542. https://doi.org/10.1515/polyeng-2019-0298.

[40] J. Han, L. Bai, B. Yang, Y. Bai, S. Luo, S. Zeng, H. Gao, Y. Nie, X. Ji, S. Zhang, X. Zhang, Highly Selective Oxygen/Nitrogen Separation Membrane Engineered Using a Porphyrin-Based Oxygen Carrier, Membr. 2019, Vol. 9, Page 115. 9 (2019) 115. https://doi.org/10.3390/MEMBRANES9090115.

[41] L. Yang, H. Yang, H. Wu, L. Zhang, H. Ma, Y. Liu, Y. Wu, Y. Ren, X. Wu, Z. Jiang, COF

membranes with uniform and exchangeable facilitated transport carriers for efficient carbon capture, J. Mater. Chem. A. 9 (2021) 12636–12643. https://doi.org/10.1039/D0TA12486A.

[42] M.R. Dilshad, A. Islam, B. Haider, A. Sabir, A. Ijaz, R.U. Khan, A.K. Durrani, Novel PVA/PEG nano-composite membranes tethered with surface engineered multi-walled carbon nanotubes for carbon dioxide separation, Microporous Mesoporous Mater. 308 (2020) 110545. https://doi.org/10.1016/J.MICROMESO.2020.110545.

[43] A.E. Amooghin, M.Z. Pedram, M. Omidkhah, R. Yegani, A novel CO_2-selective synthesized amine-impregnated cross-linked polyvinylalcohol/glutaraldehyde membrane: fabrication, characterization, and gas permeation study, Greenh. Gases Sci. Technol. 3 (2013) 378–391. https://doi.org/10.1002/GHG.1369.

[44] A. Mondal, B. Mandal, Synthesis and characterization of crosslinked poly(vinyl alcohol)/poly (allylamine)/2-amino-2-hydroxymethyl-1,3-propanediol/polysulfone composite membrane for CO_2/N_2 separation, (2013). https://doi.org/10.1016/j.memsci.2013.06.052.

[45] H. Shirvani, S. Maghami, A.P. Isfahani, M. Sadeghi, Influence of blend composition and silica nanoparticles on the morphology and gas separation performance of PU/PVA blend membranes, Membranes (Basel). 9 (2019). https://doi.org/10.3390/membranes9070082.

[46] H. Rabiee, A. Ghadimi, S. Abbasi, T. Mohammadi, CO_2 separation performance of poly(ether-b-amide6)/PTMEG blended membranes: Permeation and sorption properties, Chem. Eng. Res. Des. 98 (2015) 96–106. https://doi.org/10.1016/j.cherd.2015.03.026.

[47] H. Lin, T. Kai, B.D. Freeman, S. Kalakkunnath, D.S. Kalika, The effect of cross-linking on gas permeability in cross-linked poly(ethylene glycol diacrylate), Macromolecules. 38 (2005) 8381–8393. https://doi.org/10.1021/ma0510136.

[48] T. Zhu, X. Yang, Y. Zheng, X. He, F. Chen, J. Luo, Preparation of poly(ether-block-amide)/poly(amide-co-poly(propylene glycol)) random copolymer blend membranes for CO_2/N_2 separation, Polym. Eng. Sci. 59 (2019) E14–E23. https://doi.org/10.1002/pen.24828.

[49] N. Du, H.B. Park, G.P. Robertson, M.M. Dal-Cin, T. Visser, L. Scoles, M.D. Guiver, Polymer nanosieve membranes for CO_2-capture applications, Nat. Mater. 10 (2011) 372–375. https://doi.org/10.1038/nmat2989.

[50] P.M. Budd, K.J. Msayib, C.E. Tattershall, B.S. Ghanem, K.J. Reynolds, N.B. McKeown, D. Fritsch, Gas separation membranes from polymers of intrinsic microporosity, J. Memb. Sci. 251 (2005) 263–269. https://doi.org/10.1016/j.memsci.2005.01.009.

[51] D. Fritsch, G. Bengtson, M. Carta, N.B. McKeown, Synthesis and gas permeation properties of spirobischromane-based polymers of intrinsic microporosity, Macromol. Chem. Phys. 212 (2011) 1137–1146. https://doi.org/10.1002/macp.201100089.

[52] X. Hu, W.H. Lee, J.Y. Bae, J. Zhao, J.S. Kim, Z. Wang, J. Yan, Y.M. Lee, Highly permeable polyimides incorporating Tröger's base (TB) units for gas separation membranes, J. Memb. Sci. 615 (2020) 118533. https://doi.org/10.1016/j.memsci.2020.118533.

[53] M. Mukaddam, E. Litwiller, I. Pinnau, Gas Sorption, Diffusion, and Permeation in Nafion, Macromolecules. 49 (2016) 280–286. https://doi.org/10.1021/acs.macromol.5b02578.

[54] T. Nakagawa, T. Saito, S. Asakawa, Y. Saito, Polyacetylene derivatives as membranes for gas separation, Gas Sep. Purif. 2 (1988) 3–8. https://doi.org/10.1016/0950-4214(88)80035-5.

[55] L.M. Robeson, Correlation of separation factor versus permeability for polymeric membranes, J. Memb. Sci. 62 (1991) 165–185. https://doi.org/10.1016/0376-

7388(91)80060-J.

CHAPTER 4: ZEOLITE-13X- AND ZIF-8 FILLED PVA MIXED MATRIX MEMBRANES FOR USE IN CO_2/N_2 AND CO2/CH4 SEPARATION

4.1 ABSTRACT

Continual global warming has become a global concern for policy makers, particularly the Intergovernmental Panel on Climate Change (IPCC) warning that the earth should not warm more than 2°C higher than pre-industrial revolution temperatures. Separation of carbon dioxide (CO_2) from nitrogen (N_2) has therefore become a topic of interest in order to make fossil fuels a greener and more viable source of energy. Also, separation of CO_2 from methane (CH_4) has also been explored to reduce greenhouse gas emissions from the burning of biogas. This research focuses on the methods of improving the separation of CO_2 from CH_4 and N_2 gases by varying the feed pressure and by using mixed-matrix membranes. Poly vinyl alcohol (PVA) based polymer membranes that had previously been optimized for CO_2/N_2 and CO_2/CH_4 separation were used with and without two different filler materials: the metal organic framework zeolitic imidazolate framework-8 (ZIF-8) filler materials and zeolite 13X fillers. The loaded membranes showed a decrease in CO_2/N_2 and CO_2/CH_4 selectivity with large gas permeabilities. Feed pressure testing showed an increase in the CO_2/N_2 and CO_2/CH_4 separation with a decrease in feed pressure. At 1.5atm-absolute pressure, CO_2/N_2 and CO_2/CH_4 selectivities of 5.94 and 2.13, respectively, were observed with a CO_2 permeability of 15,813 Barrer.

Key words: CO_2/N_2 separation, CO_2/CH_4 separation, polymeric membranes, PVA membranes, mixed matrix membranes.

4.2 INTRODUCTION

Climate change and global warming resulting from greenhouse gases has been a major cause of concern over the last few years. This is because the average global temperatures have already increased by a little over 1°C since 1880 [1]. According to the Intergovernmental Panel on Climate Change (IPCC), this increase has already caused shrinkage of glaciers, thawing of permafrost in addition to later freezing and earlier breakup of ice on rivers and lakes over the last two decades. Moreover, there has also been lengthening of mid to high altitude growing seasons, which has resulted in declines in animal and plant populations as well as earlier flowering of trees, egg-laying of birds and earlier emergence of insects [2]. The negative impact that global warming has had on the seasons has also affected agriculture, which has to already compete with the growing world population. This is why the IPCC has warned that the earth should not warm more than 2°C higher than pre-industrial revolution temperatures as the latter mentioned effects of climate change will worsen [1]. Furthermore, with this growth in world population, the continued globalization and industrialization of third world countries there is a higher energy demand [3]. This all entails the need for an alternative cleaner, greener energy source.

There are five main greenhouse gases in the earth's atmosphere, namely: water vapor (H_2O), carbon dioxide (CO_2), methane (CH_4), nitrous oxide (N_2O) and ozone (O_3). Among these greenhouse gases,CO2 has a long atmospheric lifetime of about 2-20 centuries according to Archer et al and is the reason for the effects of climate change currently being experienced on earth [4]. In fact, the concentration of CO_2 has increased by 35% since preindustrial times. The source of this increase has been mainly attributed to emissions from fossil fuel combustion industries, with approximately 50% of the world's CO_2 emissions being from power generation by fossil fuel combustion [5]. Also, the International Energy Agency World Energy Outlook has predicted that

because of the increased energy demand, fossil fuels will remain significant for many decades to come [6]. Thus, there is a need to reduce the net CO_2 emitted into the atmosphere by power plants. Post-combustion CO_2 capture focuses on the separation of CO_2 from N_2 for application in power plants after the combustion of fossil fuels for energy production [7].

Separation of CO_2 from CH_4 has also been explored for application in natural gas sweetening. This process is necessary as separation of CO_2 lowers the Btu of natural gas, therefore aiding the transportation of natural gas, as well as making the natural gas less corrosive [8]. Different polymeric, inorganic and mixed matrix membranes have been explored in CO_2/N_2 and CO_2/CH_4 separation as they offer an environmentally friendly and cheaper method of gas separation [8,9]. Among polymeric membranes, PVA based membranes have shown a lot of promise when incorporated into gas separation membranes due to their hydrophilic nature as well as their good mechanical stability [10]. Unfortunately, polymeric membranes have been associated with the trade-off between the permeabilities and the selectivities as illustrated by Robeson's curve[18,19]. Facilitated transport membranes make use of the quadruple moment of CO_2 to selectively transport CO_2. This is done by incorporating amines and carboxylic groups which act as carriers and selectively interact with the CO_2 reversibly thus transporting it across the membrane [20]. This mode of transportation is facilitated transport. The other mode of transportation is through a concentration or pressure difference, the solution diffusion model. When combined with amines, PVA facilitated transport membranes have been used to overcome this tradeoff and have shown high gas permeabilities and CO_2/N_2 and CO_2/CH_4 selectivities. Jian Zou and Winston Ho observed a high CO_2/N_2 selectivity of 280 with other research papers reporting similarly high CO_2/N_2 and CO_2/CH_4 selectivities above 50 with different amine based PVA membranes [10–12]. Mixed

matrix membranes where an inorganic material is added to a polymeric membrane have also been explored as a means of overcoming this trade-off.

Different adsorbents that have already showed high gas separation properties have been incorporated into polymeric membranes in the making of these mixed matrix membranes. An example of this is the zeolite 13X adsorbent which exhibited a high CO_2/CH_4 selectivity of 3.957 at 50°C. The selectivity was imparted by the quadruple moment that CO_2 possesses which CH_4 lacks. The quadruple moment allows CO_2 to interact with the negatively charged zeolite 13X frame – negative because of the high Al^- content and balanced by electrostatic interactions with cations [15]. Similar good separation performance of zeolite 13X adsorbents was also seen with CO_2/N_2 [16]. When zeolite 13X was incorporated into polyimide polymeric membranes by Chaidou et al. (2012) it was able to increase the CO_2/N_2 selectivity from 19.1 to 67.1 with a 30wt% 13X loading. The CO_2 permeability of the membrane also increased from 3.67 Barrer to 378 Barrer with a 30wt% 13X loading to polyimide [17].

ZIF-8 (Zeolitic imidazolate Framework-8) has also shown promise in its use as an adsorbent. ZIFs have gained attention because of their molecular sieving effect, their facile synthesis, and their good compatibility with polymers. Because of these properties, ZIFs have been used as adsorbents and in mixed matrix membranes. As an adsorbent, ZIF-8 showed a high CO_2/N_2 selectivity of 11.5 and a high CO_2/N_2 adsorption capacity of 9.603 mmol/g. Amine modified ZIF-8 have shown even higher CO_2/N_2 selectivities and CO_2 adsorption capacities of 31.4 and 31.29, respectively [18,19]. When incorporated into a model polymer matrix Matrimind® 5218, 20wt% ZIF-8 was found to have high CO_2/N_2 and CO_2/CH_4 selectivities of 21.3 and 41.5 respectively [19]. PVA/PG/ZIF-8 mixed matrix membranes have also shown a high CO_2/N_2 selectivity of 370 with a 5wt% loading

of ZIF-8 [20]. However, mixed matrix membranes often have the formation of defects caused by agglomeration of the nanoparticles causing the formation of pinholes. The transport through these pinholes can be characterized as either Knudsen flow or viscous flow depending on the size of the pinholes created. Transportation though Knudsen flow involves interaction of the permeants with the membrane walls causing there to be some selectivity however transportation through viscous flow is not selective [26, 27].

This paper focuses on the effect of ZIF-8 and zeolite 13X when incorporated into PVA amine-based membranes that had been previously optimized for CO_2/N_2 and CO_2/CH_4 selectivities. The optimized membranes had CO_2/N_2 and CO_2/CH_4 selectivities of 1.83 and 2.45 respectively. It was hypothesized that the incorporation of ZIF-8 and zeolite 13X would improve this selectivity further. It was also hypothesized that addition of the fillers would enable the making of a stable film that did not need support for mechanical stability.

4.3 EXPERIMENTAL

4.3.1 Membrane development procedure

The procedure for the membrane preparation has been adapted from Zou and Ho with changes that ensured a working membrane was made [11]. A previous optimization study was done to optimize the concentrations of the base working membrane with respect to the concentrations of the constituting components: Polyvinyl alcohol (PVA), Formaldehyde, deionized water, Poly (allylamine hydroxide) (Pam-OH), Potassium hydroxide (KOH) and 2-Aminoisobutyric acid (AIBA). This was done using a 2^6 factorial design where the concentration combinations used resulted in the best performing membranes in terms of CO_2/N_2 and CO_2/CH_4 separation. The component concentrations and the results for the membranes that showed the best selectivity values from the factorial design study are shown in Table 4.1, together with the comparison to the base membrane. The base membrane is the unoptimized membrane made from the adapted procedure by Zou and Ho.

Table 4.1: Summary of results from 2^6 factorial design study on PVA amine-based membranes.

Property	Base membrane	Membrane 13	Membrane 61
% PVA	1.905	3.6	0.21
% Formaldehyde	1.185	0.3	0.3
% H20	86.645	82.65	82.65
% Pam-OH	0.5	0.7	0.7
% KOH	1.15	2	2
%AIBA	1.15	0.3	2
CO_2 permeability (Barrer)	489,604	128, 728	207,392
CO_2/N_2	1.03	1.83	1.10
CO_2/CH_4	1.01	0.94	2.45

Membranes 13 and 61 were remade for the pressure test study. Zeolite 13X and the metal organic framework, ZIF-8, were incorporated into these membranes using the procedure outlined below. 1wt%, 2wt%, 4wt% and 6wt% of the total dry weight of the adsorbents were used in this study.

4.3.1.1 Materials

- Deionized water was obtained from University of Ottawa local facilities.
- Polyacrylonitrile (PAN) I flat sheet support with a molecular weight cut-off of 30kDa and a thickness of 150µM was purchased from Synder Filtration (Vacaville, CA). Catalogue number: 500-06-9095.

The following chemicals were obtained from Sigma-Aldrich® (Oakville ON) at the highest purity available:

- Polyvinyl alcohol (PVA) (99% hydrolyzed powder)
- Poly (allylamine hydrochloride) (Pam-HCl)
- 2-Aminoisobutyric acid (AIBA)
- Formaldehyde solution (37 wt.% aqueous solution)
- Potassium hydroxide (KOH)
- Methanol
- Molecular sieve 13X, powder, ~2µm particle size
- Basolite Z1200, ZIF-8, powder ~5µm particle size

4.3.1.2 Procedure

The procedure outlined below is for the base membrane with the concentrations as outlined in Table 4.1 above. Three separate mixtures were prepared:

- The first mixture was poly(allymine) which was obtained by mixing Pam-HCl with KOH in methanol overnight (0.44 g Pam-HCl in 0.528 g KOH mixed with 60 ml of methanol). This overnight mixture was stirred in a flask covered with parafilm. The resulting KCl was precipitated after the 24 hours leaving a mixture of poly(allymine)

solution. 20 ml of deionized water was added as the solvent and the methanol was then evaporated in the fume hood at room temperature.

- The second mixture was made by first dissolving 2 g of PVA in 50 g of deionized water at 80℃ with stirring until the solution turned colourless. Separately, 0.6977 g of the 37wt% formaldehyde solution was dissolved in 1.8856 g of deionized water and 0.732 g of KOH was added. These two separate solutions were mixed, and the resulting mixture was then heated at 80℃ with stirring at level of 500 rpm for 3h 35 min. This was changed from the original 16 hours as with 16 hours a solid was formed. The solution turned from colourless to yellow to orange while thickening up due to cross-linking all through the 3h 35min of heating. A batch solution of 100g total was prepared so that an equal total weight was being heated and therefore cross-linked each time.
- The third mixture was prepared by mixing a 1:1 molar ratio of KOH and AIBA; 0.405g KOH into an aqueous solution of AIBA (0.828g AIBA in 20 ml of deionized water).

After the 3 hour 35 minute heating for the second solution, the third mixture was added to the second solution by mixing for 30 minutes. Thereafter, the first mixture was added to the second and third mixture with mixing again for another 30 minutes. This mixture is the polymeric membrane mixture before the addition of the fillers. The weight percentages were kept constant for the base/adapted membrane for a total weight of 100 grams where the amount of water in the third mixture was varied to maintain this total constant weight. This is because the total amount of water added after cross linking was all later evaporated during drying.

Depending on the concentration of adsorbent needed, the specified weight of the adsorbent is measured and then added to the membrane mixture with stirring for 30 minutes. Before mixing it

into the membrane, zeolite 13X was activated by heating it in the oven at 300°C for 4 hours [21]. This was done to remove any impurities and adsorbed gases from the zeolite 13X structure. The ZIF-8 was not activated, but it was incorporated into the membrane mixture with heating at 80°C during the 30 minutes for a more homogeneous mixed matrix membrane. This incorporation was performed as suggested by Barooah et al. (2019) study of PVA/piperazine glycinate/ ZIF-8 mixed matrix membranes [20].

Thereafter, the resulting mixture was casted using a casting knife with a thickness of 250 micrometers on top of the PAN support that was flattened and taped on the sides on top of a glass sheet and the PVA- fillers blend was spread using the casting knife. This membrane solution with the support was then dried overnight for about 16h. The formed membrane was then also heated to 120℃ for 4 hours. The membrane was then cut into a circle of diameter 6.8 cm to fit in the gas permeation device. All the membranes formed maintained a total thickness of between 160µm-165µm with an active layer thickness of about 25µm. All membranes were assumed to have the same average active layer thickness of 25 µm and this active layer thickness was used in the calculation of the permeabilities.

4.3.2 Feed pressure test procedure

Different feed pressure tests were carried out on membranes 13 and 61, which had the best selectivity values for the gases of interest in this study. The feed pressures tested were between 1.5 and 4 atm. All membranes were tested 21 days after their preparation. This is because of previous tests which indicated that the PVA membrane takes 21 days to stabilize, since the excess free volume associated with glassy polymers decreases with time [22].

4.3.3 Single gas permeation experiment procedure

All gases used were purchased by Messer Canada Ltd from Mississauga, ON and their grades and purities are displayed in Table 4.2.

Table 4.2: Gases used for the research experiment and their grades and purities

Species	Grade	Purity (%)
CO_2	4.0	99.99
CH_4	4.0	99.99
N_2	4.0	99.99

To test the membranes, a single flow of each N_2, CO_2 and CH_4 gas passed through the membrane using different membranes made from the same batch, and the flow rates were measured. The membranes were tested using the set up shown in Figure 4.1. The membranes were tested between 1.5 and 4.0 atm feed pressure and the permeate pressure was kept at 1 atm. The membrane was placed in the membrane module. The feed pressure was set and the retentate and permeate flow rates were measured using the corresponding bubble flow meters. The measurements were done every 5 minutes for 60 minutes at which time the flow rates stabilized and the last couple of readings are averaged to give the retentate flow rate and permeate flow rates for each of the individual gases. The permeabilities and selectivities were then calculated from the readings as explained below.

The permeability of component 1, P_1, was calculated in Barrer units using Equation 1:

$$P_1 = F_1 \frac{T_{STP}}{T_{feed} \times p_{STP}} \frac{L\,\Delta p}{A\,p_{feed}} \times 10^{10} \quad (1)$$

Where F_1 is the volumetric flow rate [cm^3/s] taken at STP conditions for component 1 and A is the surface area of the membrane[cm^2], T_{STP} is the temperature of gas at STP conditions in K, 273.15K

was used. p_{STP} is the pressure of 1 mol of gas at STP conditions in cmHg, 76 cmHg was used. T_{feed} is the temperature of the feed and p_{feed} is the pressure of the feed. Δp is the difference between the upstream and downstream pressure and L is the thickness of the membrane active layer measured in cm. The 10^{10} converts the permeability from {cm^3 (STP)cm/s cm^2 cmHg} units to Barrer. The permeability of gases is dependent on the solubility, size and diffusivity of the gases [23].

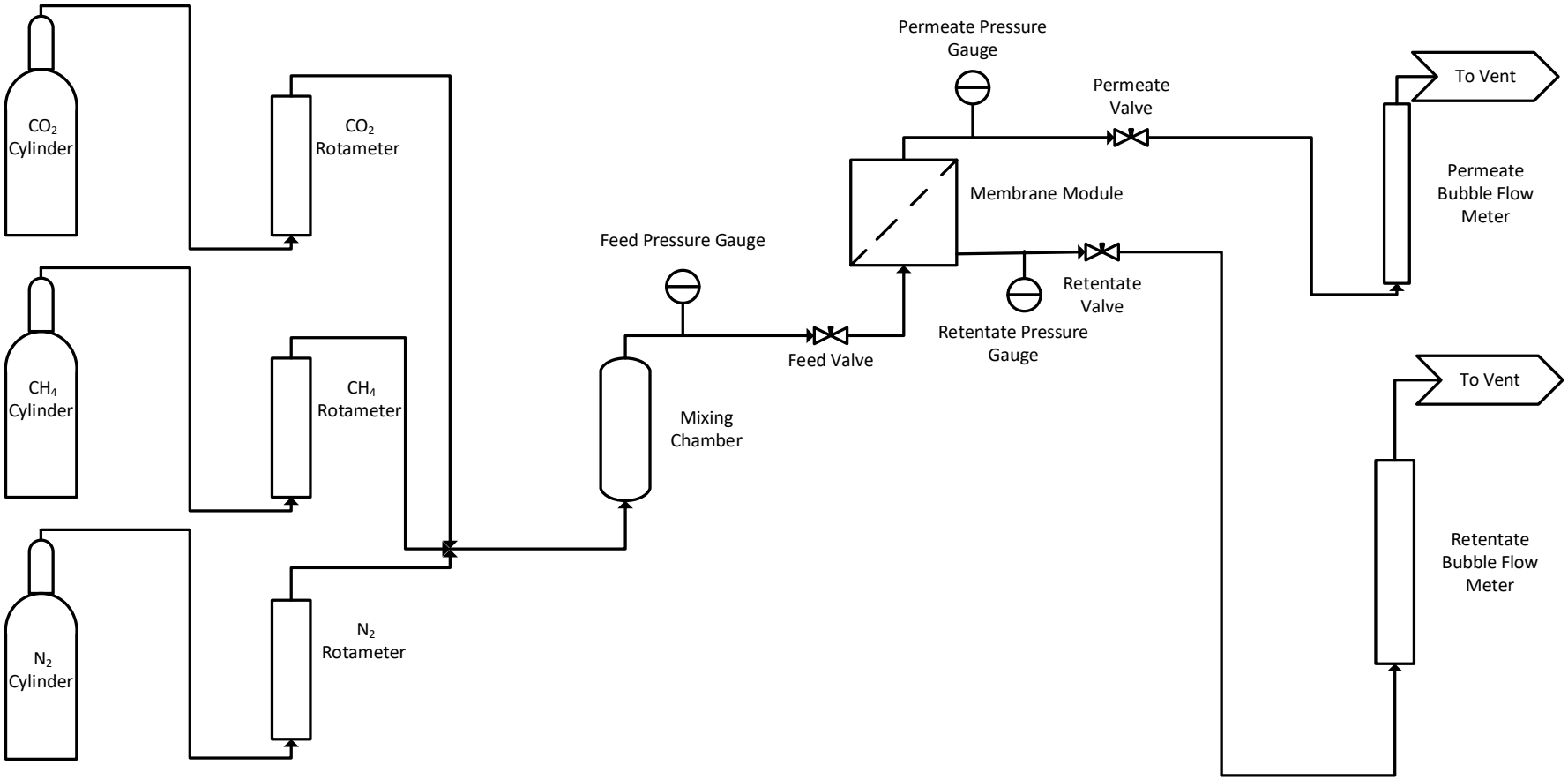

Figure 4.1: Schematic of single gas permeation setup used in this study.

The membrane selectivity is defined as the preferred permeability of the membrane for one fluid over other fluid(s). This is calculated using Equation 2 for selectivity of component 1 over component 2.

$$\alpha^*_{1/2} = \frac{P_1}{P_2} \quad (2)$$

Where $\alpha^*_{1/2}$, is the selectivity of the membrane for component 1 over component 2 and P_i is the permeability of gas i where i is either component 1 or 2 [24].

4.3.4 Characterization of synthesized membranes

Some of the good performing membranes were characterized using a Scanning Electron Microscope (SEM) which was used to verify the thickness of the active layer of the membrane. This was done using JEOL JSM-7500F FESEM series operated with 30 kV electron beams under 30 Pa of vacuum. The cross-sectional images were taken at ×100 and ×800 magnification on top surface of the membrane coated with 10 nm of gold. Imaging of the top surface of the membrane was also done by SEM imaging at ×1,000, ×5,000 and ×10,000 magnification levels on samples coated with 7 nm of gold. Fourier Transform Infrared (FTIR) Spectroscopy was also carried out with wavenumbers in the ranges of (4000-650) cm^{-1} to determine the functional groups of the best performing membranes. This was done using a Cary 630 FTIR spectrometer by Agilent. Lastly, the hydrophobicity of the membranes was established through contact angle measurements using a goniometer. Seven measurements were taken at different locations on the membrane surface and an average of those seven determined the contact angle reported. The goniometer used was the Video Contact Angle System (VCA) Optima XE from AST products.

4.4 RESULTS AND DISCUSSION

A summary of the concentrations used in the preparation of the optimized membranes 13 and 61 to which the zeolite 13X and ZIF-8 fillers were added is shown in Table 4.1 from the Experimental section above. It is important to note that although one of the goals of the research project was to form a stable film without the use of support, this was not achieved and all the membranes reported incorporated the use of PAN support.

4.4.1 Membrane characterization

The SEM imaging was done to view the morphology of the top membrane surface. As can be seen in Figure 4.2, the SEM imaging showed that when 13X was added to the membrane mixture, there was formation of agglomerations of zeolite 13X. There was also formation of cracks with the addition of zeolite 13X. Figure 4.3 shows that with ZIF-8, there was also the formation of agglomerations of the ZIF-8 crystals. The smoother regions without ZIF-8 clumps were relatively smooth without cracks and smaller clumps were observed compared to the zeolite 13X filled membranes.

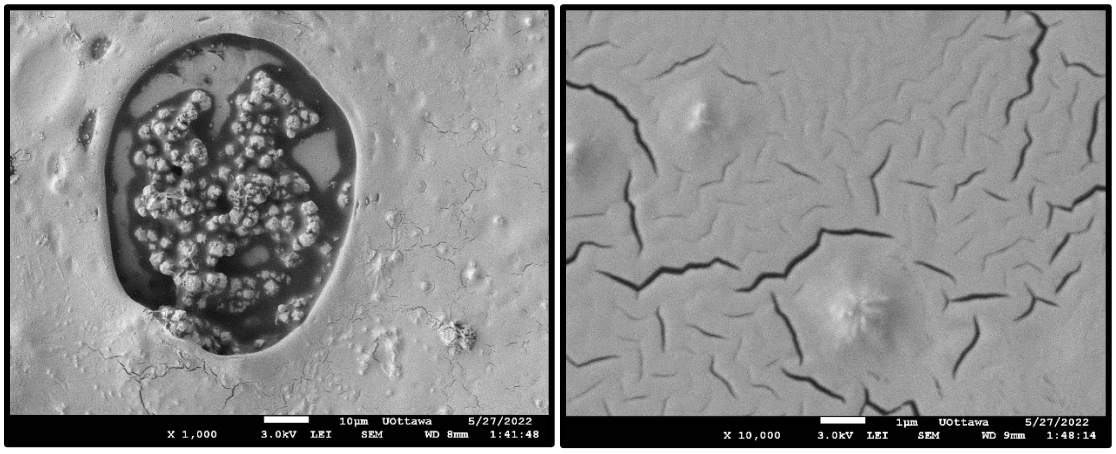

Figure 4.2: Zeolite 13X filled membranes at ×1,000 magnification (left) and at ×3,000 magnification (right).

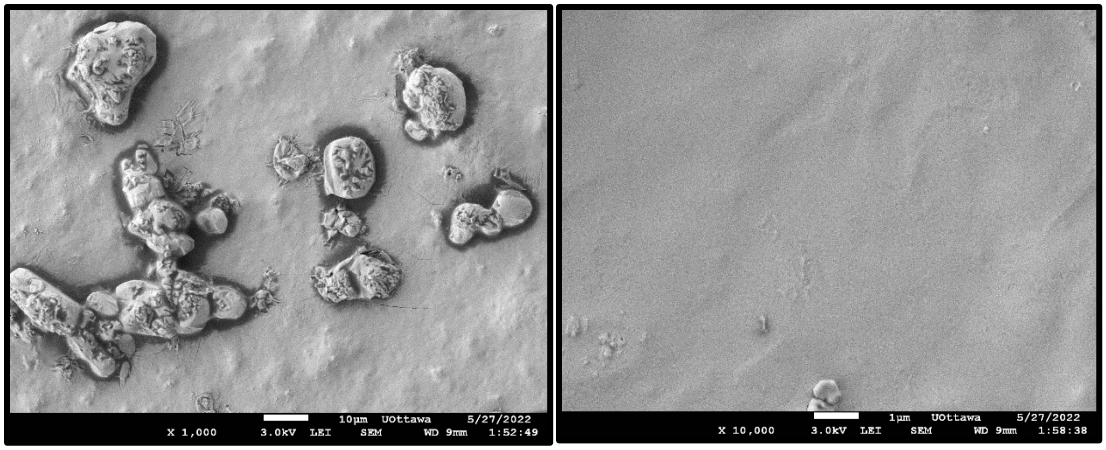

Figure 4.3: ZIF-8 filled membranes at ×1,000 magnification (left) and at ×3,000 magnification (right).

FTIR imaging was done to observe the most noticeable functional groups of the membrane before and after the addition of the two fillers, zeolite 13X and ZIF-8. FTIR analysis of membrane 13 with and without zeolite 13X and ZIF-8 is shown in Figure 4.4. FTIR analysis of membrane 61 with and without zeolite 13X and ZIF-8 fillers is shown in Figure 4.5. The characterization of the peaks was done using "Interpretation of infrared spectra, a practical approach" by John Coates (2000) [25]. As can be seen from Figure 4.4 with the addition of zeolite 13X to membrane 13, the membrane had the same general spectra, but with the addition of ZIF-8, a sharp peak at a wavenumber of 1240 cm^{-1} was observed. This was indicative of a (C-O-C) epoxy linkage and resulted in the lower contact angle seen in the goniometer readings. The size of the 3280 cm^{-1} peak characteristic of hydroxyl (O-H) and amine (N-H) groups also increased with the addition of 13X and especially with the addition of ZIF-8.

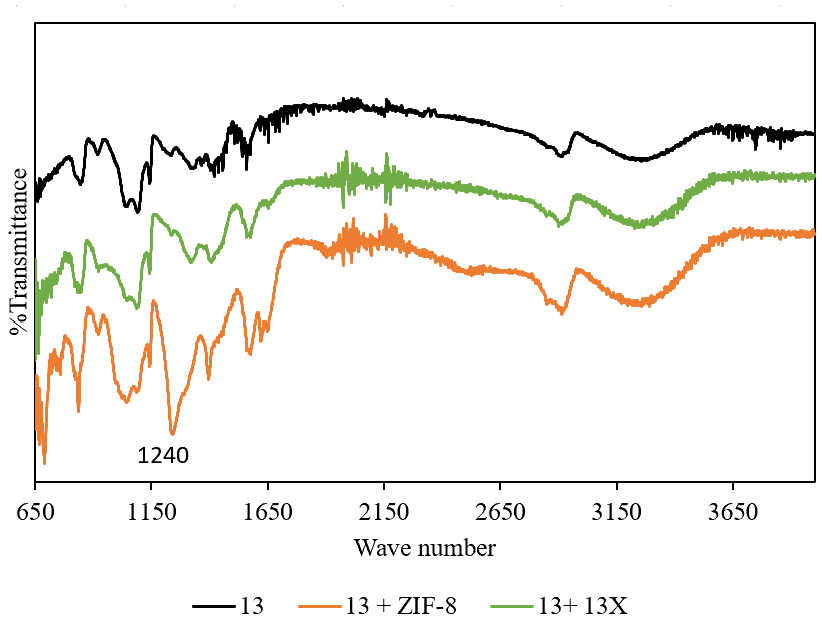

Figure 4.4: FTIR spectroscopy image of membrane 13 with and without zeolite 13X filler and ZIF-8 filler

On the other hand, with Figure 4.5, the addition of ZIF-8 to membrane 61, the membrane had the same general spectra, but with the addition of 13X, a sharp peak at a wavenumber of 940 cm^{-1} was observed. This was indicative of a Si-OH bond where the Si was imparted by the zeolite 13X. This linkage resulted in the lower contact angle seen in the goniometer readings as well. The 3280 cm^{-1} peak characteristic of hydroxyl (O-H) and amine (N-H) groups also became more pronounced with the addition of 13X [25].

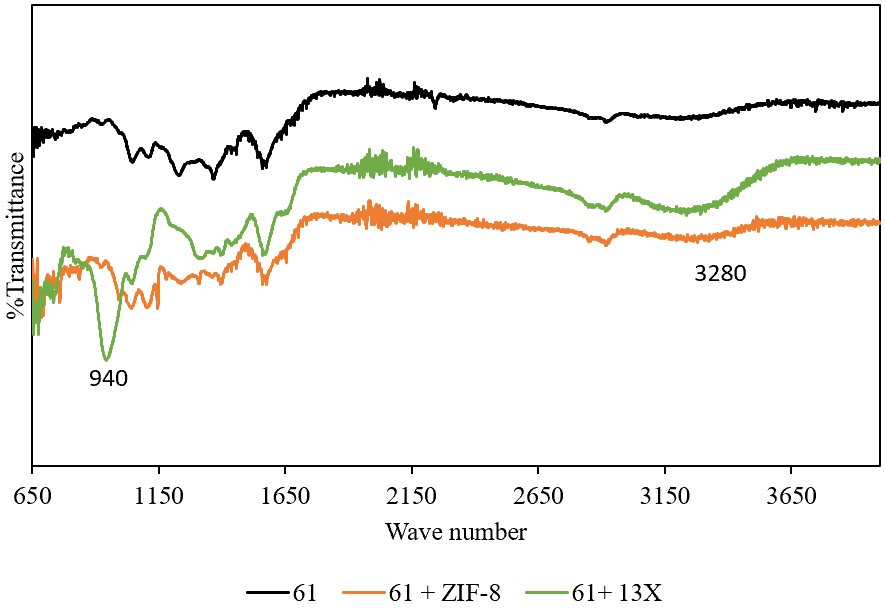

Figure 4.5: FTIR spectroscopy image of membrane 61 with and without zeolite 13X filler and ZIF-8 filler.

The results of the contact angle measurements of membrane 13 with and without the membrane fillers are shown in Figure 4.6. These contact angle measurements showed that with the addition of ZIF-8 to membrane 13, the contact angle of the membrane decreased by approximately 10°. The addition of zeolite 13X to this particular membrane however did not change the contact angle of the membrane much. These results corroborated with the FTIR results where there was an epoxy linkage peak seen with the addition of ZIF-8, but the addition of zeolite 13X didn't change the bonding of the membrane much. Contrarily, the opposite results were observed with membrane 61 in Figure 4.7, where zeolite 13X instead of ZIF-8 seemed to change the chemical structure of the membrane, leading to additional FTIR peaks and a more hydrophilic membrane with lower contact angle as seen by the goniometer readings. These observations could be due to the higher PVA content in membrane 13 as observed in Table 4.1 and the higher amine content in membrane 61.

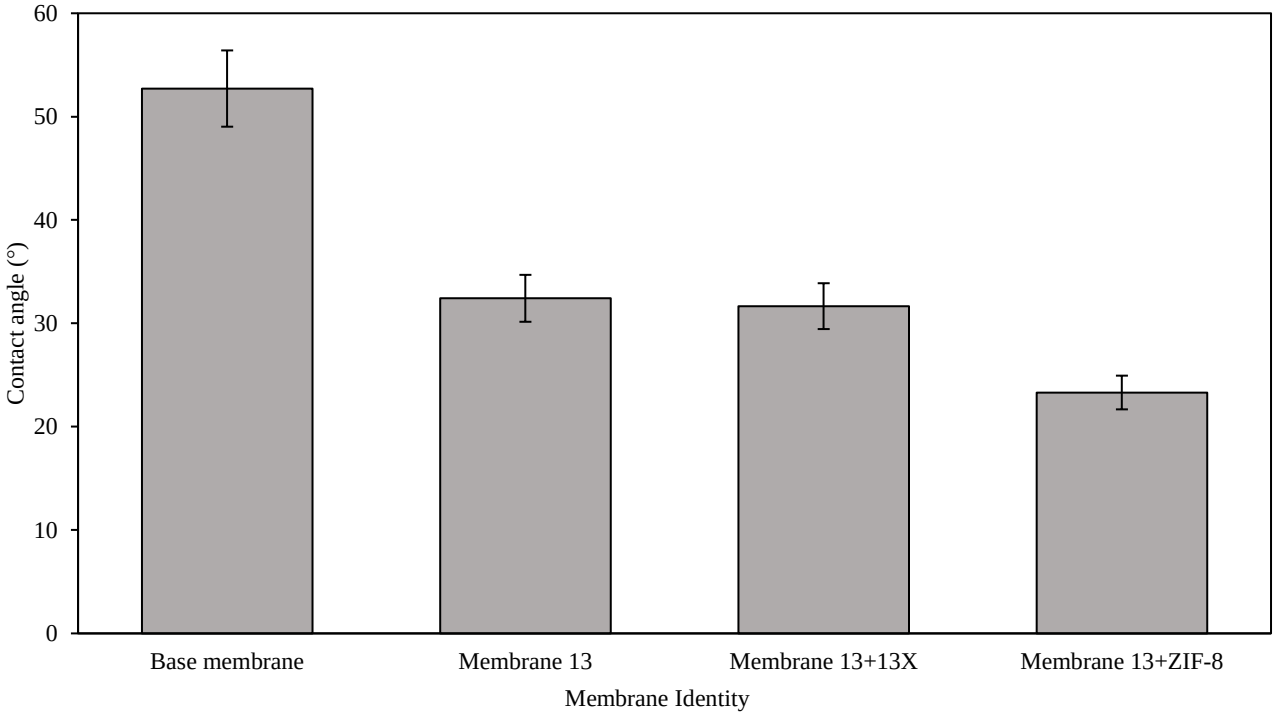

Figure 4.6: Contact angle measurements of the base membrane and membrane 13 with and zeolite 13X filler and ZIF-8 filler

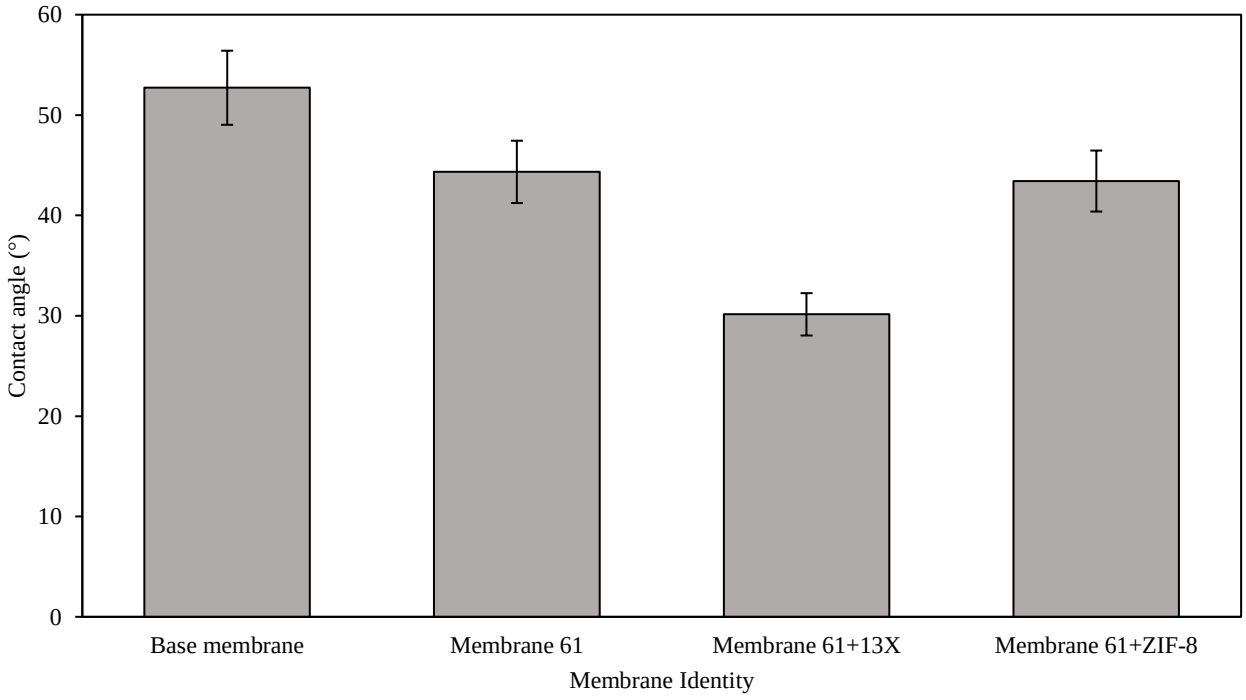

Figure 4.7: Contact angle measurements of the base membrane and membrane 61 with and without zeolite 13X filler and ZIF-8 filler

4.4.2 Zeolite 13X filler tests

With the addition of zeolite 13X filler to both membrane 13 and membrane 61, they lost their selectivity for CO_2 as shown in Figure 4.8 and Figure 4.9, since the permeability values for different gases came closer to each other with the addition of the fillers. This is because of the loss of the integrity of the membrane due to the formation of pinholes due to the agglomerations and cracks seen in the SEM images. As these defects were large enough to be seen by the SEM imaging, they would most likely result in viscous flow. In viscous flow, the mean free path is less than the pore diameter. As characteristic of viscous flow, the membrane also lost its selectivity with the addition of the fillers and the consequent increase in the defects formed [26,27]. Moreover, with the addition of 1wt% of zeolite 13X, the permeability values for membrane 13 had increased by 5-6 times. Permeability values for membrane 61 had a less dramatic increase with the addition of zeolite 13X for the 2wt% 13X loading. Moreover, membrane 13 had no selectivity for any of the gases for the 1wt% to 6wt% addition of zeolite 13X, as the permeability of different gases coincided with each other. On the other hand, membrane 61 showed a more gradual decrease in the selectivity for CO_2 gas, as the permeability values for different gases got closer to each other with the increase in zeolite 13X percentage in the membrane. Membrane 61 also showed more change in chemical structure with the addition of zeolite 13X, as observed in Figure 4.5. This shows that the high amine, low PVA composition of membrane 61 was more compatible with the zeolite 13X compared to membrane 13.

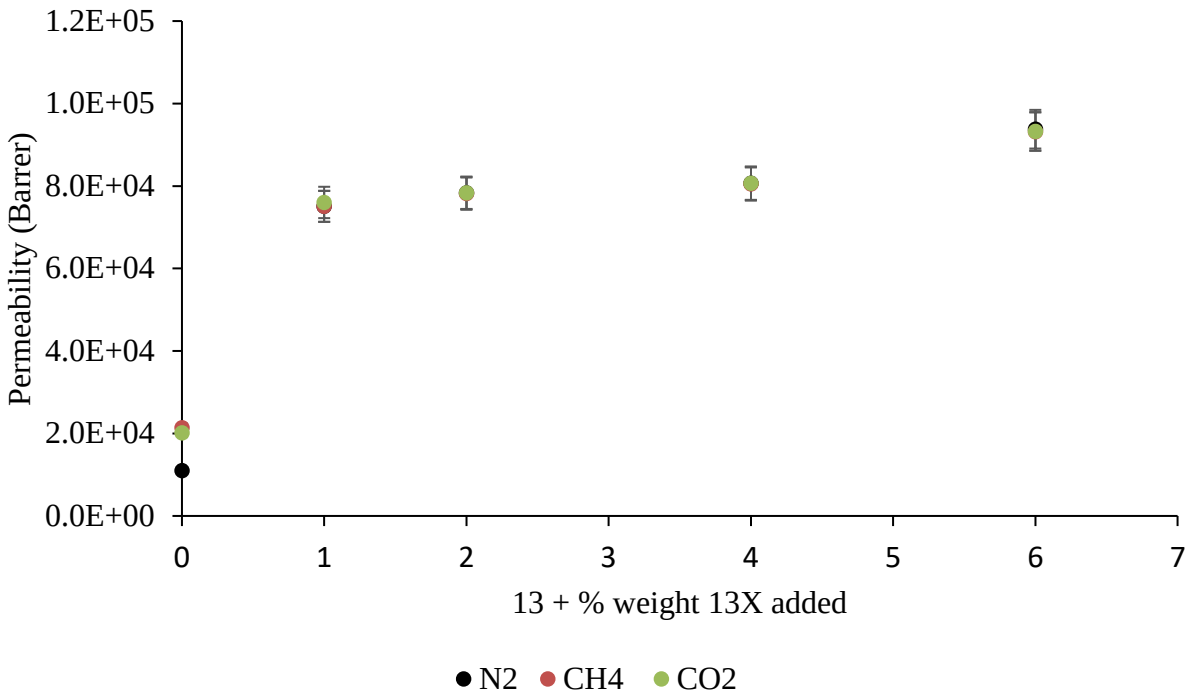

Figure 4.8: Permeation test results for different zeolite 13X weight % filled membrane 13.

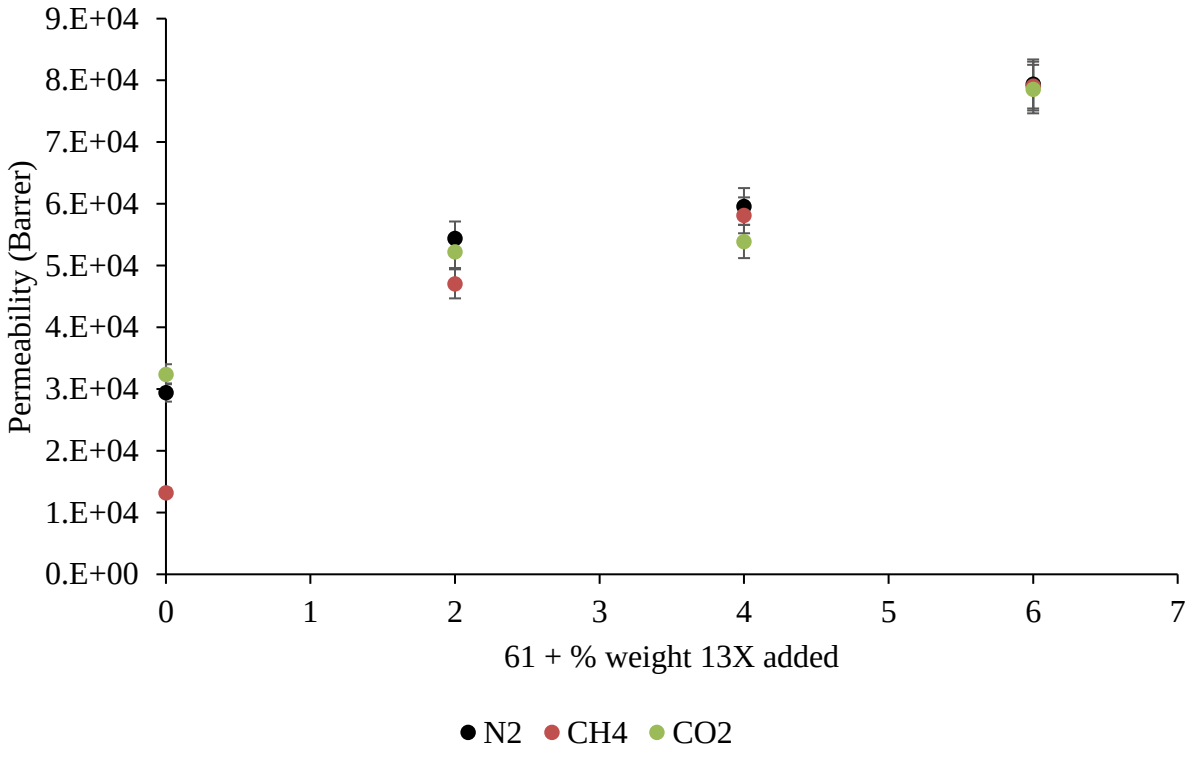

Figure 4.9: Permeation test results for different zeolite 13X weight % filled membrane 61.

4.4.3 ZIF-8 filler tests

With the addition of the MOF ZIF-8 filler to both membrane 13 and membrane 61, they lost their selectivity for CO_2 as the permeability values for different gases approached each other more with the addition of more fillers, as shown in Figure 4.10 and Figure 4.11. This is also due to the loss of the integrity of the membrane from the formation of pinholes often seen with mixed matrix membranes and as seen in the SEM images. Again the pinholes caused viscous flow to be the main means of transport through the membrane resulting in the loss of selectivity seen by the membrane [26,27]. Moreover, with the addition of 1wt% of ZIF-8, the permeability values for membrane 13 increased almost by 5 times. The permeability values for N_2 and CO_2 decreased first with the addition of ZIF-8 for membrane 61, before they increased when 4 and 6wt% ZIF-8 was added. For CH_4 gas, the permeability value kept increasing steadily with the addition of ZIF-8. For both membranes 13 and 61, the selectivity of CO_2 decreased gradually. The FTIR and contact angle measurements showed that membrane 13 was more compatible with the ZIF-8 filler, as the permeability initially increased instead of decreasing as membrane 61 did. Moreover, the FTIR showed a change in chemical structure indicative of the ZIF-8 filler. This shows that the high PVA and low amine composition of the membrane 13 was more compatible with the ZIF-8 MOF compared to membrane 61.

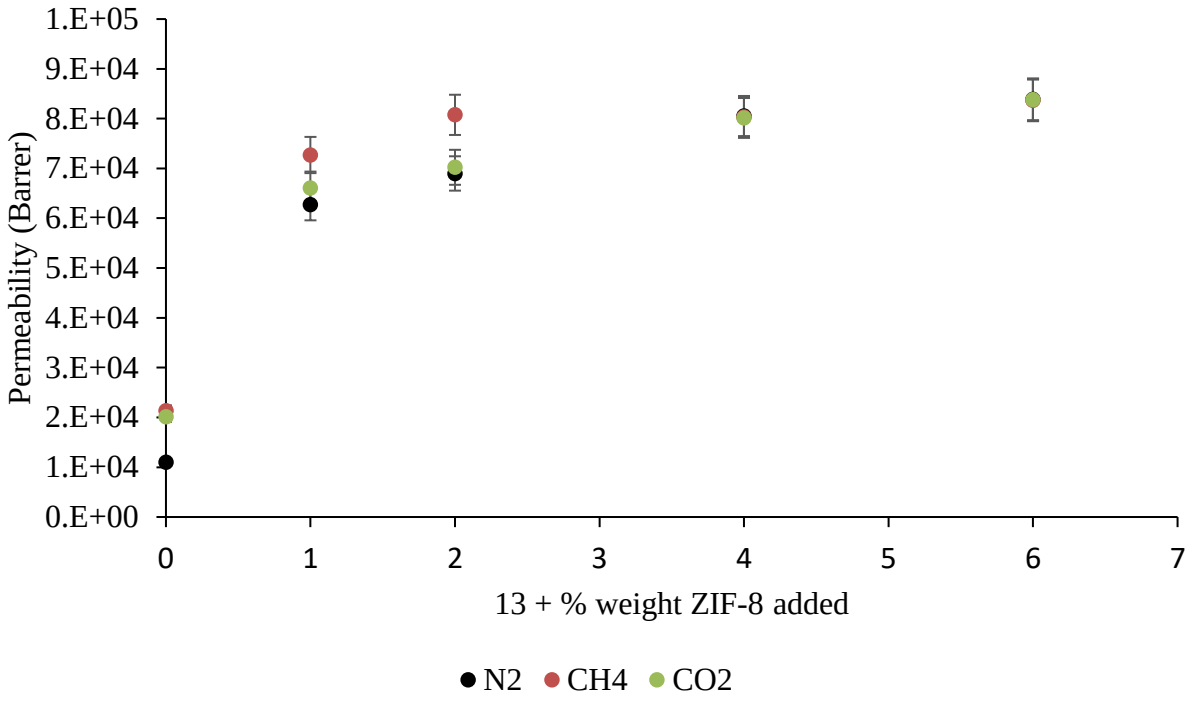

Figure 4.10: Permeation test results for different ZIF-8 weight % filled membrane 13.

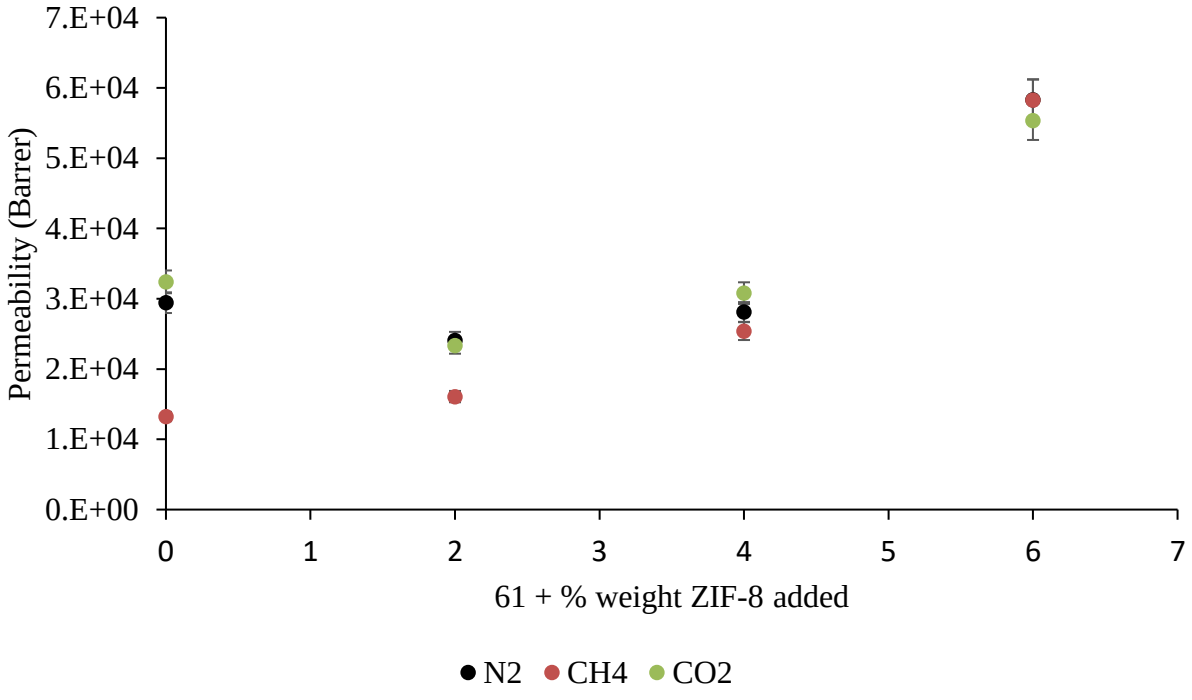

Figure 4.11: Permeation test results for different ZIF-8 weight % filled membrane 61.

4.4.4 Feed pressure tests

The optimized polymeric membranes had feed pressure tests done as they were the best performing, to test the effect of changing the feed pressure on the performance of the membrane. The permeate pressure was kept at 1 atm absolute whereas the feed pressure was varied from 1.5 to 4 atm pressure absolute. Membrane 13 had previously shown the best CO_2/N_2 separation performance with a CO_2/N_2 selectivity of 1.83. The effect of the feed pressure on the permeability of the gases for membrane 13 is shown in Figure 4.12 and the effect of the feed pressure on CO_2/N_2 and CO_2/CH_4 selectivity values for membrane 13 is seen in Figure 4.13. With a decrease in feed pressure, there is a decrease in gas permeability and an increase in the CO_2/N_2 and CO_2/CH_4 selectivity for this membrane. This observation was seen in other PVA membranes as well [11,20]. This is because a decrease in feed pressure meant that facilitated transport was the main transportation means, as with increase in pressure there was an increase in carrier saturation. This is a phenomenon described by Ho and Dalrymple[28]. With increase in pressure past a critical pressure, the membrane carriers responsible for facilitated transport of a particular penetrant become saturated with the penetrant and a further increase in penetrant's partial pressure does not increase the concentration of CO_2-carrier reaction product leading to more CO_2 transport. Therefore, past the critical pressure transport of the penetrant is mainly through solution-diffusion and dependent on the kinetic diameter of the penetrant. This describes the increase in CO_2 selectivity with decrease in pressure as facilitated transport is becoming the more relevant form of transport with decrease in pressure and the opposite with transport through solution diffusion. The CO_2/N_2 and CO_2/CH_4 selectivity values at 1.5 atm pressure were 5.94 and 2.13, respectively, with a CO_2 permeability of 2,471 Barrer, as observed in Figures 4.12 and 4.13. This facilitated transport responsible for the improved selectivity of the membrane at lower pressures could also be due to

the interaction between the permeants and the pore walls of the defects in the membrane as they are transported through Knudsen flow [26].

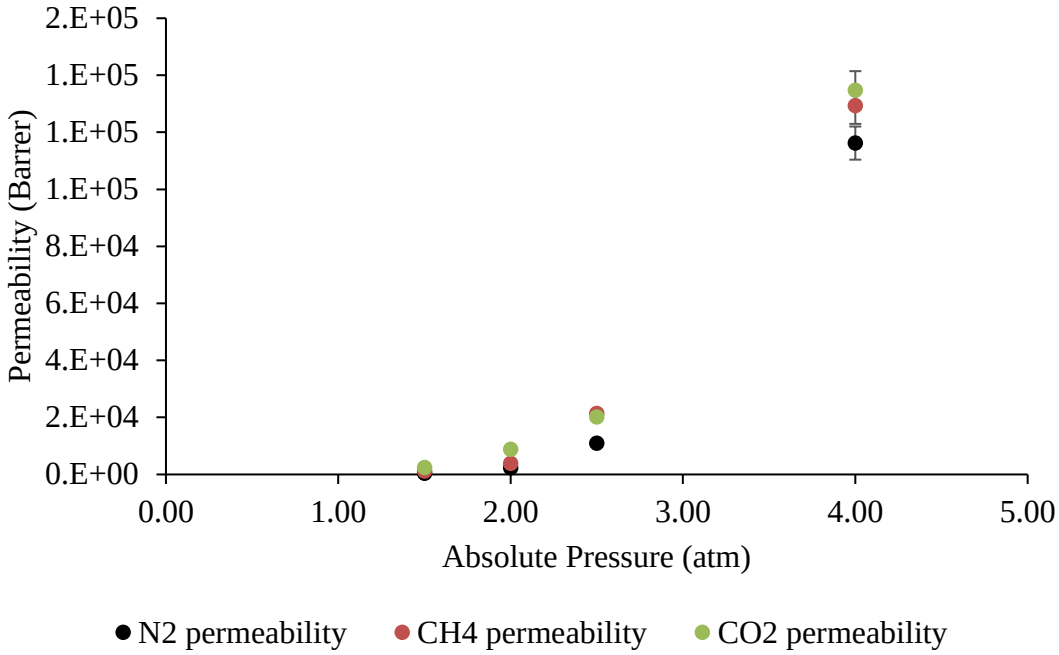

Figure 4.12: N_2, CH_4 and CO_2 permeability for membrane 13 at different feed pressures.

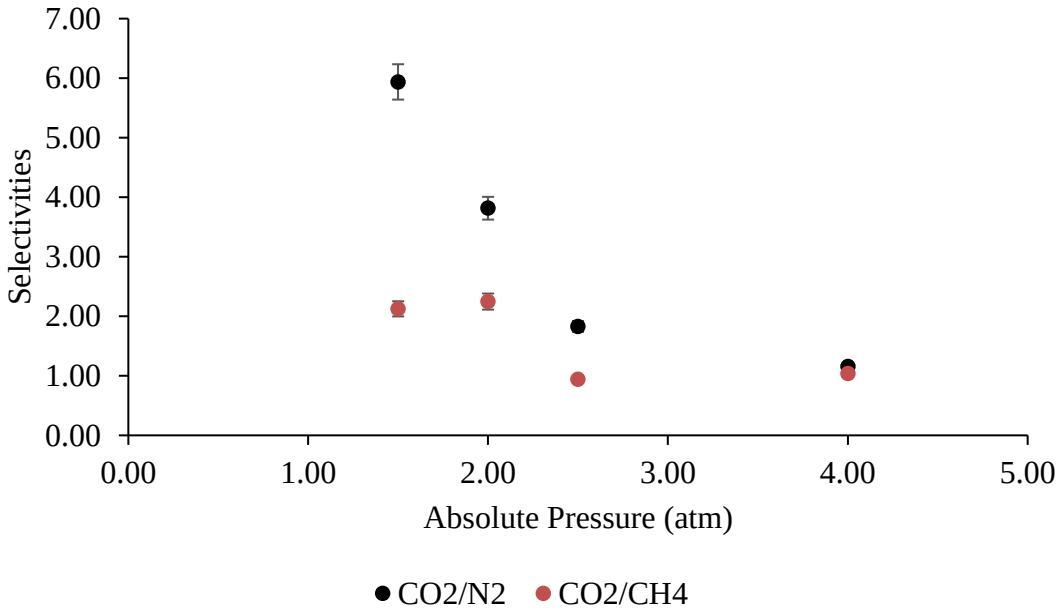

Figure 4.13: CO_2/N_2 and CO_2/CH_4 selectivity values at different feed pressures for membrane 13.

The same feed pressure test was done on the membrane 61 which showed the best CO_2/CH_4 separation performance with a CO_2/CH_4 selectivity of 2.45. The effect of the feed pressure on the permeability of membrane 61 is shown in Figure 4.14 and the effect of the feed pressure on CO_2/N_2 and CO_2/CH_4 selectivity values for membrane 61 is seen in Figure 4.15. With a decrease in feed pressure, there is an increase in the CO_2/N_2 selectivity for this membrane as was seen with membrane 13. This is because a decrease in feed pressure meant that facilitated transport was the main transportation means, as with increase in pressure there was an increase in carrier saturation [20]. The lower CO_2/N_2 and CO_2/CH_4 separation performance of this membrane compared to membrane 13 indicated that membrane 13 had more carriers and more facilitated transport than membrane 61. With membrane 61 however, the membrane's selectivity for CO_2/CH_4 seemed to increase with pressure up to 2.5 atm pressure. Although the results at 4 atm are shown in Figure 4.15, this membrane broke and could not maintain the 4atm feed pressure past 20 minutes. This data point is therefore most likely an outlier. Therefore, ignoring this point the results for the CO_2/CH_4 selectivity show an increase in selectivity with an increase in pressure up to 2.5 atm. This indicates that solution diffusion and not facilitated transport is responsible for the separation of CO_2 from CH_4 with membrane 61. This facilitated transport could also be through interaction with the membrane walls by Knudsen diffusion as the membrane was likely not defect free [26]. The CO_2/N_2 and CO_2/CH_4 selectivity at 1.5 atm pressure was 1.54 and 1.00 respectively, with a CO_2 permeability of 2,491 Barrer.

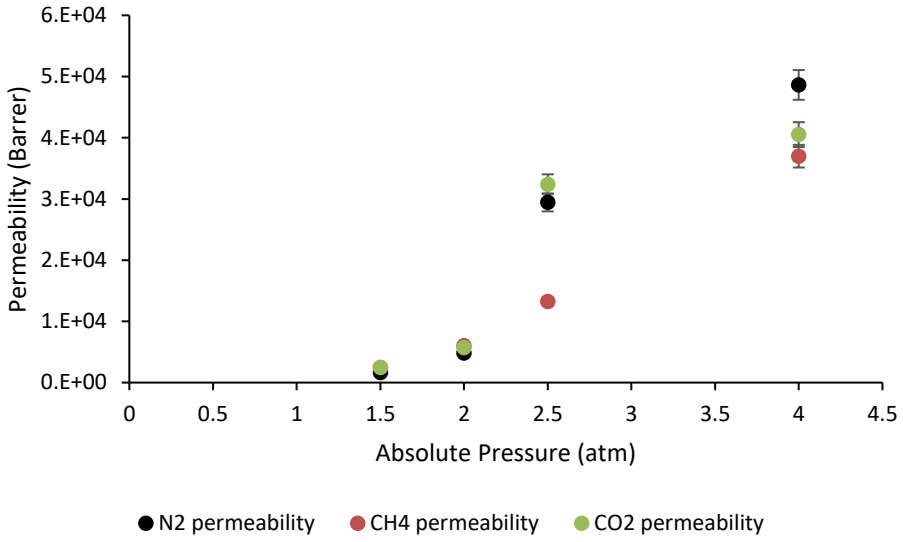

Figure 4.14: N_2, CH_4 and CO_2 permeability for membrane 61 at different feed pressures.

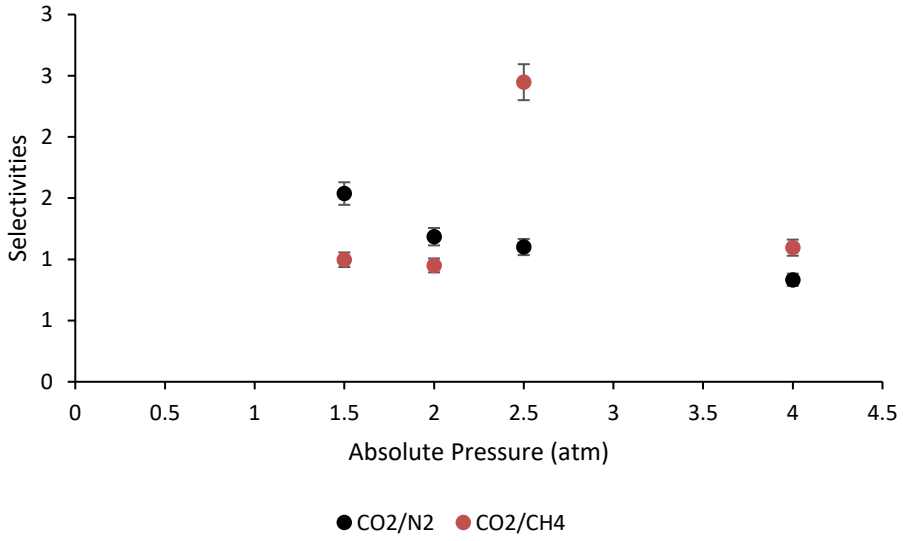

Figure 4.15: CO_2/N_2 and CO_2/CH_4 selectivity values at different feed pressures for membrane 61.

4.4.5 Comparison with membranes from literature

The mixed matrix membranes were compared to other similarly made mixed matrix membranes filled with zeolite 13X and ZIF-8. Because of the loss in selectivity with the addition of the

membrane fillers, the mixed matrix membranes prepared did not compare well in terms of separation performance. The results for mixed matrix membranes obtained from literature are presented in Table 4.3. As can be seen from this table, with a 5wt% ZIF-8 loading, the PVA/piperazine glycinate membrane had a CO_2/N_2 selectivity of 370 [20]. The Matrimind 5218 filled with 5wt% ZIF-8 on the other hand showed a CO_2/CH_4 selectivity of 35.2 [19]. The zeolite 13X filled polymeric membranes had relatively high CO_2/N_2 selectivities above 20 as well, as shown in Table 4.4.

Table 4.3: Summary of zeolite 13X and ZIF-8 filled mixed matrix membranes

Membrane filler	Membrane identity	Weight % filler	CO_2 Permeability (Barrer)	CO_2/N_2	CO_2/CH_4	Temperature (°C)	Ref
ZIF-8	PVA/ Piperazine glycinate /ZIF-8	5	328	370	-	80	[20]
	Matrimind 5218	5	10.05	22.4	35.2	230	[19]
13X	Polyimide	30	378	67.1	-	25	[17]
	Rubbery ethylenevinyl acetate copolymer (EVA)and glassy polysulfone (PSF)	30	45.4	24.7	-	22	[21]

Membrane 13 tested at 1.5 atm was also compared to other polymeric membranes from literature and to the Robeson plot. Membrane 61 was previously compared to other polymeric membranes in the previous chapter. The results are shown in Figure 4.16, Figure 4.17 and Table 4.5. Compared to the other polymeric membranes, the PVA amine-based membrane shows a lot of promise for improvement, especially in terms of the CO_2 selectivity over N_2 and CH_4 when tested at near

atmospheric conditions. Although the membrane does not meet the 2008 Modified Robeson's upper bound limit as shown in Figure 4.16 and 4.17, its performance still compares to other polymeric membranes such as PTMSP and has potential to have its performance improved through the incorporation of more compatible fillers. Other methods of filler incorporation such as priming treatments can also be attempted to reduce the formation of the agglomerations and cracks [29].

Table 4.4: Performance of common polymeric membranes for CO_2/N_2 and CO_2/CH_4 separation

Membrane	CO_2 permeability (Barrers)	CO_2/N_2	CO_2/CH_4	Temperature (°C)	Feed Pressure absolute (atm)	Reference
PVA+ amines	1800	280	-	150	2	[11]
2-PD/2-ME	$9.08 X10^6$	162	-	57	1.1	[30]
PAAm-PVA	$2.4 X10^5$	80	58	25	1	[10]
$PTMEG_{0.8}$+PEBAX	325	70	22.5	25	15.8	[31]
XL-PEGDA	145	66	19.86	35	2.2	[32]
PVA-PEG/PTFE	$1.85X10^7$	56	-	30	2	[12]
$PEBAX_{1074}$	120	51	-	35	15	[33]
PEBAX/PA-PPG	79.7	34.7	14.0	25	1	[34]
PEBA/PSF	260	32	-	25	7.8	[35]
TZPIM	3076	31	24	25	-	[36]
PEBAX	150	29	7.5	55	15.8	[31]
PNB-Si(DEt)-Si(OEtOMe)	733.3	27.5	-	35	1	[37]
PIM-7	1100	26	17.74	30	1.3	[38]
PIM-1	2300	25	18.5	30	1.2	[38]
PIM-CO15	2000	24	15.38	30	1.5	[39]
Bio-PITB-2 (air-100)	1161	23	26	35	1	[40]
Bio-PITB-1 (vac)	1123	22	23	35	1	[40]
Bio-PITB-1(vac-100)	1008	22	25	35	1	[40]
Bio-PITB-1 (air-100)	1076	22	25	35	1	[40]
Bio-PITB-2 (vac)	1201	22	24	35	1	[40]
Bio-PITB-2 (vac-100)	1087	22	27	35	1	[40]
Bio-PITB-2 (air)	1384	22	23	35	1	[40]
Bio-PITB-1 (air)	1352	21	23	35	1	[40]
PIM-CO19	6100	19	10.52	30	1.5	[39]
PDMS	3800	9.5	28	35	1	[41]
This work-61	32405	1.10	2.45	room	2.5	
This work-13	2471	5.94	2.1	room	1.5	
PTMSP	28010	5.64	2.2	20-25	-	[42]

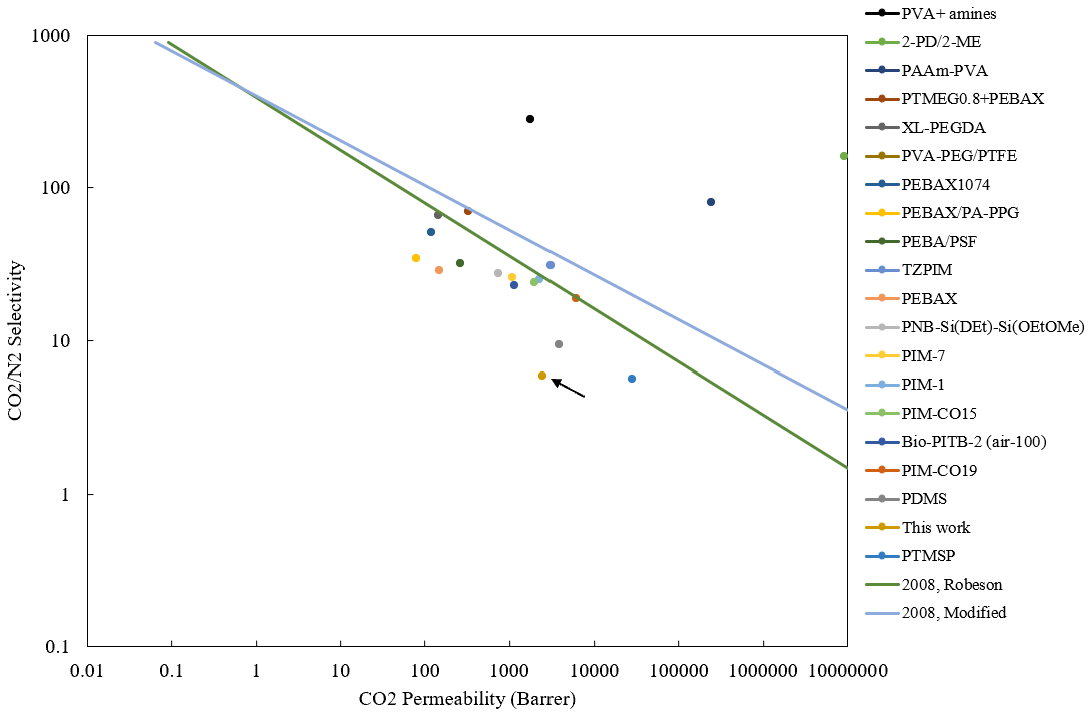

Figure 4.16: CO_2/N_2 Robeson plot of polymeric membranes

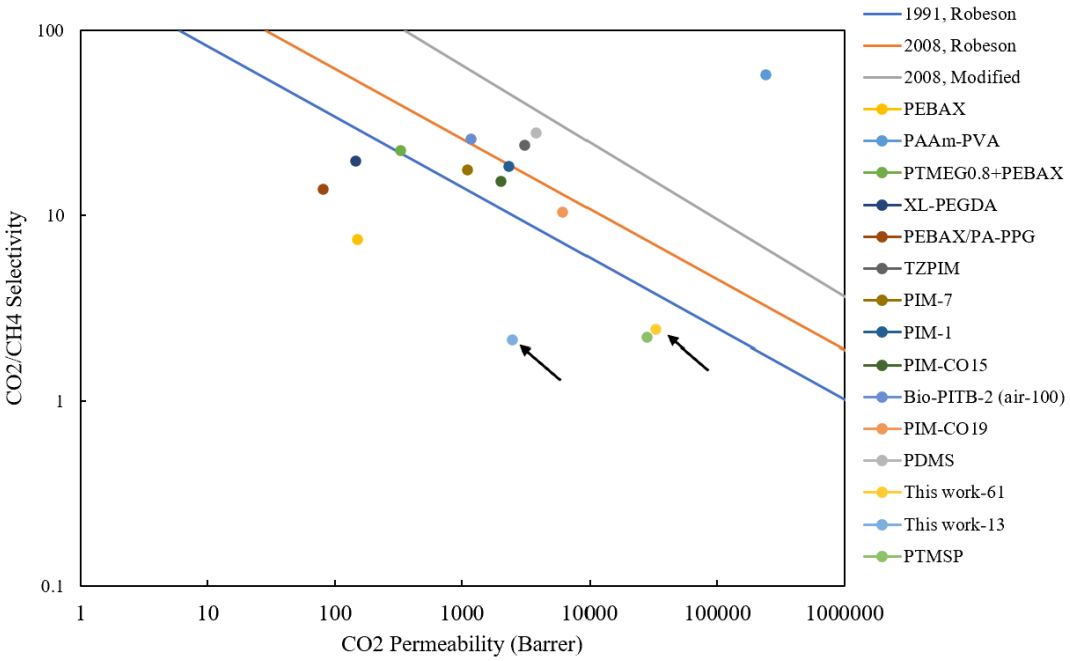

Figure 4.17: CO_2/CH_4 Robeson plot of polymeric membranes

4.5 CONCLUSIONS

PVA based polymeric membranes are a cost effective and more environmentally friendly means of separating gases that have shown good separation performance in terms of CO_2/N_2 and CO_2/CH_4 separation. In this project, an adapted membrane from Zou and Ho's procedure that had previously been optimized had zeolite 13X and the metal organic framework ZIF-8 added to it with the goal of improving the separation performance of the membrane. 1wt%, 2wt%, 4wt% and 6wt% of both fillers were added to each of the of the optimized membranes 13 and 61. Feed pressure tests were also carried out on the optimized polymeric membranes 13 and 61. The feed pressures tested were 1.5 atm, 2.0 atm, 2.5 atm and 4.0 atm with the permeate pressure being kept at atmospheric. Membrane characterization through SEM imaging, FTIR imaging and contact angle testing were performed on the filled mixed matrix membranes.

With the addition of zeolite 13X to membrane 13 and membrane 61, their permeability increased by 5 times and 2 times, respectively, with a loss in CO_2 selectivity. With the addition of ZIF-8 to membrane 13, the membrane's permeability increased by 5 times with a gradual loss in CO_2 selectivity as the filler loading weight increased. Addition of ZIF-8 to membrane 61 decreased both its permeability and selectivity. The SEM images confirmed the formation of agglomerations/cracks in the filled membranes which led to their observed loss in selectivity. The feed pressure tests on the polymeric unfilled membranes showed an increase in CO_2 selectivity with a decrease in feed pressure. Membrane 13 had the highest CO_2/N_2 selectivity of 5.94 with a CO_2 permeability of 2,471 Barrer. This membrane shows promise with better incorporated or primed filler materials in the making of mixed matrix membranes.

4.6 NOMENCLATURE

A	Area of membrane (cm^2)
Barrer	10^{-10} cm^3(STP)cm/scm^2cmHg
F_1	Volumetric flow rate taken at STP conditions (cm^3/s)
P_1	Permeability of component 1 where the component can be either CO_2, CH_4 or N_2 (Barrer)
p_{STP}	Pressure of 1 mol of gas at STP, 76cmHg was used (cmHg)
p_{feed}	Pressure of feed gas (atm)
T_{STP}	Temperature of 1 mol of gas at STP conditions, 273.15K was used (Kelvin)
T_{feed}	Temperature of feed gas (Kelvin)

4.7 GREEK SYMBOLS

$\alpha^*_{1/2}$	Ideal selectivity based on pure component permeability values
Δp	Pressure difference measured at permeate and feed side (psi)

4.8 ABBREVIATIONS

2-PD/2-ME	2-pyrrolidone/ 2-methoxyethanol
AIBA	2-Aminoisobutyric acid
Bio-PITB-1	Polyimide incorporating Tröger's Base
Bio-PITB-2	Polyimide incorporating Tröger's Base
Btu	British Thermal Unit
C=O	Carboxyl
CCS	Carbon Capture and Storage
C-O-C	Epoxy
EVA	Ethylenevinyl acetate copolymer
IPCC	Intergovernmental Panel on Climate Change
KOH	Potassium hydroxide
MOF	Metal Organic Framework
PAAm-PVA	Polyallylamine-poly(vinyl alcohol)
Pam-OH	Poly (allylamine hydroxide)
PDMS	Poly(dimethylsiloxane)
PEBA/PSF	Polyether block amide/ polysulfone
PEBAX	Polyether block amine
PEBAX/ PA-PPG	Polyether block amine / Poly(amide-c-poly(propylene glycol))
PIM-1	Polymers of intrinsic microporosity-1
PIM-7	Polymers of intrinsic microporosity-2
PIM-CO-15	Polymers of intrinsic microporosity-CO-15
PIM-CO-19	Polymers of intrinsic microporosity-CO-19
PNB-Si(DEt)-Si(OEtOMe)	Polynorborenes with alkoxy silyl pendant
PSF	polysulfone
PTMEG+PEBAX	Poly(tetramethylene ether) glycol + Polyether block amine
PTMSP	poly[1-(trimethylsilyl)-1-propyne]
PVA	Polyvinyl alcohol
PVA+amines	Poly vinyl alcohol + formaldehyde + potassium hydroxide+ methanol+ poly (allylamine hydrochloride) + 2-aminoisobutyric acid
PVA-PEG/PTFE	Poly(vinyl alcohol)- poly(ethylene glycol)/ Polytetrafluoroethylene
STP	Standard Temperature Pressure conditions, 1 atmosphere, 76cmHg and 273.15K
TZPIM	Tetrazole-modified polymers of intrinsic microporosity
XL-PEGDA	Cross linked poly(ethylene glycil) diacrylate
ZIF	Zeolitic imidazolate frameworks

4.9 REFERENCES

[1] IPCC News from Policy and Legislation News from Policy and Legislation Intergovernmental Panel on Climate Change IPCC Second Assessment Synthesis of Scientific-Technical Information Relevant to Interpreting Article 2 of the UN Framework Convention on Climate Change 1995', n.d.

[2] Intergovernmental Panel on Climate Change (IPCC) third assessment report : hearing before the Committee on Commerce, Science, and Transportation, United States Senate, One Hundred Seventh Congress, first session, May 1, 2001., Intergov. Panel Clim. Chang. Third Assess. Rep. Hear. before Comm. Commer. Sci. Transp. United States Senat. One Hundred Seventh Congr. First Sess. May 1, 2001. . (2004). https://heinonline.org/HOL/Page?handle=hein.cbhear/cbhearings71893&id=1&div=&collection=congrec (accessed June 16, 2021).

[3] T. Kober, H.W. Schiffer, M. Densing, E. Panos, Global energy perspectives to 2060 – WEC's World Energy Scenarios 2019, Energy Strateg. Rev. 31 (2020) 100523. https://doi.org/10.1016/j.esr.2020.100523.

[4] D. Archer, M. Eby, V. Brovkin, A. Ridgwell, L. Cao, U. Mikolajewicz, K. Caldeira, K. Matsumoto, G. Munhoven, A. Montenegro, K. Tokos, Atmospheric lifetime of fossil fuel carbon dioxide, Annu. Rev. Earth Planet. Sci. 37 (2009) 117–134. https://doi.org/10.1146/ANNUREV.EARTH.031208.100206.

[5] A. Lowe, B. Beasley, T. Berly, Chapter 3. Carbon Capture and Storage (CCS) in Australia, Carbon Capture. (2010) 65–101. https://doi.org/10.1039/9781847559715-00065.

[6] International Energy Agency (IEA), World Energy Outlook 2019, OECD, 2019.

https://doi.org/10.1787/caf32f3b-en.

[7] J. Gibbins, H. Chalmers, Chapter 2. Fossil Power Generation with Carbon Capture and Storage (CCS): Policy Development for Technology Deployment, Carbon Capture. (2010) 41–64. https://doi.org/10.1039/9781847559715-00041.

[8] M. Stewart, K. Arnold, Gas Sweetening and Processing Field Manual, Gas Sweeten. Process. F. Man. (2011).

[9] H. Liu, R. Idem, P. Tontiwachwuthikul, Post-combustion CO_2 Capture Technology, Springer International Publishing, Regina, 2019. https://doi.org/10.1007/978-3-030-00922-9.

[10] Y. Cai, Z. Wang, C. Yi, Y. Bai, J. Wang, S. Wang, Gas transport property of polyallylamine-poly(vinyl alcohol)/polysulfone composite membranes, J. Memb. Sci. 310 (2008) 184–196. https://doi.org/10.1016/j.memsci.2007.10.052.

[11] J. Zou, W.S.W. Ho, CO2-selective polymeric membranes containing amines in crosslinked poly(vinyl alcohol), J. Memb. Sci. 286 (2006) 310–321. https://doi.org/10.1016/j.memsci.2006.10.013.

[12] S. Kunalan, K. Dey, P.K. Roy, V. Velachi, P.K. Maiti, K. Palanivelu, N. Jayaraman, Efficient facilitated transport PETIM dendrimer-PVA-PEG/PTFE composite flat-bed membranes for selective removal of CO_2, J. Memb. Sci. 622 (2021) 119007. https://doi.org/10.1016/j.memsci.2020.119007.

[13] L.M. Robeson, The upper bound revisited, J. Memb. Sci. 320 (2008) 390–400. https://doi.org/10.1016/j.memsci.2008.04.030.

[14] E.P. Favvas, A. Figoli, R. Castro-Muñoz, V. Fíla, X. He, Polymeric membrane materials for CO_2 separations, 2018. https://doi.org/10.1016/B978-0-12-813645-4.00001-5.

[15] F.A. Abdul Kareem, A.M. Shariff, S. Ullah, N. Mellon, L.K. Keong, Adsorption of pure and predicted binary (CO_2:CH_4) mixtures on 13X-Zeolite: Equilibrium and kinetic properties at offshore conditions, Microporous Mesoporous Mater. 267 (2018) 221–234. https://doi.org/10.1016/j.micromeso.2018.04.007.

[16] D.P. Bezerra, F.W.M.D. Silva, P.A.S.D. Moura, A.G.S. Sousa, R.S. Vieira, E. Rodriguez-Castellon, D.C.S. Azevedo, CO_2 adsorption in amine-grafted zeolite 13X, Appl. Surf. Sci. 314 (2014) 314–321. https://doi.org/10.1016/j.apsusc.2014.06.164.

[17] C.I. Chaidou, G. Pantoleontos, D.E. Koutsonikolas, S.P. Kaldis, G.P. Sakellaropoulos, Gas Separation Properties of Polyimide-Zeolite Mixed Matrix Membranes, Sep. Sci. Technol. 47 (2012) 950–962. https://doi.org/10.1080/01496395.2011.645263.

[18] Z. Zhang, P. Li, T. Zhao, Y. Xia, Enhanced CO_2 Adsorption and Selectivity of CO_2/N_2 on Amine @ ZIF-8 Materials, 2022 (2022).

[19] Q. Song, S.K. Nataraj, M. V. Roussenova, J.C. Tan, D.J. Hughes, W. Li, P. Bourgoin, M.A. Alam, A.K. Cheetham, S.A. Al-Muhtaseb, E. Sivaniah, Zeolitic imidazolate framework (ZIF-8) based polymer nanocomposite membranes for gas separation, Energy Environ. Sci. 5 (2012) 8359–8369. https://doi.org/10.1039/c2ee21996d.

[20] M. Barooah, B. Mandal, Synthesis, characterization and CO_2 separation performance of novel PVA/PG/ZIF-8 mixed matrix membrane, J. Memb. Sci. 572 (2019) 198–209. https://doi.org/10.1016/J.MEMSCI.2018.11.001.

[21] A. Wolińska-Grabczyk, P. Kubica, A. Jankowski, M. Wójtowicz, J. Kansy, M. Wojtyniak, Gas and water vapor transport properties of mixed matrix membranes containing 13X zeolite, J. Memb. Sci. 526 (2017) 334–347. https://doi.org/10.1016/j.memsci.2016.11.031.

[22] P. Bernardo, F. Bazzarelli, F. Tasselli, G. Clarizia, C.R. Mason, L. Maynard-Atem, P.M.

Budd, M. Lanč, K. Pilnáček, O. Vopička, K. Friess, D. Fritsch, Y.P. Yampolskii, V. Shantarovich, J.C. Jansen, Effect of physical aging on the gas transport and sorption in PIM-1 membranes, Polymer (Guildf). 113 (2017) 283–294. https://doi.org/10.1016/J.POLYMER.2016.10.040.

[23] Y. Kudo, H. Mikami, M. Tanaka, T. Isaji, K. Odaka, M. Yamato, H. Kawakami, Mixed matrix membranes comprising a polymer of intrinsic microporosity loaded with surface-modified non-porous pearl-necklace nanoparticles, J. Memb. Sci. 597 (2020) 117627. https://doi.org/10.1016/j.memsci.2019.117627.

[24] R. Singh, Introduction to Membrane Technology, Elsevier Ltd., Colorado Springs, 2015.

[25] J. Coates, Interpretation of Infrared Spectra, A Practical Approach, (n.d.) 10815–10837.

[26] J.D. Seader, E.J. Henley, Separation process principles, Choice Rev. Online. 36 (1999) 36-5112-36–5112. https://doi.org/10.5860/choice.36-5112.

[27] M.A. Aroon, A.F. Ismail, T. Matsuura, M.M. Montazer-Rahmati, Performance studies of mixed matrix membranes for gas separation: A review, Sep. Purif. Technol. 75 (2010) 229–242. https://doi.org/10.1016/J.SEPPUR.2010.08.023.

[28] W.S. Ho, D.C. Dalrymple, Facilitated transport of olefins in Ag+-containing polymer membranes, J. Memb. Sci. 91 (1994) 13–25. https://doi.org/10.1016/0376-7388(94)00008-5.

[29] A. Figoli, A. Cassano, A. Basile, Membrane Technologies for Biorefining, Membr. Technol. Biorefining. (2016) 1–500. https://doi.org/10.1016/C2014-0-03660-X.

[30] R. Pang, K.K. Chen, Y. Han, W.S.W. Ho, Highly permeable polyethersulfone substrates with bicontinuous structure for composite membranes in CO_2/N_2 separation, J. Memb. Sci. 612 (2020) 118443. https://doi.org/10.1016/j.memsci.2020.118443.

[31] H. Rabiee, A. Ghadimi, S. Abbasi, T. Mohammadi, CO_2 separation performance of poly(ether-b-amide6)/PTMEG blended membranes: Permeation and sorption properties, Chem. Eng. Res. Des. 98 (2015) 96–106. https://doi.org/10.1016/j.cherd.2015.03.026.

[32] H. Lin, T. Kai, B.D. Freeman, S. Kalakkunnath, D.S. Kalika, The effect of cross-linking on gas permeability in cross-linked poly(ethylene glycol diacrylate), Macromolecules. 38 (2005) 8381–8393. https://doi.org/10.1021/ma0510136.

[33] V.I. Bondar, B.D. Freeman, I. Pinnau, Gas Transport Properties of Poly (ether-b-amide) Segmented, J. Polym. Sci. Part B Polym. Physics,. 38 (2000) 2051–2062.

[34] T. Zhu, X. Yang, Y. Zheng, X. He, F. Chen, J. Luo, Preparation of poly(ether-block-amide)/poly(amide-co-poly(propylene glycol)) random copolymer blend membranes for CO_2/N_2 separation, Polym. Eng. Sci. 59 (2019) E14–E23. https://doi.org/10.1002/pen.24828.

[35] L. Liu, A. Chakma, X. Feng, Preparation of hollow fiber poly(ether block amide)/polysulfone composite membranes for separation of carbon dioxide from nitrogen, Chem. Eng. J. 105 (2004) 43–51. https://doi.org/10.1016/j.cej.2004.08.005.

[36] N. Du, H.B. Park, G.P. Robertson, M.M. Dal-Cin, T. Visser, L. Scoles, M.D. Guiver, Polymer nanosieve membranes for CO_2-capture applications, Nat. Mater. 10 (2011) 372–375. https://doi.org/10.1038/nmat2989.

[37] Y. Han, W.S.W. Ho, Recent developments on polymeric membranes for CO_2 capture from flue gas, J. Polym. Eng. 40 (2020) 529–542. https://doi.org/10.1515/polyeng-2019-0298.

[38] P.M. Budd, K.J. Msayib, C.E. Tattershall, B.S. Ghanem, K.J. Reynolds, N.B. McKeown, D. Fritsch, Gas separation membranes from polymers of intrinsic microporosity, J. Memb. Sci. 251 (2005) 263–269. https://doi.org/10.1016/j.memsci.2005.01.009.

[39] D. Fritsch, G. Bengtson, M. Carta, N.B. McKeown, Synthesis and gas permeation properties of spirobischromane-based polymers of intrinsic microporosity, Macromol. Chem. Phys. 212 (2011) 1137–1146. https://doi.org/10.1002/macp.201100089.

[40] X. Hu, W.H. Lee, J.Y. Bae, J. Zhao, J.S. Kim, Z. Wang, J. Yan, Y.M. Lee, Highly permeable polyimides incorporating Tröger's base (TB) units for gas separation membranes, J. Memb. Sci. 615 (2020) 118533. https://doi.org/10.1016/j.memsci.2020.118533.

[41] M. Mukaddam, E. Litwiller, I. Pinnau, Gas Sorption, Diffusion, and Permeation in Nafion, Macromolecules. 49 (2016) 280–286. https://doi.org/10.1021/acs.macromol.5b02578.

[42] T. Nakagawa, T. Saito, S. Asakawa, Y. Saito, Polyacetylene derivatives as membranes for gas separation, Gas Sep. Purif. 2 (1988) 3–8. https://doi.org/10.1016/0950-4214(88)80035-5.

CHAPTER 5: CONCLUSIONS AND RECOMMENDATIONS

The consumption of hydrocarbons and therefore the rise in global temperatures is predicted to continue increasing with the increase in globalization and the industrialization of third world countries. Separation of CO_2, the main global warming causing greenhouse gas, from other flue gases and from biogas has therefore become of great interest. This research focuses on the separation of CO_2 from CH_4 and N_2 gases using polymeric and mixed matrix membranes. PVA based polymer membranes were chosen to work with as they provide a cost effective, environmentally friendly, are adaptable, and energy efficient solution to gas separation. In this project, an adapted membranes from Zou and Ho's procedure were prepared and tested at atmospheric conditions and their performance was optimized at these conditions. Aging tests were done first to determine the appropriate membrane testing/ use time which was established to be 21 days after which the physical aging of the membrane had slowed down. The optimization was done through a 2^6 factorial design using the membrane forming components PVA, formaldehyde, water, AIBA, KOH and Pam-OH. This design used the CO_2/N_2 and CO_2/CH_4 selectivities to optimize the membrane. The experiments were conducted at room temperature and 2.5 atm operating pressure.

From the results of incorporating the 2^6 factorial design, out of 64 experiments and 3 error experiments it was established that the maximum permeability was achieved by CO_2 at 81,552 Barrer followed by N_2 and CH_4 at 81.544 Barrer and 80,111 Barrer, respectively. The highest membrane separation selectivity of 2.45 was achieved for the CO_2/CH_4 pair by membrane 61. The most optimized CO_2/N_2 selective membrane 13 obtained a lower maximum selectivity of 1.83. CO_2/N_2 separation was most positively affected by the PVA concentration and CO_2/CH_4

separation was most positively affected by a combination of PVA, formaldehyde and Pam-OH components.

In order to further increase the CO_2 selectivities of the membranes, the previously optimized factorial design membranes had zeolite 13X and the metal organic framework ZIF-8 added to them. 1wt%, 2wt%, 4wt% and 6wt% of both fillers were added to each of the of the optimized membranes 13 and 61. Feed pressure tests were also carried out on the optimized polymeric membranes 13 and 61. The feed pressures tested were 1.5 atm, 2.0 atm, 2.5 atm and 4.0 atm with the permeate pressure being kept at atmospheric.

With the addition of zeolite 13X to membrane 13, the CO_2/N_2 optimized membrane and to membrane 61, the CO_2/CH_4 optimized membrane their permeability increased by 5 times and 2 times, respectively, with a loss in CO_2 selectivity. With the addition of ZIF-8 to membrane 13, the membrane's permeability increased by 5 times with a gradual loss in CO_2 selectivity as the filler loading weight increased. Addition of ZIF-8 to membrane 61 decreased both its permeability and selectivity. The SEM images confirmed the formation of agglomerations/cracks in the filled membranes which led to their observed loss in selectivity.

The feed pressure tests on the polymeric unfilled membranes showed an increase in CO_2 selectivity with a decrease in feed pressure. Membrane 13 was the best performing membrane with a CO_2/N_2 and CO_2/CH_4 selectivity of 5.94 and 2.1 respectively with a CO_2 permeability of 2,471 Barrer. This membrane therefore still shows promise with better incorporated filler materials in the making of mixed matrix membranes.

It could also be of interest to try other filler materials including activated carbons to see if they would be better incorporated into the PVA amine based membranes. Moreover, it would be of

interest to try using membrane lamination using commercial silicon rubber to decrease the effects of the membrane defects so as to confirm whether the selectivity displayed by some of the membranes was due to Knudsen flow through the defects or whether the selectivity was due to facilitated transport across the membrane's pores. Also, additional membrane characterization of determining the membrane pore size as well as the glass transition temperature would be of interest. Finally, it could be also recommended to add piperazine glycinate (PG) to the optimized PVA amine based membranes as Barooah et al referenced in Chapter 4 were able to have less agglomerations on their membranes when they used a PVA/PG amine blend in the making of mixed-matrix membranes with ZIF-8.